SCUOLA DI DOTTORATO
UNIVERSITÀ DEGLI STUDI DI MILANO-BICOCCA

Department of Material Science

PhD program in **Material Science and Nanotechnology** Cycle **XXXV**

NOVEL FILLERS FOR ENHANCING THERMAL CONDUCTIVITY OF RUBBER NANOCOMPOSITES

Mirizzi Lorenzo

Registration number: 859884

Supervisor: Prof. Massimiliano D'Arienzo

Industrial tutors: Dr. Luca Giannini; Dr.ssa Silvia Guerra

Coordinator: Prof. Marco Bernasconi

ACADEMIC YEAR **2021/2022**

Contents

PHD ACTIVITIES

ACTIVITY TYPE	TITLE	LOCATION
WORKSHOP	Workshop on Functional Additives	SAES-GROUP Lainate (MI)
WORKSHOP	Introduction to life cycle assessment (LCA)	WEB (Radboud University)
WORKSHOP	Author Workshops on Academic Writing and Publishing	University of Milano Bicocca
WORKSHOP	KIC SafeVulca - 1st workshop -	University of Milano Bicocca
CONFERENCE	XXIV Convegno AIM di Trento	Trento
WINTER SCHOOL	InoMat2021	Bardonecchia

PUBLICATION AND ORAL PRESENTATION

TYPE	TITLE
SCIENTIFIC PUBLICATIONS	Mirizzi, L., Carnevale, M., D'arienzo, M., Milanese, C., Di Credico, B., Mostoni, S., et al. (2021). Tailoring the thermal conductivity of rubber nanocomposites by inorganic systems: Opportunities and challenges for their application in tires formulation. MOLECULES,26(12) [10.3390/molecules26123555].
PRESENTATION AT CONFERENCES	Hybrid Al_2O_3@POSS nanofiller for the production of thermal conductive rubber nanocomposites
OTHER PUBLICATIONS	**SUBMITTED ARTICLE:** Al_2O_3 decorated with POSS units: an unconventional filler system for upgrading thermal conductivity and mechanical properties of rubber composites

Glossary

AMM	Acoustic Mismatch Model
ACN	Acrylonitrile
ATR	Attenuated Total Reflection Fourier Transform Infrared
FTIR	Spectroscopy
AIBN	Azobisisobutirronitrile
Si69, TESPT	bis-(3-triethoxy silylpropyl)-tetrasulfide
BR	Butadiene Rubber
CNTs	Carbon Nanotubes
XNBR	Carboxylated Nitryl Rubber
CTAB	Cetyltrimethylammonium Bromide
DCP	Dicumarylperoxide
DMM	Diffuse Mismatch Model
DRS	Diffuse Reflectance Spectroscopy
DMA	Dynamical Mechanical Analysis
DMTA	Dynamical Mechanical Thermal Analysis
EDS	Energy-dispersive X-ray spectroscopy
EPDM	Ethylene Propylene Diene Monomer
EG	Expanded Graphite
GO	Graphene Oxide
h-BN	Hexagonal Born Nitride
ICP	Inductively Coupled Plasma
LFA	Laser Flash Analysis
MAS	Magic Angle Spinning
MTPMS	Methacrylsilane
MTPS	Modified Transient Plane Source
MMT	Montmorillonite
MWNTs	Multiwalled Carbon Nanotubes
6PPD	N-(1,3-dimethylbutyl)-N-phenyl-p-phenylenediamine
NPs	Nanoparticles
NR	Natural Rubber
CBS	N-cyclohexyl-2-benzothiazole sulfenamide
NMR	Nuclear Magnetic Resonance
OES	Optical Emission Spectrometry
PHR	Per Hundred Rubber
PA	Polyacrylates
PB	Polybutadiene
PDA	Polydopamine
POSS	Polyhedral Oligomeric Silsesquioxanes
rGO	Reduced Graphene Oxide
RPA	Rubber Process Analyzer
SEM	Scanning Electron Microscopy

SBR	Styrene Butadiene Rubber
TC	Thermal Conductivity
TGA	Thermogravimetric Analysis
TEM	Transmission Electron Microscopy
XRD	X-Ray Diffractometer

Introduction, aims and structure of the thesis

Introduction

Polymer composites

IUPAC defines *polymer composite* as a multicomponent material comprising multiple, different (non-gaseous) phase domains in which at least one type of phase domain is a polymeric continuous phase. A *nanocomposite* is a composite in which at least one of the phase domains has one dimension of the order of nanometres.[1] Generally, we call *matrix* the continuous polymeric phase and *filler* the dispersed phase. As shown in figure I.1, polymer nanocomposite is a developing scientific field, with an increasing number of papers published in different subject areas, primarily material science, chemistry and engineering.

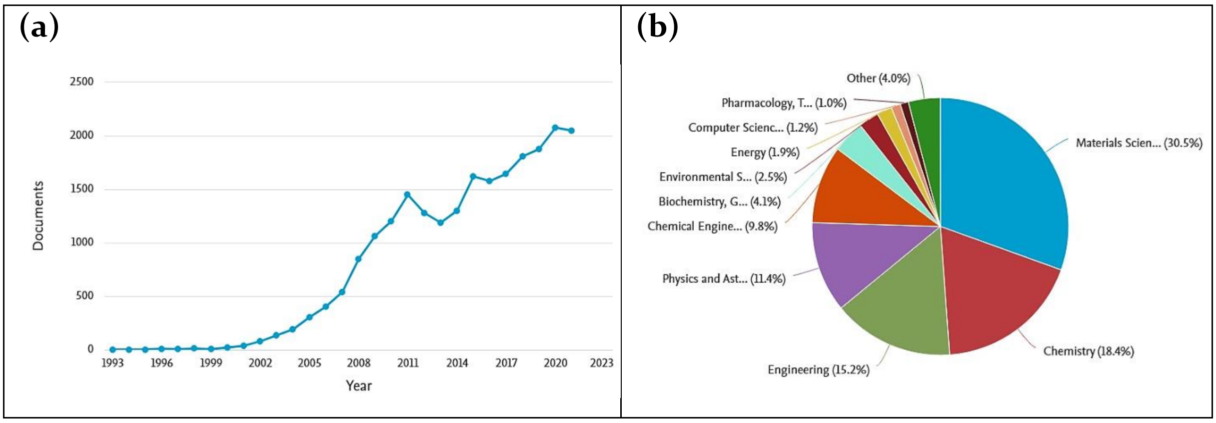

Figure I.1 – Analytical graphs of the resultant documents (a) by year and (b) by subject area obtained when searching "polymer composite" as keyword on Scopus website

Since the tuning of properties at the interface can change dramatically the macroscopic properties of the whole material, nanocomposites are an attractive field of research for many applications ranging from biomedical, catalytic process, separation science, chemical sensing, fuel cell, solar energy accumulation, hydrogen storage, capacitors, micro/nano electronics devices, etc. (Fig. I.2)

Rubber composites for tires

A strategic class of polymer nanocomposites are rubber nanocomposites, where the matrix is rubber (e.g. Natural Rubber, Isoprene, Styrene Butadiene Rubber, Polybutadiene, Nitrile Butadiene Rubber) generally combined with carbon-based and inorganic fillers, which play a fundamental role in making them applicable in various fields. [2–4] These kinds of composite materials have in fact several applications, not only in miniaturised systems, like electronic devices or gas barrier materials, but also in large-scale products, like tubes, belts, hoses seals and, remarkably, tires.

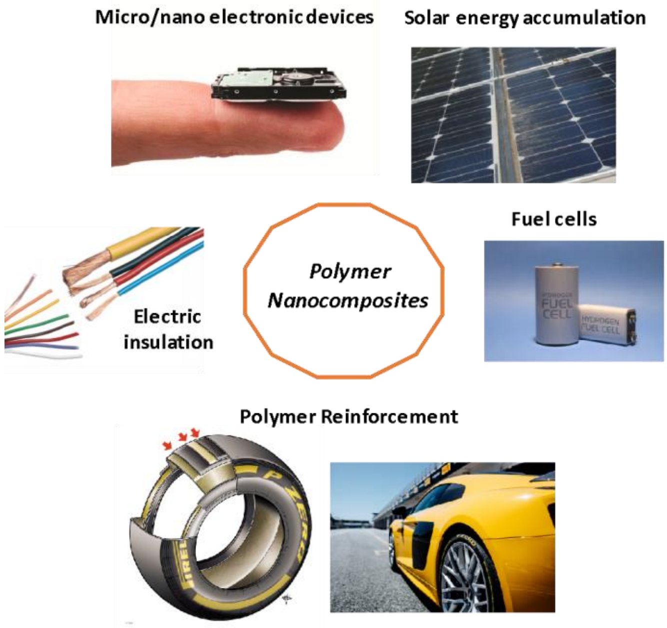

Figure I.2 - Application of polymer nanocomposites

Owing to their superior mechanical properties, enhanced modulus and dimensional stability, flame retardancy, improved scratch and mar resistance, enhanced thermal and processing features, reduced warpage of components and improved impact resistance, rubber nanocomposites are widely utilised for tires application. [5] In particular, a challenging objective is the development of "Green tires", an energy efficient system, in which the rolling resistance (the force that works against the tire motion) is lowered without affecting grip and wear. [6–9] The enhancement of these properties remarkably depends on the viscoelastic characteristics of the rubber composites. A tire is in fact an assembly of numerous components manufactured with a relatively standardized process (Fig. I.3), where the principal component is rubber, a material with unique properties, such as low hardness, high elasticity and high elongation at break. In tire industry, both natural rubber and synthetic rubber (e.g. isoprene, IR; styrene, SR; butadiene, BR) are used. Anyway, rubber itself cannot be used to produce tire thus, proper additives must be added. Different formulations are employed to obtain specific properties (like hardness, tensile strength and wear resistance), to fulfil the requirements for the specific part of the tire that they will constitute (tread, bead, etc.). Additives can be grouped as filler, vulcanizing agent (sulphur, accelerator and activator), processing oil and anti-degradant.

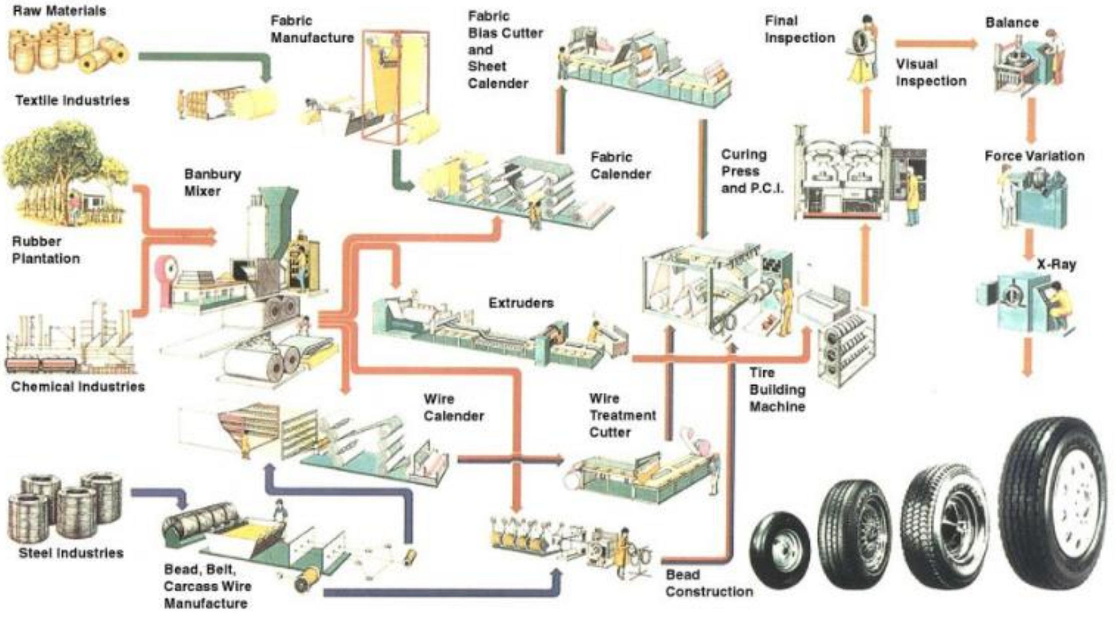

Figure I.3 - Tire manufacturing process [1]

Fillers are particles that are included in the matrix for various purposes. In tire industry it is possible to find non-reinforcing filler used to reduce the final cost of the composite and the reinforcing filler extremely useful to impart proper mechanical properties to the tire. Reinforcing filler are generally material with nanometric (1-100 nm) primary particle size and are divided into in black fillers (mainly carbon black) and white filler (silica, silicates and clays). Vulcanization is a fundamental process that permits to form crosslinks between rubber chains enhancing rigidity, durability and mechanical performance of the final tire. The term vulcanization was originally used by Goodyear that developed a way to hardening NR by introduction of sulphur and subsequent heating treatment. [10] Actually this method has been extended to other rubber and it widely diffuse in rubber industry. Sulphur itself is a slow vulcanizing agent, thus activator and accelerator are generally introduced. These substances have been historically optimized for the different matrix and all contribute to the determination of the vulcanization efficiency and rate, and thus to the final properties of the composite.

Finally, processing oils are introduced in order to improve the efficiency of mixing procedures and anti-degradant are molecules that permits to reduce the oxidation of the rubber, extending its lifetime. In particular, a challenging objective in tire industry is the development of "Green tires" i.e. energy efficient systems, in which the rolling resistance, i.e. the force that works against the tire motion, is lowered without affecting grip and wear. [6–9] The enhancement of these properties remarkably depends on the viscoelastic characteristics of the rubber composites. These, in turn, rely on different parameters such as the filler typology and amount, morphology of filler particles (aspect ratio), the degree of dispersion and aggregation of particles in the matrix (filler-filler interaction) and the interfacial adhesion between filler and polymer chains (filler-rubber interaction). [11–13] Besides Carbon Black (CB), amorphous silica is the most widely utilised inorganic filler in rubber nanocomposites for tires. [13, 14] Size, shape and surface functionalization, i.e. compatibilization with silane coupling agents [12], [15–17] (Fig. I.4), are key parameters in determining the reinforcing capability of SiO_2 in the rubber matrix.

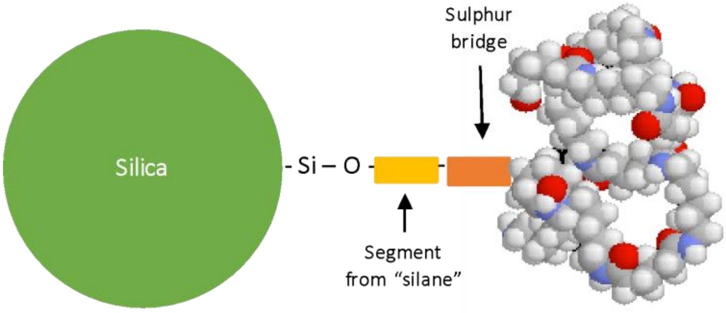

Figure I.4 - Generalized approach for SiO_2 surface modification with a silane coupling agent

In this context, our group [12, 16, 18] investigated and rationalized the effects induced by different silane coupling agents on the properties of rubber formulations, by examining both the morphology and the mechanical behavior of silica–natural rubber nanocomposites, enclosing silica nanoparticles (NPs) functionalized with trialkoxysilane bearing different functional groups (Fig. I.5).

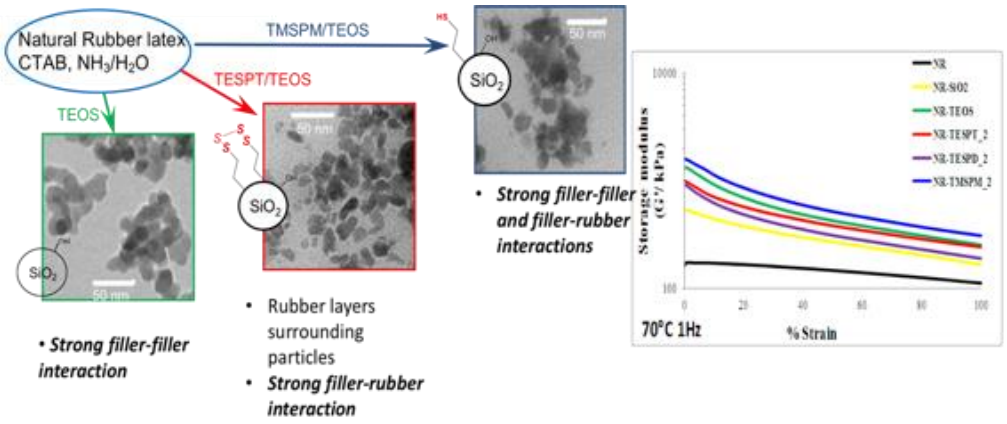

Figure I.5 - Silica surface functionalization effect on the mechanical properties of rubber nanocomposites

The study demonstrated that silane coupling agents modulate the filler-filler and the filler-rubber interactions, contributing to the tailoring of the filler networking and, consequently to the dynamic-mechanical properties of the composites. Moreover, this approach has been recently extended by using as unconventional functionalizing agents polysilsesquioxanes (POSS) units. [19, 20] More in detail, the peculiar features of OctaMethacrylPOSS modified SiO_2 NPs, forming a novel SiO_2@POSS hybrid filler, were exploited to produce styrene butadiene rubber (SBR) composites for tires which displayed outstanding reinforcement and decreased energy loss under strain, even when very low amount of POSS was enclosed in the formulations (Fig. I.6). These results suggest that polysilsesquioxanes can be promising fillers for this application, granting a transfer of the advanced properties of POSS nanounits to the final nanocomposites. Also, the shape of silica NPs has a great influence on the reinforcement of rubber nanocomposites for tires. It has been demonstrated that shape-controlled rod-like silica NPs with high aspect ratios align in the rubber matrix, providing, beside an increase of the filler-filler interactions, high percentage of immobilized rubber at the filler/rubber interface, supplying remarkable mechanical and dissipation properties (Fig. I.7).

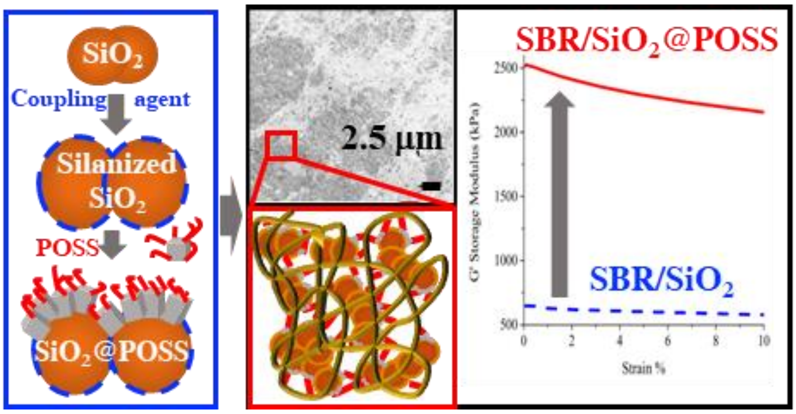

Figure I.6 - Main features and properties imparted by SiO2@POSS hybrid filler to SBR nanocomposites

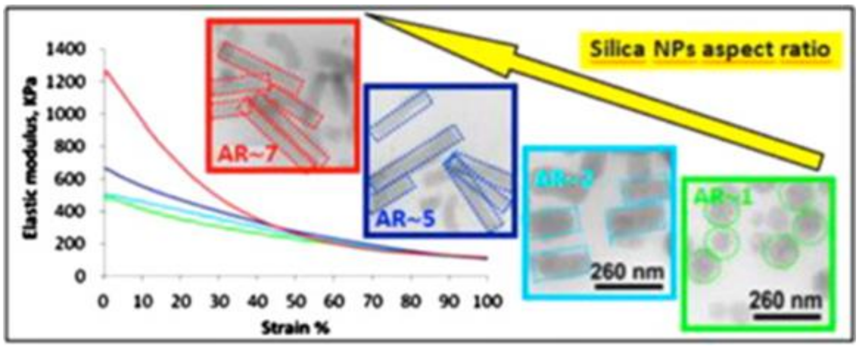

Figure I.7 - Effect of Silica NPs with different aspect ratio on the reinforcement. Reprinted with permission from [11].

In summary, a fine tuning of the filler morphology, including shape and specific surface area, surface chemistry, interfacial interactions with the polymer (filler-rubber interactions) or between the filler particles (filler-filler interactions) is necessary to control the final properties of the tire rubber formulation. Although mechanical properties are important for tire applications, recently also thermophysical properties have drawn the attention of researchers and companies. In fact, tires work under dynamic service conditions, experiencing intense low-frequency mechanical deformations arising from the internal friction at the molecular level between filler and rubber, which lead to a significant heat build-up. Due to the low thermal transport in the matrix, heat can accumulate, producing high local temperature that leads to the failure of the tread base and shoulder of tires. [21] Thus, thermal conductivity becomes an important parameter for personal safety issues and durability of tire. During the past few decades, different approaches have been utilized to enhance the thermal conductivity (λ) of rubber composites, principally using thermally conductive fillers or fabricating ordered polymer microstructures in the matrix. [22–30] Regarding the use of thermally conductive fillers, it has to be highlighted that SiO_2 filler unfortunately has a very low thermal conductivity (about 3,5 W/mK). Thus, to fulfil the target to attain high thermal dissipation, ceramic or carbon-based phases having high intrinsic λ values are additionally needed. Common thermal conductive filler that can be exploited are inorganic material like silicon carbide (SiC)[31, 32], alumina (Al_2O_3)[33, 34], boron nitride (BN) [35], zinc oxide (ZnO)[36, 37] and aluminium nitride (AlN)[38, 39], but also carbon based materials like carbon nanotubes (CNTs) [40], CB [41], graphite [42, 43], reduced graphene oxide (rGO) [44-46] and carbon fibre [47]. Various morphologies have also been analysed, finding that high aspect ratio fillers have the ability to assemble in such a way that they form continuous thermal conductive pathway in the matrix even at low loading, and thus enhance the thermal transport [48]. Another way to improve the λ of a composite is to construct a three-dimensional (3D) network of thermal conductive filler or to incorporate cooperative fillers with different nature or morphology (hybrid filler). [49–52] On the other hand, not only the filler intrinsic parameters are important, but also the interaction between filler and matrix must be considered. Fundamental is the interfacial thermal resistance that arise when a filler is incorporated in the matrix. This phenomenon, in fact, causes a drop of λ and is caused by the differences in phonon spectra of the filler and the matrix and the consequent phonon scattering at the matrix-filler interface. [30] An effective strategy that can be developed to reduce the interfacial thermal resistance deals with filler surface functionalization, in order to enhance filler-matrix interaction and reduce discontinuity between the filler. [53–56] Although recent studies report that remarkable improvements of λ can be obtained only at high filler loadings [57, 58], this must be avoided, since it dramatically changes the mechanical behaviour and the cross-linking density of the composites. [25] A detailed investigation of the effect of rubber formulation and compounding on the heat dissipation properties has to be pursued, especially for high-performance materials like rubber composites for tires, where the identification and the mitigation of overheating effects represent a difficult task. [21, 59]

Finally, it has to be observed that the tires overheating entails also permanent damages of the composites, raising concerns in terms of wastes production and, more remarkably, of safety. Thus, enhancing of thermal conductivity positively affects both the safety and sustainability of tire composites reducing the tire failure chances and increasing the average service lifetime.

In this context, smart materials which are capable of automatic healing and restoration of damage after suffering external damage look promising alternatives. [60–63] Inspired by the energy dissipation and self-healability of sacrificial bonds in nature, several recent research efforts have been devoted to the incorporation of these particular bonds into synthetic and natural rubber for imparting both mechanical strength and self-healing ability [63]. Sacrificial bonds are non-covalent bonds that generally broke before the main structural link in the matrix [64]. However, the presence of a stable covalently bonded network in these materials often hinders the restoring upon damage. Therefore, it remains challenging to develop a synergistic alliance between robust mechanical properties, virtuous self-healing ability and enhanced thermal transport properties in order to upgrade the tire durability and, consequently, their safety.

Aims of the thesis

In this context, the PhD research activity, in collaboration with Pirelli Tires, aims at **modifying commercially available materials or designing novel fillers suitable for the production of rubber composites with high thermal conductivity and satisfactory mechanical performances, trying also to reduce the filler loading**.

Among the thermally conductive filler materials **Al_2O_3 was selected as an appealing candidate**, due to its low cost, the stable chemical performance and the negligible toxicity, which compensate for the not very high intrinsic thermal conductivity. By a proper tuning of crystal phase, morphology and surface properties alumina has been widely used as filler mostly in silicon rubber nanocomposites, endowing improved thermal conductivity as well as good mechanical and electrical insulation properties.

Inspired by these results, different inorganic and hybrid alumina-based fillers have been developed:

i. Alumina nanosheets supported on silica: **$SiO_2@Al_2O_3$**

ii. Alumina decorated at the surface with polysilsesquioxanes units: **Al_2O_3@POSS**

The structural, morphological and surface features of these materials have been comprehensively investigated and the novel fillers have been utilized for the production of butadiene rubber (BR)-styrene butadiene rubber (SBR) composites, which were then characterized in terms of mechanical and thermal conductive properties.

Moreover, a **preliminary inspection** on the properties of an **innovative carbon-based filler constituted of exfoliated graphite decorated at the surface with SiO_2 NPs (EG@SiO_2)** has been carried out.

As already stressed, the mitigation of tires overheating effects represents an ambitious task which, besides dealing with the possibility to tune/improve the thermal conductivity, entails the problem of a permanent damage of the composites. Thus, a promising opportunity lies in **developing filler systems able not only to improve the thermomechanical properties but also to induce self-healing effects,** in order to extend the service-life, the sustainability and the safety of the composites.

With this aim and in collaboration with CSIC Madrid, the following activities have been pursued:

i. The exploiting of **Al_2O_3@POSS** (with methacrylic terminations) in carboxylated nitrile rubber (XNBR) employed in automotive to verify their **potential self-healing ability**

ii. The developing of an innovative filler composed by **alumina decorated at the surface with ZnO NPs (Al_2O_3@ZnO) able to assure,** upon incorporation XNBR, **both enhanced thermal conductivity and self-repairing properties**

The structural, morphological and surface features of Al_2O_3@ZnO have been investigated in depth as well as the ability of both filler systems imparting the self-healing to polymer matrices.

Finally, it has to be mentioned that, due to the COVID pandemic situation, during 2020 the experimental activities were remarkably limited and all the results reported in this work have been mainly achieved in the second and third years of the PhD.

Structure of thesis

This thesis is organized in the following chapters:

- In *Chapter 1* a general introduction regarding the thermal conductivity of polymer composites is given, with a particular focus on the rubber nanocomposites and on the exploitation of alumina thermally conductive fillers. The basic principles of thermal conductivity have been described as well as the factors affecting the thermal transport in polymer composites. Successively, the main techniques for assessing thermal conductivity have been depicted. Finally, the attention has focused on the description of the thermal conductivity in rubber nanocomposites, reporting in particular on the use of hybrid and alumina nanofillers.

- In *Chapter 2* a careful description of the synthesis and characterization of SiO_2@Al_2O_3 filler has been reported, together with its application in the formulation of rubber composites for tires. Mechanical and thermal conductivity properties of the final composites have been also outlined.

- In *Chapter 3* the promising properties of Al_2O_3@POSS have been described. The first part of the chapter focuses on the synthesis and characterization of the material, while the second one mainly deals with the influence of the POSS presence at the filler surface on the mechanical and thermal conductive properties. Finally, in the last part of the section the versatility of the synthetic approach has been demonstrated by reporting the application on elongated alumina nanoparticles.

- In *Chapter 4* the synthesis and the characterization of Al_2O_3@ZnO have been illustrated. Successively, the capability of the novel filler and of Al_2O_3@POSS to impart self-healing properties to XNBR nanocomposites has been reported.

- In *Chapter 5* the preliminary results obtained on carbon-based filler in SBR nanocomposites are presented.

- In *Chapter 6* conclusions and perspectives of the thesis are drawn.

Acknowledgement

The author would like to thank university of Trento for solid state NMR analysis on the fillers and for the mechanical and thermal conductivity determination on PB based composites; University of Pavia and Polytechnic of Milano for thermal conductivity analysis on SBR/BR composites.

Bibliography

[1] A. W. A. D. McNaught, *The IUPAC Compendium of Chemical Terminology*. Research Triangle Park, NC: International Union of Pure and Applied Chemistry (IUPAC), 2019.

[2] S. Thomas and R. Stephen, Eds., *Rubber Nanocomposites*. Chichester, UK: John Wiley & Sons, Ltd, 2010.

[3] V. E. Borisenko and S. Ossicini, *What is What in the Nanoworld*. Wiley, 2008.

[4] A. B. Morgan, "Hybrid Materials: Synthesis, Characterization, and Applications. Edited by Guido Kickelbick (Technische Universität Wien, Austria). Wiley-VCH Verlag GmbH & Co. KGaA: Weinheim. 2007. xviii + 498 pp. $200.00. ISBN 978-3-527-31299-3.," *J. Am. Chem. Soc.*, vol. 130, no. 3, pp. 1111–1112, Jan. 2008.

[5] M. El Fray and L. A. Goettler, "Application of Rubber Nanocomposites," in *Rubber Nanocomposites*, 2010, pp. 675–696.

[6] S. Uhrlandt and A. Blume, "Silica in green tyres - Processes, products, properties," *Kautschuk Gummi Kunststoffe*, vol. 54, no. 10, p. 520, 2001.

[7] A. R. Payne, "Rubber Plast," *Age (Omaha).*, vol. 111, p. 963, 1961.

[8] A. R. Payne and R. E. Whittaker, "Low Strain Dynamic Properties of Filled Rubbers," *Rubber Chem. Technol.*, vol. 44, no. 2, pp. 440–478, May 1971.

[9] A. I. Medalia, "Morphology of aggregates," *J. Colloid Interface Sci.*, vol. 32, no. 1, pp. 115–131, Jan. 1970.

[10] J. E. Mark, B. Erman, and M. Roland, The Science and Technology of Rubber. Elsevier Science, 2013.

[11] R. Scotti *et al.*, "Shape controlled spherical (0D) and rod-like (1D) silica nanoparticles in silica/styrene butadiene rubber nanocomposites: Role of the particle morphology on the filler reinforcing effect," *Polymer (Guildf).*, vol. 55, no. 6, pp. 1497–1506, Mar. 2014.

[12] R. Scotti *et al.*, "Rubber–silica nanocomposites obtained by in situ sol–gel method: particle shape influence on the filler–filler and filler–rubber interactions," *Soft Matter*, vol. 8, no. 7, p. 2131, 2012.

[13] L. Tadiello *et al.*, "The filler–rubber interface in styrene butadiene nanocomposites with anisotropic silica particles: morphology and dynamic properties," *Soft Matter*, vol. 11, no. 20, pp. 4022–4033, 2015.

[14] R. Scotti, M. D'Arienzo, B. Di Credico, L. Giannini, and F. Morazzoni, "Silica-Polymer Interface and Mechanical Reinforcement in Rubber Nanocomposites," in *Hybrid Organic-Inorganic Interfaces*, Weinheim, Germany: Wiley-VCH Verlag GmbH & Co. KGaA, 2017, pp. 151–198.

[15] V. A. E. Barrios and M. Garcia-Ramirez, "EFFECT OF FUNCTIONALIZATION ON SBR'S INTERACTION WITH CARBON BLACK AND SILICA," *Int. J. Polym. Mater.*, vol. 52, no. 11–12, pp. 985–998, Nov. 2003.

[16] L. Wahba *et al.*, "In situ sol–gel obtained silica–rubber nanocomposites: influence of the filler precursors on the improvement of the mechanical properties," *RSC Adv.*, vol. 3, no. 17, p. 5832, 2013.

[17] P. Thaptong, P. Sae-Oui, and C. Sirisinha, "Effects of silanization temperature and silica type on properties of silica-filled solution styrene butadiene rubber (SSBR) for passenger car tire tread compounds," *J. Appl. Polym. Sci.*, vol. 133, no. 17, p. n/a-n/a, May 2016.

[18] L. Wahba *et al.*, "A novel non-aqueous sol–gel route for the in situ synthesis of high loaded silica–rubber nanocomposites," *Soft Matter*, vol. 10, no. 13, pp. 2234–2244, Jan. 2014.

[19] M. D'Arienzo *et al.*, "Hybrid SiO 2 @POSS nanofiller: a promising reinforcing system for rubber nanocomposites," *Mater. Chem. Front.*, vol. 1, no. 7, pp. 1441–1452, 2017.

[20] M. Redaelli *et al.*, "On the key role of SiO2@POSS hybrid filler in tailoring networking and interfaces in rubber nanocomposites," *Polym. Test.*, vol. 65, pp. 429–439, Feb. 2018.

[21] S. M. Danilova-Tret'yak, "On Thermophysical Properties of Rubbers and Their Components," *J. Eng. Phys. Thermophys.*, vol. 89, no. 6, pp. 1388–1393, Nov. 2016.

[22] C. I. Idumah and A. Hassan, "Recently emerging trends in thermal conductivity of polymer nanocomposites," *Rev. Chem. Eng.*, vol. 32, no. 4, Jan. 2016.

[23] X. Yang *et al.*, "A review on thermally conductive polymeric composites: classification, measurement, model and equations, mechanism and fabrication methods," *Adv. Compos. Hybrid Mater.*, vol. 1, no. 2, pp. 207–230, Jun. 2018.

[24] S. N. Leung, "Thermally conductive polymer composites and nanocomposites: Processing-structure-property relationships," *Compos. Part B Eng.*, vol. 150, pp. 78–92, Oct. 2018.

[25] H. Chen *et al.*, "Thermal conductivity of polymer-based composites: Fundamentals and applications," *Prog. Polym. Sci.*, vol. 59, pp. 41–85, Aug. 2016.

[26] C. Huang, X. Qian, and R. Yang, "Thermal conductivity of polymers and polymer nanocomposites," *Mater. Sci.*

Eng. R Reports, vol. 132, pp. 1–22, Oct. 2018.

[27] J. Eastoe, M. J. Hollamby, and L. Hudson, "Recent advances in nanoparticle synthesis with reversed micelles," *Adv. Colloid Interface Sci.*, vol. 128–130, no. 2006, pp. 5–15, 2006.

[28] X. He and Y. Wang, "Recent Advances in the Rational Design of Thermal Conductive Polymer Composites," *Ind. Eng. Chem. Res.*, vol. 60, no. 3, pp. 1137–1154, Jan. 2021.

[29] Y. Cui, M. Li, and Y. Hu, "Emerging interface materials for electronics thermal management: experiments, modeling, and new opportunities," *J. Mater. Chem. C*, vol. 8, no. 31, pp. 10568–10586, 2020.

[30] N. Burger, A. Laachachi, M. Ferriol, M. Lutz, V. Toniazzo, and D. Ruch, "Review of thermal conductivity in composites: Mechanisms, parameters and theory," *Prog. Polym. Sci.*, vol. 61, pp. 1–28, Oct. 2016.

[31] T. Zhou, X. Wang, G. U. Mingyuan, and X. Liu, "Study of the thermal conduction mechanism of nano-SiC/DGEBA/EMI-2,4 composites," *Polymer (Guildf).*, vol. 49, no. 21, pp. 4666–4672, Oct. 2008.

[32] D. Shen *et al.*, "Enhanced thermal conductivity of epoxy composites filled with silicon carbide nanowires," *Sci. Rep.*, vol. 7, no. 1, p. 2606, Dec. 2017.

[33] Y. Hu, G. Du, and N. Chen, "A novel approach for Al 2 O 3 /epoxy composites with high strength and thermal conductivity," *Compos. Sci. Technol.*, vol. 124, pp. 36–43, Mar. 2016.

[34] Y. Yao, X. Zeng, K. Guo, R. Sun, and J. Xu, "The effect of interfacial state on the thermal conductivity of functionalized Al2O3 filled glass fibers reinforced polymer composites," *Compos. Part A Appl. Sci. Manuf.*, vol. 69, pp. 49–55, Feb. 2015.

[35] H. Fang, S.-L. Bai, and C. P. Wong, "'White graphene' – hexagonal boron nitride based polymeric composites and their application in thermal management," *Compos. Commun.*, vol. 2, pp. 19–24, Nov. 2016.

[36] Q. Mu, S. Feng, and G. Diao, "Thermal conductivity of silicone rubber filled with ZnO," *Polym. Compos.*, vol. 28, no. 2, pp. 125–130, Apr. 2007.

[37] H. Du, Y. Qi, W. Yu, J. Yin, and H. Xie, "T-shape ZnO whisker: A more effective thermal conductive filler than spherical particles for the thermal grease," *Int. J. Heat Mass Transf.*, vol. 112, pp. 1052–1056, Sep. 2017.

[38] C. Jiang, D. Zhang, X. Gan, R. Xie, F. Zhang, and K. Zhou, "Preparation of high performance AlN/Hydantion composite by gelcasting and infiltration processes," *Ceram. Int.*, vol. 40, no. 1, pp. 2535–2538, Jan. 2014.

[39] A. Ma, W. Chen, Y. Hou, and G. Zhang, "The Preparation and Cure Kinetics Researches of Thermal Conductivity Epoxy/AlN Composites," *Polym. Plast. Technol. Eng.*, vol. 49, no. 4, pp. 354–358, Mar. 2010.

[40] J. Nanda *et al.*, "Thermal Conductivity of Single-Wall Carbon Nanotube Dispersions: Role of Interfacial Effects," *J. Phys. Chem. C*, vol. 112, no. 3, pp. 654–658, Jan. 2008.

[41] R. A. Hauser, J. A. King, R. M. Pagel, and J. M. Keith, "Effects of carbon fillers on the thermal conductivity of highly filled liquid-crystal polymer based resins," *J. Appl. Polym. Sci.*, vol. 109, no. 4, pp. 2145–2155, Aug. 2008.

[42] I. M. Afanasov, D. V. Savchenko, S. G. Ionov, D. A. Rusakov, A. N. Seleznev, and V. V. Avdeev, "Thermal conductivity and mechanical properties of expanded graphite," *Inorg. Mater.*, vol. 45, no. 5, pp. 486–490, May 2009.

[43] J. Gu, X. Yang, Z. Lv, N. Li, C. Liang, and Q. Zhang, "Functionalized graphite nanoplatelets/epoxy resin nanocomposites with high thermal conductivity," *Int. J. Heat Mass Transf.*, vol. 92, pp. 15–22, Jan. 2016.

[44] A. A. Balandin *et al.*, "Superior Thermal Conductivity of Single-Layer Graphene," *Nano Lett.*, vol. 8, no. 3, pp. 902–907, Mar. 2008.

[45] S. H. Song *et al.*, "Enhanced Thermal Conductivity of Epoxy-Graphene Composites by Using Non-Oxidized Graphene Flakes with Non-Covalent Functionalization," *Adv. Mater.*, vol. 25, no. 5, pp. 732–737, Feb. 2013.

[46] L.-H. Liu and M. Yan, "Functionalization of pristine graphene with perfluorophenyl azides," *J. Mater. Chem.*, vol. 21, no. 10, p. 3273, 2011.

[47] T. Ji *et al.*, "Thermal conductive and flexible silastic composite based on a hierarchical framework of aligned carbon fibers-carbon nanotubes," *Carbon N. Y.*, vol. 131, pp. 149–159, May 2018.

[48] R. F. Hill and P. H. Supancic, "Thermal Conductivity of Platelet-Filled Polymer Composites," *J. Am. Ceram. Soc.*, vol. 85, no. 4, pp. 851–857, Dec. 2004.

[49] G.-W. Lee, M. Park, J. Kim, J. I. Lee, and H. G. Yoon, "Enhanced thermal conductivity of polymer composites filled with hybrid filler," *Compos. Part A Appl. Sci. Manuf.*, vol. 37, no. 5, pp. 727–734, May 2006.

[50] C.-C. Teng, C.-C. M. Ma, K.-C. Chiou, and T.-M. Lee, "Synergetic effect of thermal conductive properties of epoxy composites containing functionalized multi-walled carbon nanotubes and aluminum nitride," *Compos. Part B Eng.*, vol. 43, no. 2, pp. 265–271, Mar. 2012.

[51] S. N. Leung *et al.*, “Synergistic effects of hybrid fillers on the development of thermally conductive polyphenylene sulfide composites,” *J. Appl. Polym. Sci.*, vol. 127, no. 5, pp. 3293–3301, Mar. 2013.

[52] J. Zeng, R. Fu, Y. Shen, H. He, and X. Song, “High thermal conductive epoxy molding compound with thermal conductive pathway,” *J. Appl. Polym. Sci.*, vol. 113, no. 4, pp. 2117–2125, Aug. 2009.

[53] J. Song and Y. Zhang, “Effect of an interface layer on thermal conductivity of polymer composites studied by the design of double-layered and triple-layered composites,” *Int. J. Heat Mass Transf.*, vol. 141, pp. 1049–1055, Oct. 2019.

[54] A. Giri and P. E. Hopkins, “A Review of Experimental and Computational Advances in Thermal Boundary Conductance and Nanoscale Thermal Transport across Solid Interfaces,” *Adv. Funct. Mater.*, vol. 30, no. 8, p. 1903857, Feb. 2020.

[55] C.-W. Nan, R. Birringer, D. R. Clarke, and H. Gleiter, “Effective thermal conductivity of particulate composites with interfacial thermal resistance,” *J. Appl. Phys.*, vol. 81, no. 10, pp. 6692–6699, May 1997.

[56] A. Kotia, S. Borkakoti, P. Deval, and S. K. Ghosh, “Review of interfacial layer’s effect on thermal conductivity in nanofluid,” *Heat Mass Transf.*, vol. 53, no. 6, pp. 2199–2209, Jun. 2017.

[57] A. Oluwalowo, N. Nguyen, S. Zhang, J. G. Park, and R. Liang, “Electrical and thermal conductivity improvement of carbon nanotube and silver composites,” *Carbon N. Y.*, vol. 146, pp. 224–231, May 2019.

[58] R. Aradhana, S. Mohanty, and S. K. Nayak, “Novel electrically conductive epoxy/reduced graphite oxide/silica hollow microspheres adhesives with enhanced lap shear strength and thermal conductivity,” *Compos. Sci. Technol.*, vol. 169, pp. 86–94, Jan. 2019.

[59] Z. Wang, Y. Lu, J. Ding, L. Zhang, and T. W. Chan, “Preparation of nano-reinforced thermal conductive natural rubber composites,” *Polym. Compos.*, vol. 37, no. 3, pp. 771–781, Mar. 2016.

[60] M. A. Sattar and A. Patnaik, “Design Principles of Interfacial Dynamic Bonds in Self-Healing Materials: What are the Parameters?,” *Chem. – An Asian J.*, vol. 15, no. 24, pp. 4215–4240, Dec. 2020.

[61] M. Nakahata, Y. Takashima, H. Yamaguchi, and A. Harada, “Redox-responsive self-healing materials formed from host–guest polymers,” *Nat. Commun.*, vol. 2, no. 1, p. 511, Sep. 2011.

[62] Y. Shi, M. Wang, C. Ma, Y. Wang, X. Li, and G. Yu, “A Conductive Self-Healing Hybrid Gel Enabled by Metal–Ligand Supramolecule and Nanostructured Conductive Polymer,” *Nano Lett.*, vol. 15, no. 9, pp. 6276–6281, Sep. 2015.

[63] R. P. Wool, “Self-healing materials: a review,” *Soft Matter*, vol. 4, no. 3, p. 400, 2008.

[64] J. Araujo-Morera, M. Hernández Santana, R. Verdejo, and M. A. López-Manchado, “Giving a Second opportunity to tire waste: An alternative path for the development of sustainable self-healing styrene–butadiene rubber compounds overcoming the magic triangle of tires,” *Polymers (Basel).*, vol. 11, no. 12, p. 2122, 2019.

Chapter 1 - Thermal conductivity in polymer composites

1.1 - Basic principles, models and factors affecting the thermal transport in polymer nanocomposites

Basic principles and models

Thermal conductivity is the physical quantity that measure the ability of a material to conduct heat when heat transport by convention and irradiation mechanisms are not present, and can be expressed by Fourier's law (1):

$$q = \lambda \cdot A \cdot \frac{\Delta T}{L} \qquad (1)$$

where q is the rate of heat conduction (W); λ the thermal conductivity (W m^{-1} K^{-1}); A the cross-sectional area for the heat transfer (m^2); ΔT the temperature difference (K); and L the length of the conduction path (m).

In solids, heat conduction is mediated both by normal mode of vibrations and collisions of molecules and diffusion and collisions of free electrons. Normal modes of vibration are elementary vibrational motion in which in a lattice of atoms or molecules uniformly oscillates at a single frequency. While normal modes are wave-like phenomena in classical mechanics, quantum mechanics describes them as phonons, with particle-like properties in a way related to the wave–particle duality of quantum mechanics. Carriers of heat in solid accordingly to this are phonons and electrons, and thermal conductivity is the sum of the contribution of these two carriers. Depending on the material families, contribution from electrons or phonons can be negligible, and so for example in metals heat is transferred almost exclusively by electrons, while in non-metallic crystal and amorphous materials by phonons. In these last type of materials, thermal conductivity depends on the phonon mean free path, which can be described as the average travelling distance between two consecutive scattering events. Scattering occurs at any defect and principally with three possible mechanisms [1]:

- *Phonon/defect scattering*

Defects in crystalline scattering represent an obstacle for phonon transmission, and so it is easy to think that in this point scattering occurs.

- *Phonon/interface scattering*

Interfaces or disconnection which arise due to the finite dimension of a material, represents an inevitable type of scattering.

- *Phonon/phonon scattering*

This scattering occurs because during heat transfer by conduction, several frequencies or normal modes of vibration are present in the material.[2] These different waves can interact and merge producing a new wave that can have a flipped direction respect to the starting wave. This scattering is also known as Umklapp scattering due to the German word for flipped.

Amorphous materials, including polymers, can be thermally compared to a crystalline material with lots of defects. Therefore, polymers possess a low phonon mean free path. Phonon mean free path is an important parameter to define the λ of a material. An estimation of the thermal conductivity of solids can be obtained by Debye model [3, 4] (2):

$$\lambda = \frac{C_p \cdot v \cdot l}{3V} \tag{2}$$

where λ is the thermal conductivity (W m^{-1} K^{-1}), C_p is the specific heat capacity (J K^{-1}), υ is the speed of sound (m s^{-1}), λ the length of the phonon mean free path (m) and V the volume of the sample (m^3). This simple mathematical model can explain the poor thermal conductivity (0,1 - 0,5 W m^{-1} K^{-1}) of polymers just considering the phonon mean free path. Due to their advantageous features, increasing the λ of polymers is becoming an arising scientific challenge for novel purposes. Thermal conductive polymers have been produced by maximizing the presence of strong intermolecular bonds connecting the polymer backbones replacing weak Van der Waals interactions. [1, 5] However, to design and fabricate polymeric materials with much higher λ values, production of composite enclosing thermally conductive fillers is mandatory. In this context, the models to predict thermal conductivity of polymer composites are generally complex and equation try to relate the λ of the final composites with that of the polymer matrix and of the filler, as well as to their relative volumetric fractions. Maxwell–Eucken and Bruggerman models [6, 7] are the simplest models and provide good agreements with experimental data only when spherical filler are used and interfacial scattering at the interface filler/matrix is negligible. [8] In fact, the interface plays a key role in determining the effective λ value of polymer composites. It can be assumed that, though filler particles are surrounded by polymer chains in a composite, only smaller parts of those chains are readily in contact with the fillers.

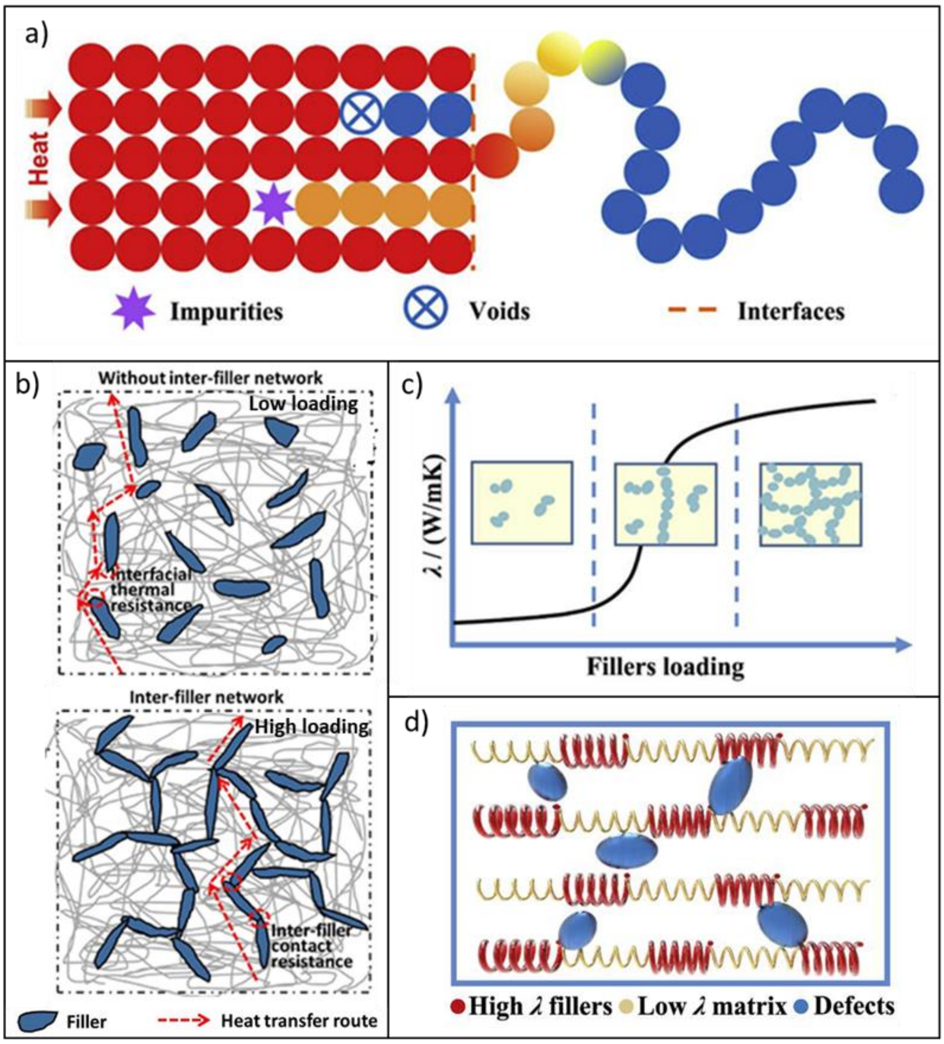

Figure 1.1 - a) Mechanism of heat transport in polymer composites; b) generation of thermally conductive pathways in polymer composites as a function of filler loading; schematic pictures of c) percolation and d) thermoelastic coefficient theories for describing thermal conductivity in polymer composites. [9]

This situation leads to large phonon scattering and, consequently, thermal resistance at the interface (Fig. 1.1a). [8, 9] Several endeavours have been recently made in order to consider the interfacial thermal resistance and the influence of fillers with different morphological features (e.g. aligned continuous fibres, layered materials, and inhomogeneously and misoriented ellipsoidal particles), offering the possibility to retrieve more accurately the λ of the composites. Assimilating phonons transfer mechanism through the interface to the behaviour of acoustic waves, acoustic mismatch (AMM) and diffuse mismatch (DMM) models have been conventionally exploited for calculating the thermal boundary conductance of interfaces. [7] In AMM, heat diffusion coefficient and, in turn, the interfacial thermal resistance will depend on the density of the materials in contact and on the group velocity of the longitudinal phonons in the two media. However, this model works perfectly only at low temperatures (< 15K) and does not consider the phonon scattering at the interfaces, which is instead examined by the diffuse mismatch model (DMM). In DMM scattering at the interfaces are introduced by assuming that at the interface phonons lose their original state and scatter diffusively and elastically in the two components. DMM model works well at higher temperature compared to AMM but overestimates the interfacial thermal resistance when the tow media have large mismatch between phonon's state density and inelastic phonon scattering is not considered. [1, 7, 10]

In addition to these theories, several other models have been proposed for explaining thermal conduction in polymer composites, such thermal conduction path, thermal percolation and thermoelastic coefficient models (Fig. 1.1b-d). [9] In the thermal conduction path theory [9], the heat transfer within the composite is granted by the generation of a continuous conductive network of thermally conductive filler. When the filler loading is low, isolated filler particles or aggregates surrounded by polymer matrix with low *λ* value, can be observed, with a negligible shift of the *λ* value of the composite. Increasing the filler volume fraction, the formation of thermally occur and, consequently, an effective thermal transport can be achieved (Fig. 1.1b). Describing the thermal transport in polymer composites referring to a percolation theory is still controversial (Fig. 1.1c). In fact, though high filler volume fractions may provide interconnected clusters inside the polymer matrix and an increase of the λ, no sharp changes of its value as a function of the filler loadings can be generally detected, hindering the possibility to define a "thermal percolation threshold". This effect may be reasonably correlated to the difference in the vibrational modes of the filler and the matrix, which make phonon scattering severe and prevents the heat transfer. Hence, though some studies report the occurrence of percolation phenomena for composites enclosing fillers with particularly high λ values, it remains an open issue to determine the relative contribution of thermal transport occurring via the filler network or via the polymer matrix. [7, 11] More interesting is the model based on thermoelastic coefficient theory, which relate the thermal conductivity to the thermoelastic coefficient of phonon propagation. The model treats λ of the composite as a macroscopic property that will depend on the intrinsic λ of the composite components, which are closely in contact and share interfaces in the composite (Fig. 1.1d). Like the interference phenomenon that undergo the vibration and the waves at the interfaces between two phases with different elastic coefficient, the phonon will also scatter and hinder the thermal conduction. According to this model, λ will gradually grow with the loading of the filler without a sharp increase in accordance with the combined enhancement mechanism of the thermoelastic coefficients of the materials.[1, 7, 12, 13]

Factors affecting the thermal transport

The above-described theories and many laboratory practices point out that the effective thermal conductivity of a polymer composite is a function of several factors, i.e. the λ of the constituents the filler volume fraction, their particle shape and size, the particle dispersion, and their surface functionalization (Fig.1.2).

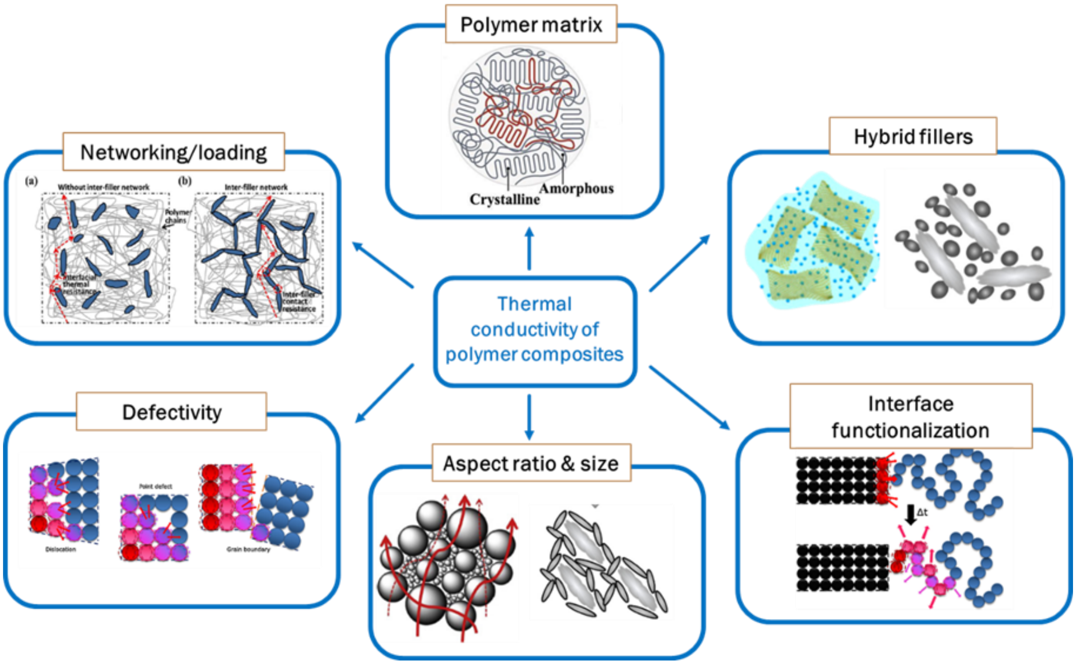

Figure 1.2 – Parameters influencing the thermal conductivity in polymer nanocomposites. [14]

Polymeric matrix represents the main component of a composite; therefore, it strongly affects the thermal conductivity of the composite. Polymers due to their complex microstructure that includes the presence of several interfaces and defects and due to the anharmonic vibrations of the polymer chains [15–18] own low thermal conductivity. It is anyway possible to increase λ of these material by introduction of small molecule that coordinates the polymer chain or by introduction of thermal conductive fillers. Chaudhry et al. [19] for example review the thermal conductivity of two polyolefins finding that thermal conductivity depends on the crystallinity, chain alignment and draw ratio. Moreover, combining those strategies with incorporation of conductive nanofillers, a new class of polymer nanocomposites with remarkable thermal conductivity and mechanical properties can be produced. On the side of the filler, high loadings are generally required to form thermally conductive pathways and to achieve high λ, inevitably depressing the mechanical and processing performances of the composite and raising their fabrication costs. [6, 20] Furthermore, a clear percolation threshold in thermally conductive composites is hard to define, even if some studies report λ values firstly increasing and then decreasing upon a determined fillers volume fraction is reached, claiming the occurrence of filler agglomeration phenomena which destroy the thermal conduction paths. [21, 22] Filler size is also critical for tuning the thermal conductivity of polymer composites. Large fillers provide lower filler/polymer interface, thus suppressing the interfacial thermal resistance and increasing λ [23–27] However, practical observation reveal that this behaviour is not always true. In fact, when the filler size is in the nanometric range, an increase of λ could be also observed. For example, the melting point of nanometallic particles is generally significantly lower than that in their bulk state; this effect may result in an easier sintering of the nanoparticles during polymer curing process with the formation of heat conductive network. Hence, besides the size, the chemical nature and the balance between the filler ability to form particle chains and reduction of phonon scattering at the surface have to be considered. Filler polydispersity can promote the assembly of thermal conductive pathways, since small particles may form conductive bridge between large particles. [28] This is also the case of the so-called *"hybrid fillers"*, i.e. the combination of thermally conductive fillers with different size, shape and chemical nature (see Section 1.4), which have been demonstrated to impart better dispersion and effective thermal conduction paths in the polymer matrix. [29–31] Filler morphology represents another key parameter, since it could aid to increase the thermal conductive pathways, while reducing scattering at the interface, simultaneously. 1D and 2D materials with high aspect ratio have been extensively exploited to increase the λ of composites materials due to their ability to form thermal conductive pathways at low filler loadings with respect to 3D filler. High aspect ratio fillers are generally nanometric only in one direction, allowing to reduce phonon scattering at the interfaces between filler and matrix and consequently to obtain higher λ. [11, 32] On the other hand, this kind of filler, due to their shape, provide anisotropic thermal conductivity, which is dependent on the filler orientation in the matrix. This depicts a delicate point, since peculiar properties can be hindered or enhanced as a function of filler alignment, upon composite processing. Therefore, the use of these filler requires a fine control of the processing route. The interfacial thermal resistance has a leading role in determining the thermal transport in polymer composites. As already mentioned, interfacial resistance can originate generally from the mismatch in the surface conditions of the two phases in contact (i.e. thermal contact resistance) or from the difference in the phonon spectra between the filler and the polymer matrix [33] Filler surface functionalization exploiting surfactants [34], silane coupling agents [35–53], grafting of functional polymers [54–57], or by generating core-shell structures [58–71] can be effective strategies to attain a significant reduction of the thermal resistance at the interface. These approaches have the common effect of improving the adhesion between filler and polymer and reducing the interfacial phonons scattering. However, surface modification may also induce the generation of defectivity, which has a detrimental influence on the phonon transport. In fact, the presence of point (vacancy and interstitial atoms), line (dislocations), surface (grain boundary and phase interfaces) and body (cavities and bubbles) defects result in phonon scattering phenomena [72–77], which may impact on the thermal transport in the composite. In summary, the λ of a composite is affected by many factors. The understanding of such factors may help to find the composition and conditions to design effective thermal conductive composites. This challenge results to be more complex when increase of λ has to deal with other functional properties (i.e. mechanical or electrical) typical of several common application of polymer composites, like tires. These aspects will be described and recalled in the next sections referring to the filler systems utilized for the development of thermally conductive rubber compounds, with specific insights for those applied in tires technology.

1.2 - Techniques for measuring thermal conductivity in polymer composites

Figure 1.3 shows some of the methods currently available for the determination of thermal conductivity. They can be divided into two main groups, the steady state and the transient methods.

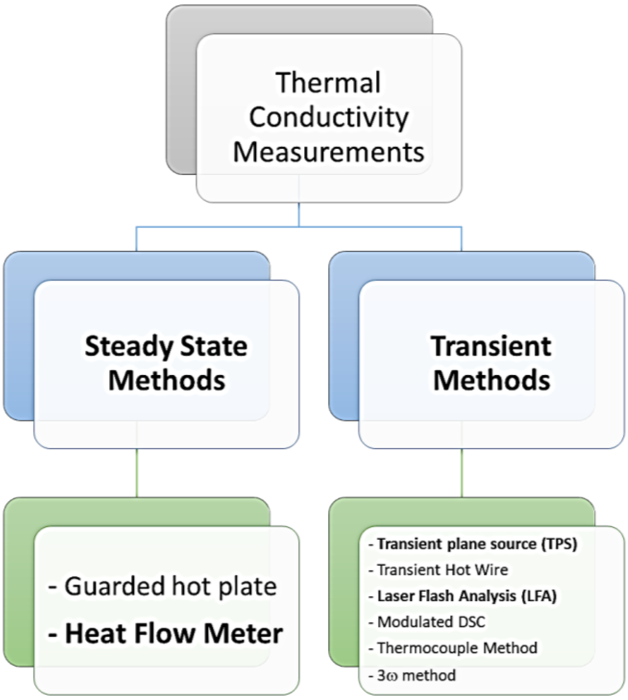

Figure 1.3 – Methods used to determine thermal conductivity

The steady state methods measure the λ by direct use of Fourier law (3), by measuring the difference in temperature (ΔT) when the heat flow (q) through the thickness (L) is in a steady state condition. [78]

$$\lambda = \frac{q \cdot L}{A \cdot \Delta T} \tag{3}$$

These methods result to be the best in determining the λ of low thermal conductive and composites materials, moreover the measure is made in one directional heat flow over a larger area which reduces the error on samples with anisotropic thermal conductivity or composites. On the contrary these techniques require large sample and present other drawback, in particular the longer time necessary to reach the steady state, the possible parasitic heat losses and the contact resistance due to the imperfect contact between the sample and temperature sensor. [79]

In transient methods the measure of λ is made by the measure of the transitional thermal flow during a pulsed heating process. This permits to reduce the measurements time and simultaneously the chances of developing convection that must be avoided especially in fluids. On the other hand, more complex mathematical model are used and particular attention must be given to the assumption that are made to calculate the λ. In this thesis heat flow meter, modified transient plane source (MTPS) and LFA methodologies have been utilized.

In heat flow meter method, sample is placed between two plates with different temperature. This temperature gradient permits to have a heat flow through the sample that is measured by transducers present in both plates. As already said this method results to be the most suitable for composite materials, anyway it is a comparative measurement method, since the thermal conductivity is determined by means of calibration of a reference sample and not directly. For this reason, particular attention must be done on the instrument calibration.

Transient plane source methods utilize a plane sensor consisted of a continuous double spiral of electrical conducting nickel placed between two layer of polyimide films that provide electrical insulation and mechanical stability to the sensor. Generally, the sensor is placed between two identical halves of the sample to be measured. During the measure the sensor is heated by Joule effect and temperature versus time is recorded. Using mathematical model, thermal conductivity, thermal diffusivity and specific heat capacity of the material can be calculated. A variation of the above-described method is the MTPS. In opposition with traditional method the MTPS sensor is included in a backing and a single sample is needed due to the use of a single-sided sensor.

LFA is a powerful technique that utilises a pulsed laser as a non-contact heating source, allowing to increase accuracy of the measures. [80] Generally a vertical setup is utilized, where on the bottom of the sample the laser furnishes heat and a detector on top detects the time-dependent temperature rise. This methodology does not measure directly λ but thermal diffusivity. Thermal diffusivity (α) measures the rate of heat transfer throughout the material and it is related with λ by the equation (4):

$$\alpha = \frac{\lambda}{\rho \cdot C_p} \tag{4}$$

where r is the density and C_p the heat capacity of the material. [81, 82] Consequently, to know the value of λ density and heat capacity must be known or measured, and this unavoidably increases the error on the obtained λ values. [83]

1.3 - Thermal dissipation in tires: many patents only few scientific papers

Tires work under dynamic service condition, in particular, it is subjected alternatively at compression and expansion motion. Due to the hysteresis properties of the rubber, energy dissipation takes places and increase of temperature inevitably occurs.[84]

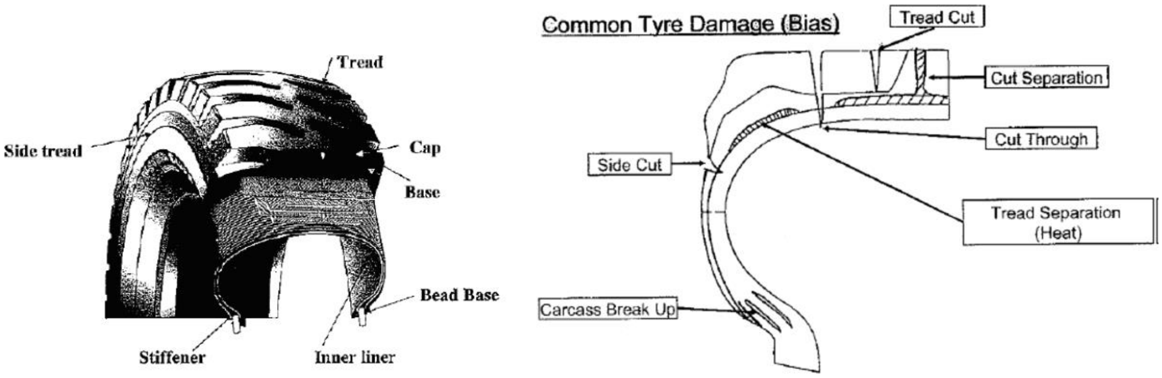

Figure 1.4 – Common tire components and heat correlated tire damage [85]

Moreover, friction of the tire with the ground and at molecular levels between rubber chains, rubber-filler and filler-filler contribute to generation of heat. But, as already mentioned, rubber possess a low thermal conductivity, thus heat building up of the tire inevitably arise. [86] This phenomenon affects the tire in various way as shown in figure 1.4. Change in temperature leads to modification in the rubber properties that makes it more vulnerable to mechanical failures [87]; moreover, it has been demonstrated that higher temperature is correlated to a higher degree of oxidative degradation. [88]

Therefore, to increase safety and durability, improving the thermal conductivity of tire represent a fundamental task, which can be accomplished by study: i) the thermal behaviour on the specific operative conditions; ii) the basic mechanisms of heat dissipation in tire under use. In addition, an in-depth investigation of the influence of rubber formulation and compounding on the heat dissipation properties is mandatory [89, 90]. Different patents [85] have been published involving heat dissipation in tires; however, these works involve the introduction of new structures or elements in the tires that lead them not suitable for the scale up of the process. Patents that modify common tire formulation to increase the λ of the composites result more attractive. Some examples are presented in the table 1.1.

Table 1.1 – Example of patented thermal conductive formulation for tire

Patent	Company	Thermal Conductive Filler	Tire Component Claimed
US8735487B2 [91]	Bridgestone Corp	**Boron Nitride (with two different sizes)**	Tread, sidewall, belt package, bead or carcass.
US9090756B2 [92]	Goodyear Tire and Rubber Co	**Nano-scale exfoliated graphene platelets**	Various tyre component
CN102250393B [93]	Beijing University of Chemical Technology	**Carbon Black and n-Alumina**	Heavy truck tire shoulder
EP1557294A1 [94]	Goodyear Tire and Rubber Co	**Two or more kind of carbon black**	Heavy tires components

As concerns on the scientific literature, very few reports deal with the tailoring of thermal conductivity of rubber composites for tire application. In the following section some examples will be given, with a more specific attention on ceramic systems like Al_2O_3, BN and ZnO, which represent promising candidates in terms of performance, availability and costs. The effects of their loading, structure, morphology, surface functionalization and combination in hybrid fillers on the generation of thermally conductive pathways in the rubber matrix, will be described.

1.4 - Filler Systems for Improving the Thermal Conductivity of Rubber Nanocomposites

Numerous types of thermally conductive nanofillers were tested in the last years: ceramic (Al_2O_3, BN, and ZnO), carbon-based fillers (graphite, graphene, carbon nanotubes), metallic. An overview of different filler will be here discussed grouping them as: carbon-based, inorganic and hybrid.

Carbon-Based Fillers

Carbon nanotubes (CNTs), carbon fibres, graphene, and graphite are examples of carbon filler extensively used to increase thermal conductivity of polymer composite. In fact, these kind of filler have high λ values (100-4000 W m^{-1} K^{-1}), though this property is generally anisotropic and strongly depends on the direction of heat propagation. [6]

If on one side this has represented an opportunity to produce highly conductive composite by filler alignment, on the other side, applications where anisotropic thermal conductivity composites are needed, like tires, are not affordable for these materials. Moreover, a consistent volume fraction in the matrix is usually required, inducing delamination or peeling phenomena which sacrifice the composite processability and finally damage the composites. Among carbon-based filler, CNTs have been employed to produce various thermally conductive rubber nanocomposites [95–98]. However, their utilization still presents issues to be solved: i) a reduction of the necessary amount for an effective thermal conduction enhancement in order to lower the cost of the final composites [99] and to retain the mechanical performance of the matrix; ii) improving dispersion and disentanglement of CNTs [100] in the matrix with consequent decrease of the high thermal resistance at the interface between the filler and the rubber; iii) using defect free and uniform CNTs. [101] It has to be mentioned also that, since CNTs are highly electrically conductive, their use in formulation for electrical insulation could be complicated. Graphene is another interesting material largely studied due to its promising properties, i.e. the zero-gap band structure, high electron mobility, and high thermal conductivity [102]. However, studies focused on the thermal conductivity of graphene–rubber composites have only recently arisen [103–108]. Homogeneous dispersion of graphene in the matrix and again interfacial compatibilization are the main issues to solve in graphene-rubber composites. A limit of graphene is also connected to its cost, due to the low yield synthesis; as a consequence, graphene derivates like graphene oxide (GO) and reduced graphene oxide (rGO) are replacing neat graphene in several applications. [109] This is not only due to the higher yield of production of these materials, but also because of the presence of polar groups at their surface which can be exploited to improve filler dispersion. [104] Graphite based fillers can be a cost-effective conductive alternative to CNTs and graphene. Due to its high theoretical intrinsic thermal conductivity (500-1000 W m^{-1} K^{-1}) and the platelet like morphology, graphite has attracted a lot of attention as conductive filler, especially in silicone rubber nanocomposites. [110] Another form of graphite is expanded graphite (EG), which is produced by intercalation of compounds that when heated release gases that separate the layers of the graphite, in fact this kind of material is also known as exfoliated graphite. This process leads to the production of a graphite with wide surface area and high aspect ratio that, when included in polymer, leads to outstanding thermal and electrical conductivity as well as good mechanical properties. [111, 112] Due to these properties, EG results to be the best choice between carbon-based materials to produce industrial-scale composites. However, a severe drawback is provided by the lubricant properties of graphite, which results in risk of peeling and delamination phenomena that, for tire applications, must be reduced. Song et al. [113] improved the dispersion and interaction between EG and natural rubber (NR) in a tire formulation by modification of the EG surface by polyacrylates (PA) composed of different ratio of two monomers (Fig. 1.5).

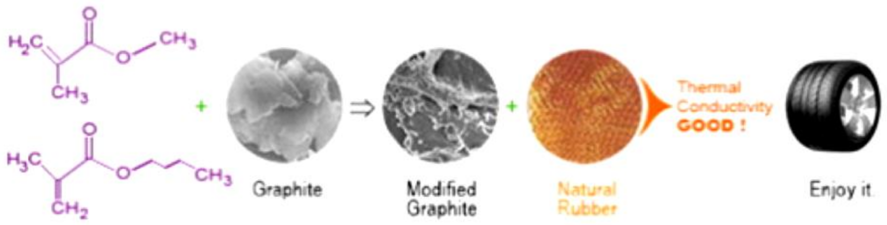

Figure 1.5 - Scheme of the graphite's modification with polyacrylates and introduction into NR and production of rubber composites for tire applications by Song et al. [108]

Authors found that λ increases when EG surface is modified with PA, and the enhancement depends on the ratio between the monomers (Fig. 1.6).

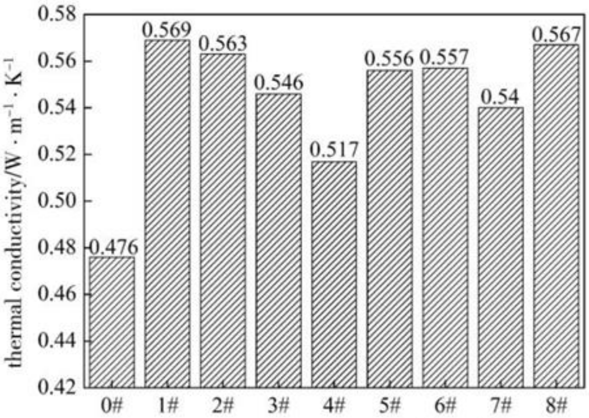

Figure 1.6 - Trend of the thermal conductivity for neat (0#) and differently surface modified (1#-8#) graphite/NR composites [113].

In summary, carbon-based fillers constitute a class of materials widely used for the thermal management in rubber nanocomposites. Because of their peculiar properties like high thermal and electrical conductivities, light weight, and generally affordable costs they result the best choice as thermal conductive filler to be introduced in tire formulation. On the other hand, the necessity to provide either filler orientation or networking inside the rubber matrix to achieve satisfactory λ enhancements, lead to a consequent risk of peeling and delamination phenomena. This kind of composite are anyway used for large scale production of non-tread components of tire.

Inorganic Based Fillers

Ceramic materials, such as alumina (Al_2O_3), boron nitride (BN), and zinc oxide (ZnO), have good thermal conductivity and their structure, particle shape and size, and surface features can be tailored to readily build up thermally conductive pathways within the rubber matrix. Moreover, they can also be utilized in combination with carbon-based thermally conductive fillers in hybrid systems, supplying a decisive upgrade in the heat transfer performance.

Al_2O_3 is the filler mainly studied in this thesis, therefore it will be extensively discussed in Section 1.5.

Boron nitride thermally and chemically resistant refractory compound that exists in various crystalline forms. The hexagonal form of BN (h-BN) displays a graphite-like structure and is sometimes called “white graphene”. [114] As graphite, h-BN can easily be exfoliated to a single or a few atomic layer sheets. Intrinsic thermal conductivity of h-BN strongly depends on the exfoliation degree and ranges from approximately 400 W m^{-1} K^{-1} for bulky from one of the highest in-plane thermal conductivity coefficients (around 2000 W m^{-1} K^{-1}), for the single layer. [115] Same issue ascribed to the carbon analogous can be translated to the h-BN. In particular, the anisotropic structure can lead to orientation and anisotropic thermal conductivity enhancement. Moreover, filler functionalization is needed in order to minimize the interfacial thermal resistance and to promote the generation of thermally conductive pathways avoiding filler aggregation. Various covalent and non-covalent functionalization have been developed. Although covalent approaches can supply strong interfacial adhesion between the filler and the matrix, with a consequent reduction in the thermal resistance and an improvement in mechanical properties, they create defects to the original BN structure. [116] Therefore, non-covalent functionalization is preferably suitable for thermal conductivity application of h-BN. An interesting study done by Yang et al. [117] propose a double functionalization of h-BN to minimize the introduction of defect but improving the interaction between the filler and the matrix. The double step functionalization consists of a first coating of h-BN platelet with polydopamine (PDA), followed by modification of the PDA with a covalently bonded silane containing a reactive methacrylate group. The filler was then introduced in NR. Authors found that PDA help to improve compatibilization of the filler with the matrix, while the presence of silane leads to the improve the dispersion and the interaction with the matrix, moreover a self-orientation of the filler in the matrix takes place. These leads of course to the formation of useful thermally conductive pathways and so to an increase of λ of the composite including non-functionalized filler. However, an exfoliation step is not included in this works, therefore high loading of h-BN is used to increase the TC, as result degradation of mechanical performance could arise. Exfoliation of the h-BN could extremely improve the λ at lower loading, as for example showed by Wu et al. [118] Anyway, the unscalable composite production methodologies and production of exfoliated h-BN, and the problem already seen for graphite lead this material still not suitable for mass tire production.

ZnO is a widely diffused semiconductor with lot of application ranging from optoelectronics to cosmetics. ZnO have also a good thermal conductivity of about 50 W m^{-1} K^{-1} but it strongly depends on the crystallinity of the ZnO. [119] ZnO is already included in rubber compound due to its use as activator for the vulcanization process and it is becoming an attractive material for tailoring the thermal management and heat dissipation of polymers, however, very few examples are present in the literature regarding its application in rubber nanocomposites as a single filler.

Generally, experiments shows that though compound enclosing submicrometric ZnO possess good mechanical performance compared to silica or carbon black, thermal conductivity is enhanced only at high filler volume fraction. [120, 121]

Optimization of the micro/nano structure of the material as well as suitable surface functionalization approaches must be developed that may enable its application in tire formulations as a multifunctional filler imparting enhanced reinforcing, vulcanizing, and thermal conductivity properties. [122]

Hybrid Fillers

Hybrid fillers are mixtures of different kinds of thermally conductive fillers or mixtures of the same material with different morphology or structure. Use of hybrid fillers permits to improve the dispersion and packing fraction, promoting the generation of thermally conductive pathways. This lower percolation threshold may facilitate the processing of composites, reduce the cost, and preserve mechanical properties of the matrix.[28] For example, silicone rubber composites enclosing ZnO with different nanoparticles size [121] or morphology [123] have been developed, where high thermal conductivity was achieved at lower filler fraction respect to the single filler, due to the generation of a 3D thermally conductive network which boosts the thermal transport throughout the whole matrix. More interesting feature can be achieved when two different fillers are introduced in the rubber, exploiting covalent or weak interaction between them. For instance, Yang et al. [124] produced a multilayer core-shell hybrid filler. Alumina was firstly surface functionalized with a non-covalent functionalization by a polyamine and subsequently graphene oxide was bonded using a peptide bond. The filler was then included in a carboxylated nitryl rubber (XNBR). The authors found that combination of Al_2O_3 and GO leads to the formation of a network made of alumina “islands” and GO “bridges” that boosts both the λ value and the mechanical properties of the composite. With the aim of increasing thermal conductive path in rubber matrix, Li et al. [125] constructed a three-dimensional network of alumina and reduced GO (rGO). The hybrid filler was obtained utilizing electrostatic self-assembly between alumina and rGO and then mixed by solution-blending with natural rubber (NR) latex (Fig. 1.7a). As expected, the resulting composite (rGO@Al_2O_3-NR) exhibited a higher λ than that of the random oriented filler nanocomposites (rGO-Al_2O_3-NR) at the same filler loading (Fig. 1.7b). According to fracture surface SEM images, this has been ascribed to the generation of a 3D interconnected structure, which enables efficient heat transfer paths, thus upgrading the thermal conductivity (Fig. 1.7c). Interestingly, λ increases (Fig. 1.7d) increasing the alumina coverage on rGO, confirming the ability of hybrid fillers to promote the heat transfer and suggesting that a simple modulation the Al_2O_3 proportions provide the chance to control the thermal management of the material. However, the production process of these composite results to be hardly scalable up to the industrial scale.

An unconventional and poorly explored way to improve the thermal transport of rubber nanocomposites consists in the modification of ceramics with polyhedral oligomeric silsesquioxanes (POSS), realizing a new class of thermally conductive hybrid filler, where the term “hybrid” implies the combination of inorganic and organic components on the same filler material. In detail, POSS are hybrid inorganic-organic molecules with $[RSiO_{1,5}]_n$ general formula and composed of a rigid core of cage-like silicon oxide and a shell of R organic groups. [126] The high number of tuneable organic functionalities on the same small unit provides a remarkable compatibility with the polymer matrix, due to the enhanced possibility of chemical or physical interactions at the polymer–POSS interface. [127] These peculiar characteristics stimulated their wide utilization in polymer nanocomposites for upgrading different properties, e.g. thermal stability, dielectric behaviour, mechanical and chemical resistance, biocompatibility, while retaining the lightweight and ductile features of the materials. [128] On the other hand, one of the main issues of POSS is their tendency to aggregate in the polymer matrix. To avoid this phenomenon, they are usually grafted to polymer chain terminations or to particle surfaces, thus acting as building blocks or providing chemical compatibilization between the filler and the polymer matrix. [129]

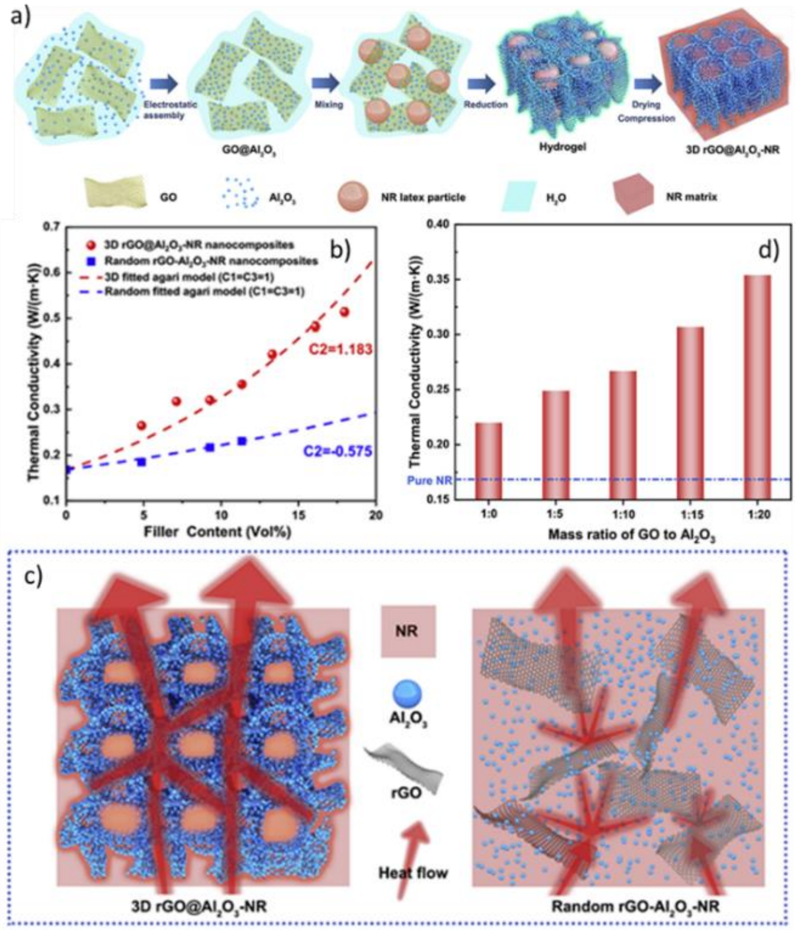

Figure 1.7 - a) Scheme of the fabrication procedure of 3D rGO@Al_2O_3-NR nanocomposites; b) Trend of thermal conductivity for 3D rGO@Al_2O_3-NR and random rGO-Al_2O_3-NR nanocomposites as function of filler loading; c) Illustration of the heat transfer mechanism in both the compounds; d) thermal conductivity of 3D rGO@Al_2O_3-NR nanocomposites vs. rGO/Al_2O_3 mass ratio. [125]

For instance, the group of Milano Bicocca has widely investigated the properties of silsesquioxanes in polymer composites and, in particular, of OctaMethacrylPOSS units in conjunction with SiO_2 (i.e. SiO_2@POSS hybrid filler) to produce rubber composites for tire application with relevant reinforcement and decreased energy loss under strain. [130] This behaviour may be exploited to enhance thermal conductivity of composites. In fact, POSS units can one hand promote the interaction between filler aggregates enhancing the number of thermal conductive paths in the matrix, and on the other hand provide rubber immobilization at the filler interface, improving the phonon transmission and reducing the scattering. In the literature thermal conductive filler modified or blended with POSS units are reported, but they mainly introduced in thermoplastic polymers like UHMWPE [131], epoxy resins [132] or bismaleimide matrix [133]. For instance, Gu et al. [131] have taken advantage of POSS properties by grafting it on SiC particles and fabricating high thermally conductive composites with ultrahigh molecular weight polyethylene (POSS-g-SiC/UHMWPE). SiC surface functionalization has been performed using NH_2-POSS and KH-560 as coupling agent, then the composites are obtained via mechanical ball milling and hot-pressing method at different filler loadings (Fig. 1.8). Thermal conductivity measurements (Fig. 1.9) reported an enhancement in comparison with original UHMWPE. However, any definite role was imputed by the authors to the nanocages, if not the ability in improving the dispersion and the compatibilization of filler in the rubbery matrix. On the other hand, these proprieties enhancements are not sufficient to justify the increase of cost of the final composite due to the addition of POSS.

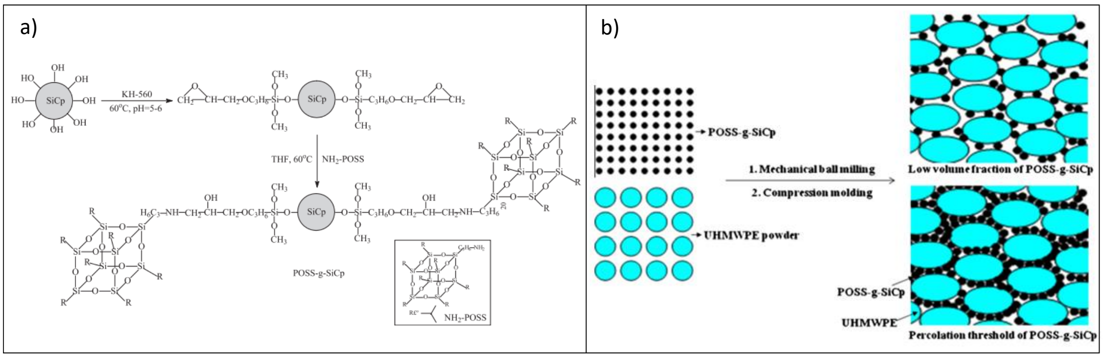

Figure 1.8 – (a) Functionalization of SiC filler and (b) POSS-g-SiC/UHMWPE composites fabrication process. [131]

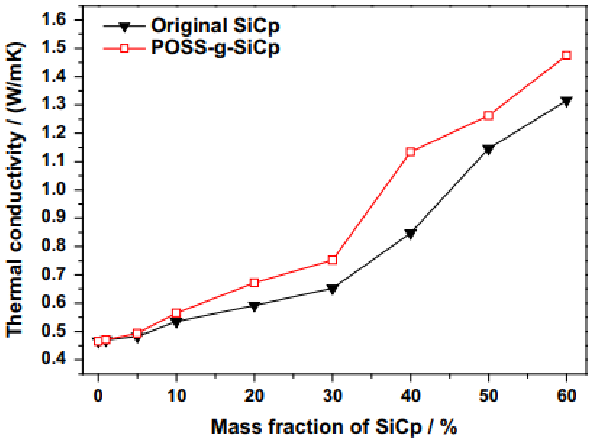

Figure 1.9 - Thermal conductivities of UHMWPE composites. [131]

More recently, Hu et al. [134] introduced octavinyl-POSS (OVPOSS) modified alumina and aluminium nitride (AlN) spherical particles in an elastomeric matrix (silicon rubber). Filler functionalization was achieved by a two-step functionalization (Fig. 1.10a). The as produced functionalized filler was then mixed with the liquid rubber precursor, casted in a mold and heated to induce the polymerization. The thermal conductivity analysis made on the composites shows that POSS functionalization effectively induces an enhancement of λ values as a function on the quantity of POSS grafted at the filler surface (Figure 1.10b, up). Authors attributed this behaviour to the decrease of the interfacial thermal resistance imparted by POSS functionalization which, simultaneously, improves the contact area and the interconnection between the filler particles of different dimensionality (Fig. 1.10b, bottom). However, this interpretation is scarcely supported by other experimental evidence in the manuscript.

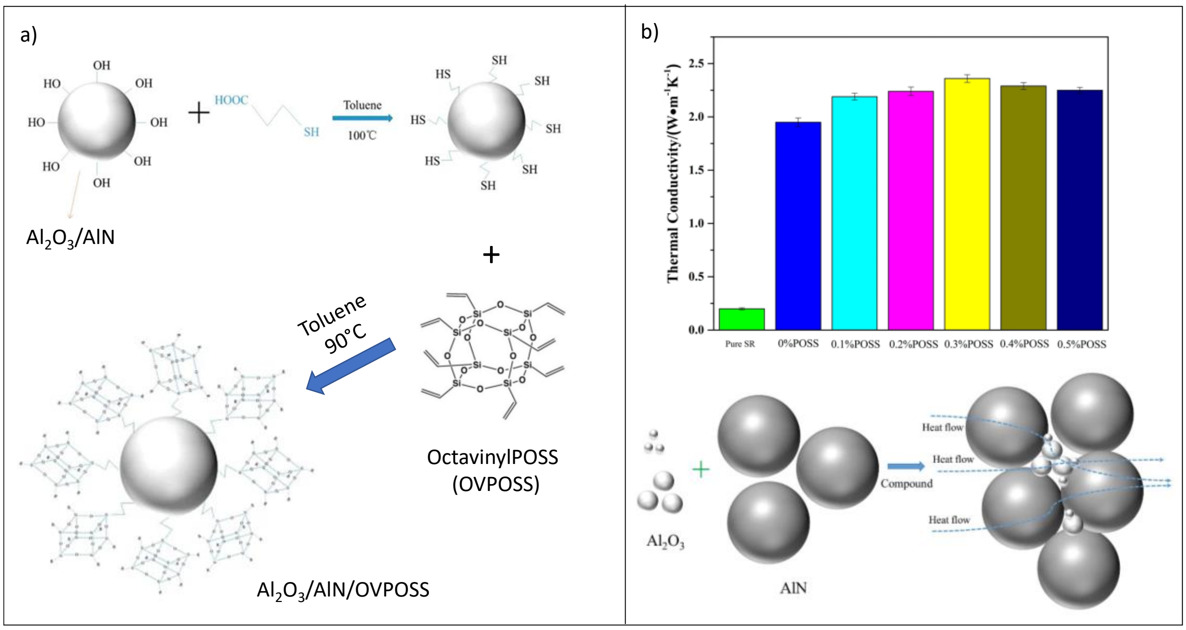

Figure 1.10 - (a) Scheme of functionalization of Al_2O_3/AlN with OVPOSS, (b) thermal conductivity analysis and scheme of heat flux in the composite. [134]

Focalizing the attention of hybrid filler for tire application, some examples can be found in literature, such as silica/carbon black [135, 136] modified layered silicates carbon/black [137]. Although their effect on the mechanical properties of SBR-based tire tread formulations has been well documented, their exploitation for attaining also improved heat dissipation properties still represents a challenge [138]. In this context, Song et al. [139] combined exfoliated montmorillonite (E-MMT) as reinforcing filler and multi walled carbon nanotubes (MWNTs) as thermal conductive filler. The E-MMT was hydroxylated to introduce polar functionalities on the surface (FE-MMT), while MWNTs was superficially covered with the cetyltrimethylammonium bromide (C-MWNTs), an amphiphilic molecule which prevents the aggregation of MWNTs and, simultaneously, improves the dispersion of the filler in the polymer matrix. Composites were produced by co-coagulation from SBR latex (S-MM, Fig. 1.11a). A remarkable improvement in both mechanical (Fig. 1.11b) and thermal conductive properties (Fig. 1.11c) of S-MM composites was observed even at low hybrid filler loadings, particularly if compared to composite obtained by simply mixing FE-MMT and C-MWNT with SBR, and with respect to the compounds enclosing neat C-MWNT and FE-MMT fillers.

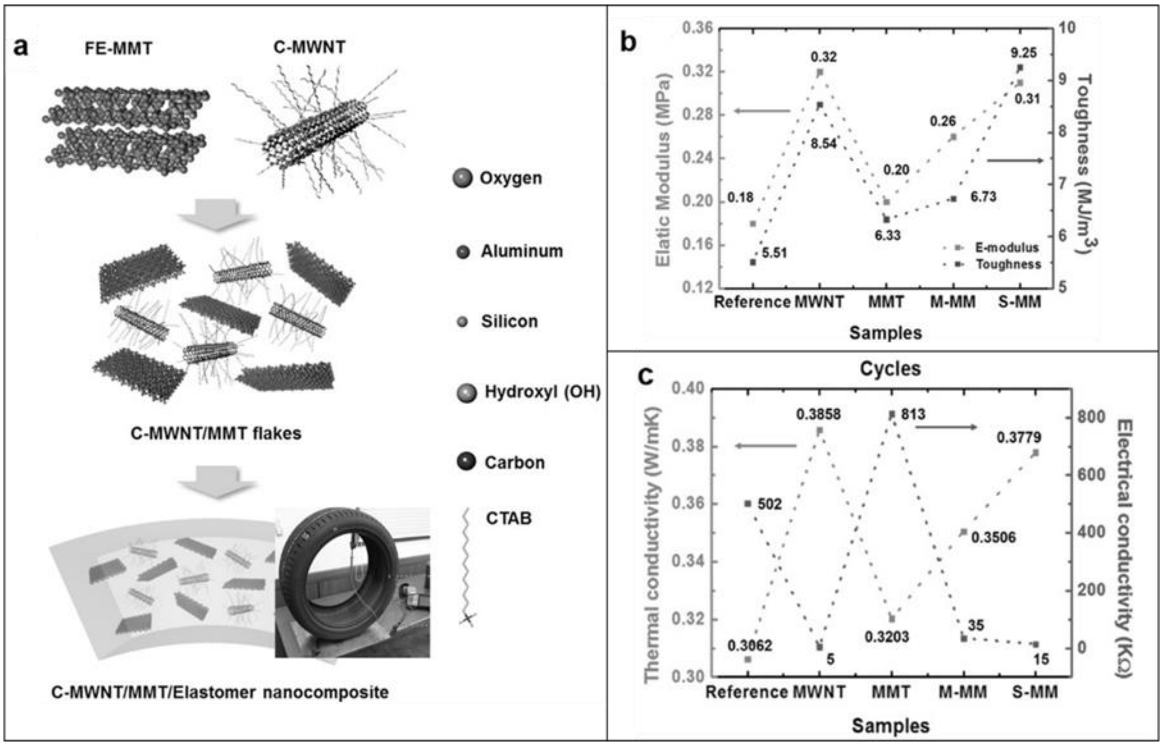

Figure 1.11 - (a) Scheme of nanocomposite filled with a hybrid filler according to Song et al.; (b) Elastic modulus and toughness of the composites enclosing neat fillers (MWNT, MMT), hybrid filler (S-MM), and mixed fillers (M-MM); (c) Thermal and electrical conductivities analysis of the nanocomposites [139]

Based on their promising properties, these materials were exploited in the formulation of tire tread of a pneumatic tire, which showed enhanced wet grip and low-rolling resistance, thus indicating the potentiality deriving from the synergistic action of clays and CNTs in the hybrid filler. The same authors also proposed the production of a hybrid filler made of graphene and silica nanoparticles where the interaction between the different filler was mediated by a fatty acid [140, 141] which were finally utilized for producing SBR nanocomposites for tires. In detail, masterbatches of SBR/graphene-silica nanohybrids (Hybrid filler/SBR) were obtained by a fast, inexpensive, scalable, and versatile latex co-coagulation approach (Fig. 1.12a). The composites displayed remarkably higher mechanical properties, thermal and electrical conductivities than similar SBR nanocomposites enclosing silica decorating carbon black, graphite and rGO, prepared by the same procedure (Fig. 1.12b). These results were attributed to the peculiar characteristics of the new hybrid filler, which providing an enhanced interfacial filler adhesion with the rubber and the generation of a continuous filler network, grants a remarkable reinforcement and an improved thermal transport through the matrix. The produced master batches were then added to silica/SBR-based tread formulations, to produce the so-called "green tires". Lower rolling resistance and highly improved grip, compared to a reference compound (control), were achieved, supporting the great potentiality of hybrid fillers for the design of tire with tailored performances (Fig. 1.12c).

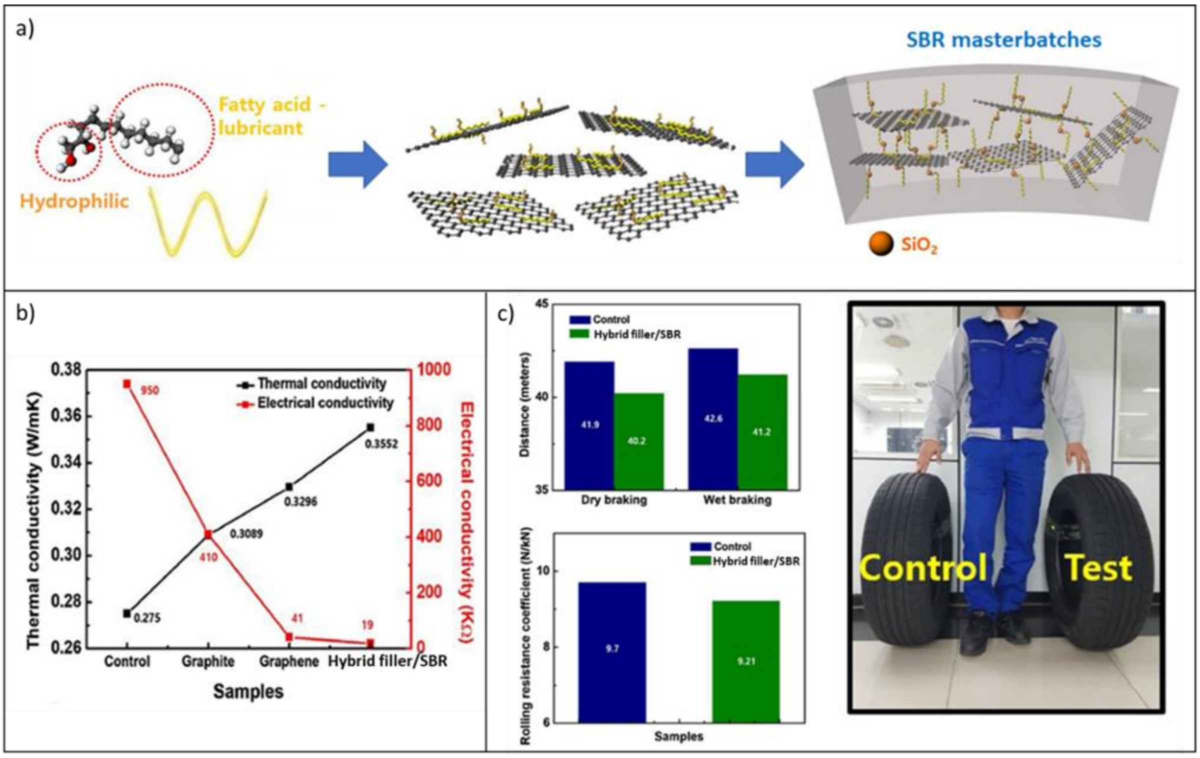

Figure 1.12 – (a) General scheme of the Hybrid/SBR nanocomposites' preparation; (b) Thermal and electrical conductivities of the SBR nanocomposites with different filler materials; (c) characterization of tread compounds (control and those made with nanocomposites enclosing hybrid fillers). [140, 141]

However, production of composite by co coagulation is not the best choice for industrial-scale production, due to the less understood dependency of this method to external factors respect to melt processing techniques. [142] Moreover, it must be considered that the composite must be separated from the wastewater. The liquid part needs to be treated, while the composite washed and dried, increasing the time and the costs of the process.

1.5 - Alumina-based filler for improving the thermal conductivity of rubber composites: an efficient and cost-effective alternative

Alumina is one of the most widely diffused metal oxide both in research and industrial field due to its peculiar properties that are strongly dependent on its crystal structure. [143] Al_2O_3 exist as amorphous material but more commonly it can be found in several metastable crystal phases (γ, δ, θ, ι, δ, κ, η) and a thermodynamically stable phase (α). Starting from different precursors which are generally different kind of aluminium oxide hydroxide, it is possible to obtain a specific crystalline phase by choosing a specific thermal treatment (Fig. 1.13). [144]

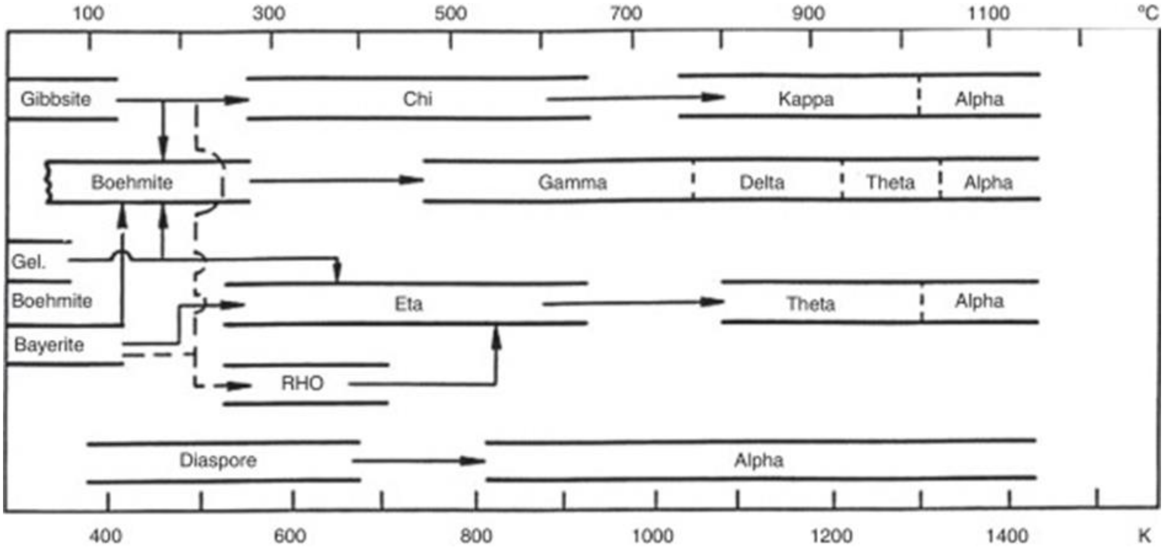

Figure 1.13 – scheme of evolution of crystalline phase of alumina starting from different precursors [145]

Moreover, it is possible to modify the properties of the alumina by simply change its morphology. Structure like spherical, irregular, fibrous and flake-like shape can be easily synthesized. Regarding the use of alumina as thermal conductive filler, it has been widely acknowledged both from industry and academia that spherical alumina has the greatest advantage in enhancing thermal conductivity compared with other fillers with different shapes. [146, 147] On of the main advantages in using spherical alumina is the improvement of composite processability. In fact, the smooth surface of alumina spheres favours the reduction of the viscosity of the system. [6] Synthesis of this kind of alumina can be produced by different approaches, the most important are homogeneous precipitation, sol-emulsification-gel, oil-drop, templated and spray method. (Fig. 1.14)

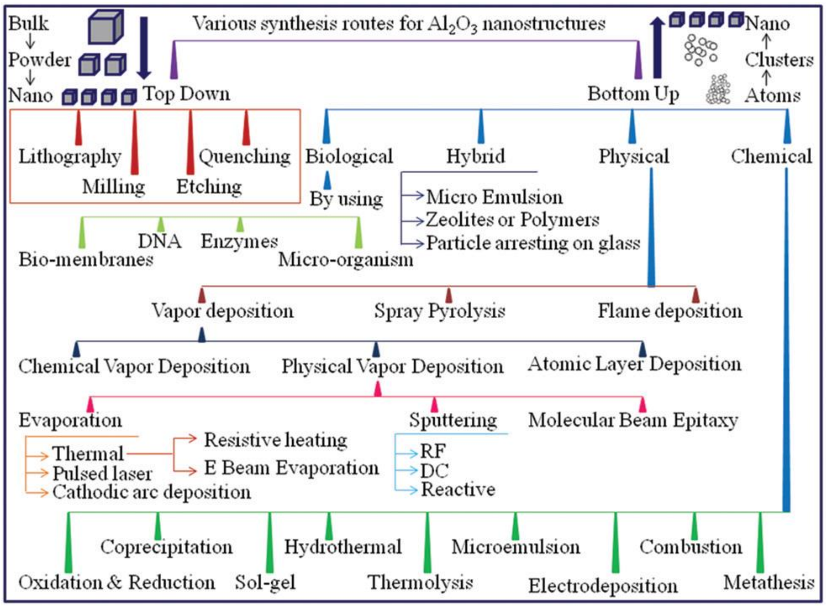

Figure 1.14 – summary of synthesis possible to produce nanometric alumina. [143]

In the homogeneous precipitation generally an aluminium source and a precipitating agent like urea or formamide are used. [148, 149] From this approach, aluminium hydroxide is firstly produced and then it is calcined in an air atmosphere to obtain spherical alumina. It is also possible to adjust the particle size of the spherical particle generally by using different aluminium sources or mixture at fixed rate of them. [149–151] Sol-emulsification-gel method permits to obtain particles with high sphericity. The Al_2O_3 is produced in a water in oil (WO) emulsion stabilized with surfactant, subsequently the as obtained powder is separated from the solvent and dried. Generally, to obtain the α-Al_2O_3, calcination is required this process may change the morphology of the particles. Oil drop method is an improved type of sol-emulsification-gel technology. In this technique the sol and gelling agent are added into organic liquid (paraffine or mineral oil). Due to difference in superficial tension, the sol forms spherical droplets in the oil and the gelation is completed in this shape. Washing, drying and calcination are then required to produce the final spherical Al_2O_3 particles. Templated methods exploit the templating proprieties of inorganic particles or micron or nanospheres of high molecular polymers. In this technique, hollow structures are synthetized by depositing the precursor on the template surface and then removing it by high temperature calcination or solvent extraction. Spray methods consist of spray drying, spray pyrolysis and spray melting. Spry drying method is the most promising and conventional method suitable for large-scale production, high-purity and high-sphericity alumina powder. In this technique, a liquid slurry is atomized into liquid droplets that arranges in spherical shape due to surface tension. The solvent is evaporated from the droplet at high temperature and calcination is then performed to remove the eventual binder and to obtain spherical particles with larger particle size. (Fig. 1.15) [152]

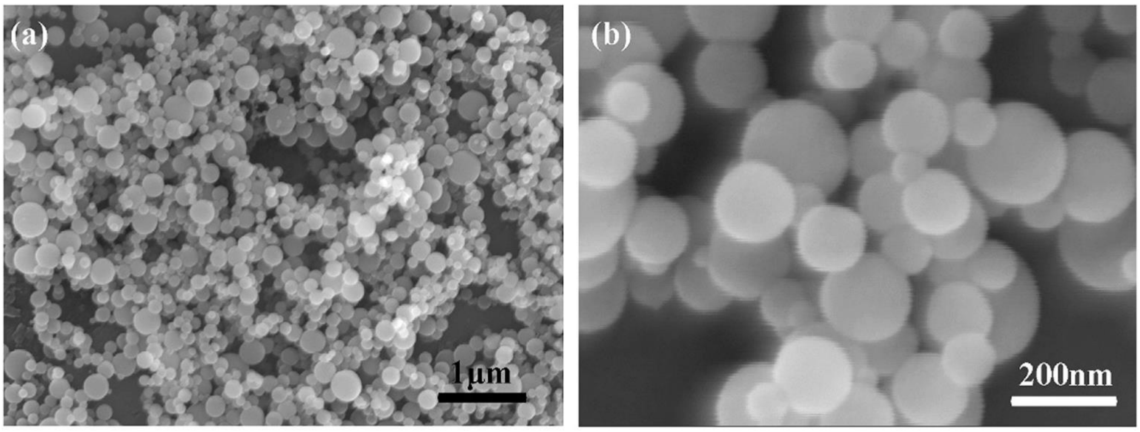

Figure 1.15 - SEM images of Al_2O_3 nanospheres prepared by thermal plasma. [152]

Of course, alumina has been widely used as filler in the field of rubber nanocomposites, endowing improved thermal conductivity as well as good mechanical and electrical properties. This material has a relatively high thermal conductivity for a ceramic, and it ranges from 38 to 42 W m^{-1} K^{-1}, depending on the crystalline phase. [28] Surely this is not the best values for ceramic fillers, however, alumina is cheap, non-toxic and can easily be obtained in various sizes and shapes, prompting its application in several rubber formulations. [153] The effect of alumina particle size on both thermal conductivity and mechanical properties of silicon rubber nanocomposites was studied by Zhou et al. [154]. In detail, a comparison between the thermal transport afforded by micrometric β-alumina with different particle size and nanometric α-alumina surface modified with 3-methacryloyloxypropyltrimethoxysilane, as compatibilizing coupling agent, was performed. The results showed silicone rubber enclosing nanometric Al_2O_3 particles at volume fraction above 50 % displays the highest λ values. This was ascribed to the high packing density attainable with these particles, which guarantee thermal transport channels in the composites. However, at such high filler concentration, the tensile strength and elongation at break of the remarkably drop, preventing a satisfactory application of the materials. Trying to slightly reduce the filler friction Ouyang et al. [155] developed a novel synthesis of α-alumina nanoparticles by the use of a high-frequency thermal plasma. These particles exhibit smooth surfaces, without edges or corners that can cause significant filler–matrix and filler–filler friction. As a result, SR nanocomposites with high alumina percolation thresholds (~50–60 v/v %) have been produced. The materials show both satisfactory mechanical performance and significant thermal conductivity (Fig. 1.16a), even at relatively low filler loadings (~20–35 $\%_{v/v}$). This work points out the importance of the dispersion and suitable compatibility between alumina fillers and the rubber matrix, for the formation of networks to promote thermal diffusion and lower the transfer of stress. (Fig. 1.16b)

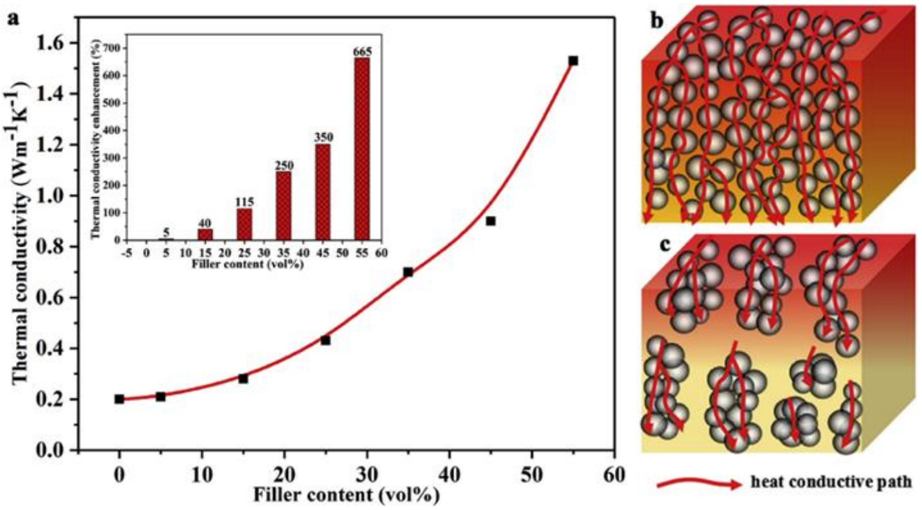

Figure 1.16 – a) Thermal conductivity of the SR composites filled with different contents of Al_2O_3 nanospheres and heat flow models of composites with good dispersion (b) and poor dispersion (c). [155]

To further lower the volume fraction of alumina, Song et al [156] produced a branched alumina particles that introduced in a SR composite constituted a thermally conductive 3D network. (Fig. 1.17) Authors demonstrated that due to the branched structure, a continuous pathway is produced in the matrix and this permits to reduce the number of the interfaces and consequently the interfacial thermal resistance. Moreover, tensile strength, elastic modulus and toughness of the composites were also improved by addiction of this filler.

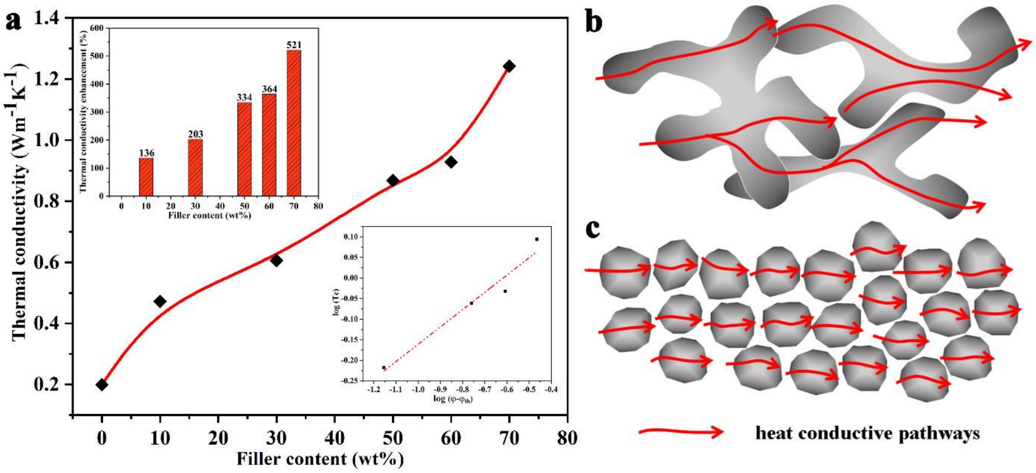

Figure 1.17 – (a) Thermal conductivity of the composites filled with different contents of Branched-Al_2O_3 and heat conductive pathways of composites with (b) Branched-Al_2O_3 and (c) common nanoparticles fillers. [156]

Very few reports in the literature focus on the exploitation of Al_2O_3 for tires applications. Wang et al. [39] utilized α-Al_2O_3 for the fabrication of thermally conductive ethylene propylene diene monomer (EPDM) nanocomposites. The authors specifically study the effects on the thermal transport and mechanical properties of the filler volume fraction; the surface functionalization with a common coupling agent utilized in tires formulation (i.e. Si69, bis-(3-triethoxy silylpropyl)-tetrasulfide, Fig. 1.18); the pre-treatment of the filler with stearic acid. The results evidenced that the incorporation of high-volume fractions of alumina can effectively upgrade the λ in EPDM nanocomposites, notwithstanding the surface chemical modification of the nanoparticles. However, the high filler loading (149 PHR) affects the tan δ values, which increases as a function of the applied strain, particularly for the naked α-Al_2O_3 nanoparticles.

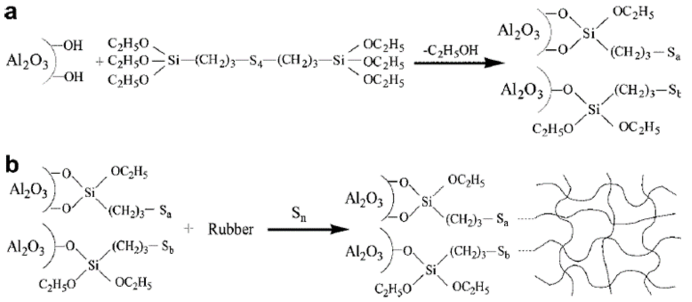

Figure 1.18 – a) In-situ surface silanization of α-Al_2O_3 nanoparticles; (b) expected reaction between functionalized α–Al_2O_3 and rubber chains during the vulcanization process. [39]

The same authors extended the use of α and γ-alumina in NR composites. [90] It was demonstrated that the different crystalline phases impart different properties to the final nanocomposite. In particular, γ-Al_2O_3 results to be impart superior mechanical feature to NR compared with the α phase. On the contrary α-Al_2O_3 results to be better in imparting superior λ. (Fig. 1.19) Authors point out that the different mechanical and λ properties depend on the difference in size of the nanoparticles. γ-Al_2O_3 possess smaller particle that leads to higher mechanical performance, but a lower intrinsic λ accompanied with worse dispersion, uncontrolled aggregation that cause lower λ enhancement, and moreover a higher filler–filler friction and thus higher heat build-up. The picture retrieved from the described studies, indicate that alumina fillers are attractive materials for improving the thermal conductivity properties of rubber composites and for large-scale applications due to abundance and low cost. Though some benefits both in the reinforcing action and thermal conductivity enhancement can be achieved by modulating the filler's crystalline phase, morphology, and surface functionalization, the reduction of the alumina loading is still a challenging point.

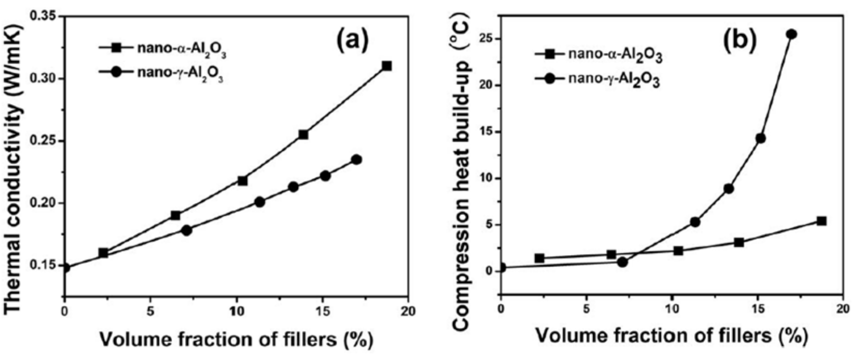

Figure 1.19 – (a) thermal conductivity and (b) heat build-up properties of NR composites filled with γ-Al_2O_3 or α-Al_2O_3 nanoparticles [90]

In summary, besides high thermally conductive carbon-based filler, ceramics and hybrid filler possess great potentialities in upgrading the thermal conductivity of rubber polymers, though some important issues still limit their utilization, especially in industrial technologies. In particular, lowering both filler loading and thermal interfacial resistance appear crucial tasks to be pursued by tailoring surfaces and, more importantly, networking in the rubber matrix. A real breakthrough may be attained by the development of suitable hybrid filler, since one can combine, for instance, enhanced cross-linking abilities with high intrinsic thermal conductivity, thus deriving significant advantages compared to the use of a single filler.

1.6 - Bibliography

[1] S. L. Shindé and J. S. Goela, Eds., *High Thermal Conductivity Materials*. New York: Springer-Verlag, 2006.

[2] J. S. Dugdale and D. K. C. MacDonald, "Lattice Thermal Conductivity," *Phys. Rev.*, vol. 98, no. 6, pp. 1751–1752, Jun. 1955.

[3] S. Zhai, P. Zhang, Y. Xian, J. Zeng, and B. Shi, "Effective thermal conductivity of polymer composites: Theoretical models and simulation models," *Int. J. Heat Mass Transf.*, vol. 117, pp. 358–374, Feb. 2018.

[4] R. W. Keyes, "High-Temperature Thermal Conductivity of Insulating Crystals: Relationship to the Melting Point," *Phys. Rev.*, vol. 115, no. 3, pp. 564–567, Aug. 1959.

[5] G.-H. Kim *et al.*, "High thermal conductivity in amorphous polymer blends by engineered interchain interactions," *Nat. Mater.*, vol. 14, no. 3, pp. 295–300, Mar. 2015.

[6] H. Chen *et al.*, "Thermal conductivity of polymer-based composites: Fundamentals and applications," *Prog. Polym. Sci.*, vol. 59, pp. 41–85, Aug. 2016.

[7] X. He and Y. Wang, "Recent Advances in the Rational Design of Thermal Conductive Polymer Composites," *Ind. Eng. Chem. Res.*, vol. 60, no. 3, pp. 1137–1154, Jan. 2021.

[8] Z. L. Wang, H. T. Mu, J. G. Liang, and D. W. Tang, "Thermal boundary resistance and temperature dependent phonon conduction in CNT array multilayer structure," *Int. J. Therm. Sci.*, vol. 74, pp. 53–62, Dec. 2013.

[9] Y. Guo, K. Ruan, X. Shi, X. Yang, and J. Gu, "Factors affecting thermal conductivities of the polymers and polymer composites: A review," *Compos. Sci. Technol.*, vol. 193, p. 108134, Jun. 2020.

[10] N. Burger, A. Laachachi, M. Ferriol, M. Lutz, V. Toniazzo, and D. Ruch, "Review of thermal conductivity in composites: Mechanisms, parameters and theory," *Prog. Polym. Sci.*, vol. 61, pp. 1–28, Oct. 2016.

[11] P. Reddy, K. Castelino, and A. Majumdar, "Diffuse mismatch model of thermal boundary conductance using exact phonon dispersion," *Appl. Phys. Lett.*, vol. 87, no. 21, p. 211908, Nov. 2005.

[12] X. Yang *et al.*, "A review on thermally conductive polymeric composites: classification, measurement, model and equations, mechanism and fabrication methods," *Adv. Compos. Hybrid Mater.*, vol. 1, no. 2, pp. 207–230, Jun. 2018.

[13] T. M. Tritt, Ed., *Thermal Conductivity*. Springer US, 2004.

[14] L. Mirizzi *et al.*, "Tailoring the Thermal Conductivity of Rubber Nanocomposites by Inorganic Systems: Opportunities and Challenges for Their Application in Tires Formulation," *Molecules*, vol. 26, no. 12, p. 3555, Jun. 2021.

[15] A. Henry and G. Chen, "Anomalous heat conduction in polyethylene chains: Theory and molecular dynamics simulations," *Phys. Rev. B*, vol. 79, no. 14, p. 144305, Apr. 2009.

[16] O. Yamamoto, "Thermal Conductivity of Cross-linked Polymers," *Polym. J.*, vol. 2, no. 4, pp. 509–517, Jul. 1971.

[17] S. Araby, L. Zhang, H.-C. Kuan, J.-B. Dai, P. Majewski, and J. Ma, "A novel approach to electrically and thermally conductive elastomers using graphene," *Polymer (Guildf).*, vol. 54, no. 14, pp. 3663–3670, Jun. 2013.

[18] J. Ma, "Effects of compatibilizing agent and in situ fibril on the morphology, interface and mechanical properties of EPDM/nylon copolymer blends," *Polymer (Guildf).*, vol. 43, no. 3, pp. 937–945, Feb. 2002.

[19] A. U. Chaudhry, A. Mabrouk, and A. Abdala, "Thermally enhanced pristine polyolefins: fundamentals, progress and prospective," *J. Mater. Res. Technol.*, vol. 9, no. 5, pp. 10796–10806, Sep. 2020.

[20] Y.-X. Fu, Z.-X. He, D.-C. Mo, and S.-S. Lu, "Thermal conductivity enhancement with different fillers for epoxy resin adhesives," *Appl. Therm. Eng.*, vol. 66, no. 1–2, pp. 493–498, May 2014.

[21] L. M. Guiney, N. D. Mansukhani, A. E. Jakus, S. G. Wallace, R. N. Shah, and M. C. Hersam, "Three-Dimensional Printing of Cytocompatible, Thermally Conductive Hexagonal Boron Nitride Nanocomposites," *Nano Lett.*, vol. 18, no. 6, pp. 3488–3493, Jun. 2018.

[22] D.-L. Zhang *et al.*, "Enhanced thermal conductivity and mechanical property through boron nitride hot string in polyvinylidene fluoride fibers by electrospinning," *Compos. Sci. Technol.*, vol. 156, pp. 1–7, Mar. 2018.

[23] S. Moradi, Y. Calventus, F. Román, and J. M. Hutchinson, "Achieving High Thermal Conductivity in Epoxy Composites: Effect of Boron Nitride Particle Size and Matrix-Filler Interface," *Polymers (Basel).*, vol. 11, no. 7, p. 1156, Jul. 2019.

[24] W. Yu, D. M. France, J. L. Routbort, and S. U. S. Choi, "Review and Comparison of Nanofluid Thermal Conductivity and Heat Transfer Enhancements," *Heat Transf. Eng.*, vol. 29, no. 5, pp. 432–460, May 2008.

[25] W. Zhou, J. Zuo, and W. Ren, "Thermal conductivity and dielectric properties of Al/PVDF composites," *Compos. Part A Appl. Sci. Manuf.*, vol. 43, no. 4, pp. 658–664, Apr. 2012.

[26] B. L. Zhu, J. Ma, J. Wu, K. C. Yung, and C. S. Xie, "Study on the properties of the epoxy-matrix composites filled with thermally conductive AlN and BN ceramic particles," *J. Appl. Polym. Sci.*, vol. 118, no. 5, pp. 2754–2764, Dec. 2010.

[27] H. Y. Ng, X. Lu, and S. K. Lau, "Thermal conductivity of boron nitride-filled thermoplastics: Effect of filler characteristics and composite processing conditions," *Polym. Compos.*, vol. 26, no. 6, pp. 778–790, Dec. 2005.

[28] X. Huang, P. Jiang, and T. Tanaka, "A review of dielectric polymer composites with high thermal conductivity," *IEEE Electr. Insul. Mag.*, vol. 27, no. 4, pp. 8–16, 2011.

[29] J. Gu, Z. Lv, X. Yang, G. Wang, and Q. Zhang, "Fabrication and Properties of Thermally Conductive Epoxy Resin Nanocomposites Filled with fGNPs/PNBRs Hybrid Fillers," *Sci. Adv. Mater.*, vol. 8, no. 5, pp. 972–979, May 2016.

[30] S. Chen, Y. Feng, M. Qin, T. Ji, and W. Feng, "Improving thermal conductivity in the through-thickness direction of carbon fibre/SiC composites by growing vertically aligned carbon nanotubes," *Carbon N. Y.*, vol. 116, pp. 84–93, May 2017.

[31] Z. Lule and J. Kim, "Thermally conductive and highly rigid polylactic acid (PLA) hybrid composite filled with surface treated alumina/nano-sized aluminum nitride," *Compos. Part A Appl. Sci. Manuf.*, vol. 124, p. 105506, Sep. 2019.

[32] S. N. Leung, "Thermally conductive polymer composites and nanocomposites: Processing-structure-property relationships," *Compos. Part B Eng.*, vol. 150, pp. 78–92, Oct. 2018.

[33] R. J. Warzoha and A. S. Fleischer, "Heat flow at

nanoparticle interfaces," *Nano Energy*, vol. 6, pp. 137–158, May 2014.

[34] K. Wattanakul, H. Manuspiya, and N. Yanumet, "The adsorption of cationic surfactants on BN surface: Its effects on the thermal conductivity and mechanical properties of BN-epoxy composite," *Colloids Surfaces A Physicochem. Eng. Asp.*, vol. 369, no. 1–3, pp. 203–210, Oct. 2010.

[35] X. Huang, T. Iizuka, P. Jiang, Y. Ohki, and T. Tanaka, "Role of interface on the thermal conductivity of highly filled dielectric epoxy/AlN composites," *J. Phys. Chem. C*, vol. 116, no. 25, pp. 13629–13639, Jun. 2012.

[36] J. Guo, P. Saha, J. Liang, M. Saha, and B. P. Grady, "Multi-walled carbon nanotubes coated by multi-layer silica for improving thermal conductivity of polymer composites," in *Journal of Thermal Analysis and Calorimetry*, 2013, vol. 113, no. 2, pp. 467–474.

[37] B. Lee and G. Dai, "Influence of interfacial modification on the thermal conductivity of polymer composites," *J. Mater. Sci.*, vol. 44, no. 18, pp. 4848–4855, Sep. 2009.

[38] W. Zhou, "Effect of coupling agents on the thermal conductivity of aluminum particle/epoxy resin composites," *J. Mater. Sci.*, vol. 46, no. 11, pp. 3883–3889, Jun. 2011.

[39] Z.-H. H. Wang, Y.-L. L. Lu, J. Liu, Z.-M. M. Dang, L.-Q. Q. Zhang, and W. Wang, "Preparation of nanoalumina/EPDM composites with good performance in thermal conductivity and mechanical properties," *Polym. Adv. Technol.*, vol. 22, no. 12, pp. 2302–2310, Dec. 2011.

[40] S. Li, S. Qi, N. Liu, and P. Cao, "Study on thermal conductive BN/novolac resin composites," *Thermochim. Acta*, vol. 523, no. 1–2, pp. 111–115, Aug. 2011.

[41] G.-W. Lee, M. Park, J. Kim, J. I. Lee, and H. G. Yoon, "Enhanced thermal conductivity of polymer composites filled with hybrid filler," *Compos. Part A Appl. Sci. Manuf.*, vol. 37, no. 5, pp. 727–734, May 2006.

[42] J. H. Yu, J. K. Duan, W. Y. Peng, L. C. Wang, P. Peng, and P. K. Jiang, "Influence of nano-ALN particles on thermal conductivity, thermal stability and cure behavior of cycloaliphatic epoxy/trimethacrylate system," *Express Polym. Lett.*, vol. 5, no. 2, pp. 132–141, Feb. 2011.

[43] C.-Y. Hsieh and S.-L. Chung, "High thermal conductivity epoxy molding compound filled with a combustion synthesized AlN powder," *J. Appl. Polym. Sci.*, vol. 102, no. 5, pp. 4734–4740, Dec. 2006.

[44] W. Peng, X. Huang, J. Yu, P. Jiang, and W. Liu, "Electrical and thermophysical properties of epoxy/aluminum nitride nanocomposites: Effects of nanoparticle surface modification," in *Composites Part A: Applied Science and Manufacturing*, 2010, vol. 41, no. 9, pp. 1201–1209.

[45] S. Ganguli, A. K. Roy, and D. P. Anderson, "Improved thermal conductivity for chemically functionalized exfoliated graphite/epoxy composites," *Carbon N. Y.*, vol. 46, no. 5, pp. 806–817, Apr. 2008.

[46] H. Hirano, J. Kadota, T. Yamashita, and Y. Agari, "Treatment of Inorganic Filler Surface by Silane-Coupling Agent: Investigation of Treatment Condition and Analysis of Bonding State of Reacted Agent," *Int. J. Chem. Mol. Nucl. Mater. Metall. Eng.*, 2012.

[47] F. Tan, X. Qiao, J. Chen, and H. Wang, "Effects of coupling agents on the properties of epoxy-based electrically conductive adhesives," *Int. J. Adhes. Adhes.*, vol. 26, no. 6, pp. 406–413, Sep. 2006.

[48] Y. Xu and D. D. L. Chung, "Increasing the thermal conductivity of boron nitride and aluminum nitride particle epoxy-matrix composites by particle surface treatments," *Compos. Interfaces*, vol. 7, no. 4, pp. 243–256, 2000.

[49] G. Yu, M. Q. Zhang, and H. M. Zeng, "Carbon-black-filled polyolefine as a positive temperature coefficient material: Effect of composition, processing, and filler treatment," *J. Appl. Polym. Sci.*, vol. 70, no. 3, pp. 559–566, Oct. 1998.

[50] K. Yang and M. Gu, "Enhanced thermal conductivity of epoxy nanocomposites filled with hybrid filler system of triethylenetetramine-functionalized multi-walled carbon nanotube/silane-modified nano-sized silicon carbide," *Compos. Part A Appl. Sci. Manuf.*, vol. 41, no. 2, pp. 215–221, Feb. 2010.

[51] K. C. Yung and H. Liem, "Enhanced thermal conductivity of boron nitride epoxy-matrix composite through multi-modal particle size mixing," *J. Appl. Polym. Sci.*, vol. 106, no. 6, pp. 3587–3591, Dec. 2007.

[52] K. Sato, A. Ijuin, and Y. Hotta, "Thermal conductivity enhancement of alumina/polyamide composites via interfacial modification," *Ceram. Int.*, vol. 41, no. 8, pp. 10314–10318, Sep. 2015.

[53] J.-P. Hong, S.-W. Yoon, T.-S. Hwang, Y.-K. Lee, S.-H. Won, and J.-D. Nam, "Interphase control of boron nitride/epoxy composites for high thermal conductivity," 2010.

[54] K. Wattanakul, H. Manuspiya, and N. Yanumet, "Effective surface treatments for enhancing the thermal conductivity of BN-filled epoxy composite," *J. Appl. Polym. Sci.*, vol. 119, no. 6, pp. 3234–3243, Mar. 2011.

[55] C. C. Teng, C. C. M. Ma, K. C. Chiou, T. M. Lee, and Y. F. Shih, "Synergetic effect of hybrid boron nitride and multi-walled carbon nanotubes on the thermal conductivity of epoxy composites," *Mater. Chem. Phys.*, vol. 126, no. 3, pp. 722–728, Apr. 2011.

[56] M. Zhang, A. Gu, G. Liang, and L. Yuan, "Preparation of high thermal conductive aluminum nitride/cyanate ester nanocomposite using a new macromolecular coupling agent," *Polym. Adv. Technol.*, vol. 23, no. 11, pp. 1503–1510, Nov. 2012.

[57] J. Yu, X. Huang, C. Wu, X. Wu, G. Wang, and P. Jiang, "Interfacial modification of boron nitride nanoplatelets for epoxy composites with improved thermal properties," *Polymer (Guildf).*, vol. 53, no. 2, pp. 471–480, Jan. 2012.

[58] C. Chen *et al.*, "High-performance epoxy/silica coated silver nanowire composites as underfill material for electronic packaging," *Compos. Sci. Technol.*, vol. 105, pp. 80–85, Dec. 2014.

[59] N. Badi and R. Mekala, "Heat-Sink Solution Through Artificial Nanodielectrics for LED Lighting Application."

[60] Y. Zhou, Y. Bai, K. Yu, Y. Kang, and H. Wang, "Excellent thermal conductivity and dielectric properties of polyimide composites filled with silica coated self-passivated aluminum fibers and nanoparticles," *Appl. Phys. Lett.*, vol. 102, no. 25, p. 252903, Jun. 2013.

[61] Q. Liang, K. S. Moon, Y. Zhang, and C. P. Wong, "Low stress and high thermal conductive underfill for Cu/low-k application," in *Proceedings - Electronic Components and Technology Conference*, 2008, pp. 1958–1962.

[62] S. Choi, K. Kim, J. Nam, and S. E. Shim, "Synthesis of silica-coated graphite by enolization of polyvinylpyrrolidone and its thermal and electrical conductivity in polymer composites," *Carbon N. Y.*, vol. 60, pp. 254–265, Aug. 2013.

[63] J. Zhao, F. Du, W. Cui, P. Zhu, X. Zhou, and X. Xie, "Effect of silica coating thickness on the thermal conductivity of polyurethane/SiO2 coated multiwalled carbon nanotube

composites," *Compos. Part A Appl. Sci. Manuf.*, vol. 58, pp. 1–6, Mar. 2014.

[64] S. Yu, B. I. Park, C. Park, S. M. Hong, T. H. Han, and C. M. Koo, "RTA-treated carbon fiber/copper core/shell hybrid for thermally conductive composites," *ACS Appl. Mater. Interfaces*, vol. 6, no. 10, pp. 7498–7503, May 2014.

[65] S. W. Kim, H. S. Choi, and K. S. Lee, "Thermal conductivity of thermally conductive composites consisting of core-shell particles with nanostructured shell layers," *Mater. Res. Bull.*, vol. 60, pp. 843–848, Dec. 2014.

[66] W. Yan *et al.*, "Polyimide nanocomposites with boron nitride-coated multi-walled carbon nanotubes for enhanced thermal conductivity and electrical insulation," *J. Mater. Chem. A*, vol. 2, no. 48, pp. 20958–20965, Dec. 2014.

[67] A. Gomathi, M. Ramya Harika, and C. N. R. Rao, "Urea route to coat inorganic nanowires, carbon fibers and nanotubes by boron nitride," *Mater. Sci. Eng. A*, vol. 476, no. 1–2, pp. 29–33, Mar. 2008.

[68] Y. Zheng and S. Wang, "Synthesis of boron nitride coatings on quartz fibers: Thickness control and mechanism research," *Appl. Surf. Sci.*, vol. 257, no. 24, pp. 10752–10757, Oct. 2011.

[69] Y. Hwang, M. Kim, and J. Kim, "Effect of Al2O3 coverage on SiC particles for electrically insulated polymer composites with high thermal conductivity," *RSC Adv.*, vol. 4, no. 33, pp. 17015–17021, Apr. 2014.

[70] H. Im and J. Kim, "Effect of homogeneous Al(OH)3 covered MWCNT addition on the thermal conductivity of Al2O3/epoxy-terminated poly(dimethylsiloxane) composites," *J. Mater. Sci.*, vol. 47, no. 16, pp. 6025–6033, Aug. 2012.

[71] H. T. Chiu, T. Sukachonmakul, M. T. Kuo, Y. H. Wang, and K. Wattanakul, "Surface modification of aluminum nitride by polysilazane and its polymer-derived amorphous silicon oxycarbide ceramic for the enhancement of thermal conductivity in silicone rubber composite," *Appl. Surf. Sci.*, vol. 292, pp. 928–936, Feb. 2014.

[72] J. Dong *et al.*, "Reducing Lattice Thermal Conductivity of MnTe by Se Alloying toward High Thermoelectric Performance," *ACS Appl. Mater. Interfaces*, vol. 11, no. 31, pp. 28221–28227, Aug. 2019.

[73] D. An *et al.*, "Low Thermal Conductivity and Optimized Thermoelectric Properties of p-Type Te-Sb2Se3: Synergistic Effect of Doping and Defect Engineering," *ACS Appl. Mater. Interfaces*, vol. 11, no. 31, pp. 27788–27797, Aug. 2019.

[74] H. Wang *et al.*, "Efficient and scalable high-quality graphene nanodot fabrication through confined lattice plane electrochemical exfoliation," *Chem. Commun.*, vol. 55, no. 41, pp. 5805–5808, May 2019.

[75] S.-H. Lo, J. He, K. Biswas, M. G. Kanatzidis, and V. P. Dravid, "Phonon Scattering and Thermal Conductivity in p-Type Nanostructured PbTe-BaTe Bulk Thermoelectric Materials," *Adv. Funct. Mater.*, vol. 22, no. 24, pp. 5175–5184, Dec. 2012.

[76] K. Watari, K. Ishizaki, and F. Tsuchiya, "Phonon scattering and thermal conduction mechanisms of sintered aluminium nitride ceramics," *J. Mater. Sci.*, vol. 28, no. 14, pp. 3709–3714, Jan. 1993.

[77] K. Takahata, Y. Iguchi, D. Tanaka, T. Itoh, and I. Terasaki, "Low thermal conductivity of the layered oxide Another example of a phonon glass and an electron crystal," *Phys. Rev. B - Condens. Matter Mater. Phys.*, vol. 61, no. 19, pp. 12551–12555, May 2000.

[78] D. Zhao, X. Qian, X. Gu, S. A. Jajja, and R. Yang, "Measurement Techniques for Thermal Conductivity and Interfacial Thermal Conductance of Bulk and Thin Film Materials," *J. Electron. Packag.*, vol. 138, no. 4, Dec. 2016.

[79] T. M. Tritt, *Thermal conductivity: theory, properties, and applications*. Springer Science & Business Media, 2005.

[80] S. Min, J. Blumm, and A. Lindemann, "A new laser flash system for measurement of the thermophysical properties," *Thermochim. Acta*, vol. 455, no. 1–2, pp. 46–49, Apr. 2007.

[81] H. Mehling and L. F. Cabeza, "Heat and cold storage with PCM," *Heat mass Transf.*, pp. 11–55, 2008.

[82] Y. A. Cengel, S. Klein, and W. Beckman, *Heat transfer: a practical approach*, vol. 141. WBC McGraw-Hill Boston, 1998.

[83] Y. Li *et al.*, "Improving the accuracy of the transient plane source method by correcting probe heat capacity and resistance influences," *Meas. Sci. Technol.*, vol. 25, no. 1, p. 015006, Jan. 2014.

[84] S. K. Srirangam, K. Anupam, A. Scarpas, and C. Kasbergen, "Development of a thermomechanical tyre–pavement interaction model," *Int. J. Pavement Eng.*, vol. 16, no. 8, pp. 721–729, Sep. 2015.

[85] N. Netscher, S. Aminossadati, and K. Hooman, "A Review of Patents in Tyre Cooling," *Recent Patents Eng.*, vol. 2, no. 2, pp. 87–94, Jun. 2008.

[86] S. L. Sokolov, "Analysis of the heat state of pneumatic tires by the finite element metho[1] S. L. Sokolov, 'Analysis of the heat state of pneumatic tires by the finite element method,' J. Mach. Manuf. Reliab., vol. 38, no. 3, pp. 310–314, Jun. 2009.d," *J. Mach. Manuf. Reliab.*, vol. 38, no. 3, pp. 310–314, Jun. 2009.

[87] P. Kainradl and G. Kaufmann, "Viscoelastic Properties of Truck Tire Compounds and the Related Heat Build-Up," *Rubber Chem. Technol.*, vol. 45, no. 1, pp. 1–9, Jan. 1972.

[88] L. R. Ocone, "Wheel assembly with tire cooling means." Google Patents, 11-Jul-1972.

[89] S. M. Danilova-Tret'yak, "On Thermophysical Properties of Rubbers and Their Components," *J. Eng. Phys. Thermophys.*, vol. 89, no. 6, pp. 1388–1393, Nov. 2016.

[90] Z. Wang, Y. Lu, J. Ding, L. Zhang, and T. W. Chan, "Preparation of nano-reinforced thermal conductive natural rubber composites," *Polym. Compos.*, vol. 37, no. 3, pp. 771–781, Mar. 2016.

[91] M. P. F. Afsari, "(12) United States Patent Date of Patent :," *Syst. Method Program. a Weigh. Scale Usinga Key Signal To Enter a Program. Mode*, vol. 1, no. 12, p. 14, 2009.

[92] T. R. Pulford, R. Cited, U. S. P. Documents, and P. P. Data, "(12) United States Patent (71) Applicant : The Goodyear Tire & Rubber," vol. 2, no. 12, 2015.

[93] 张立群, 王振华, 丁金波, and 卢咏来, "Strengthened and heat-conducting rubber for heavy truck tire shoulder," CN102250393B, 2013.

[94] L. Randolph and P. Harry, "* EP001557294A1 *," no. 19, pp. 1–14, 2005.

[95] Z. Han and A. Fina, "Thermal conductivity of carbon nanotubes and their polymer nanocomposites: A review," *Progress in Polymer Science (Oxford)*, vol. 36, no. 7. Elsevier Ltd, pp. 914–944, Jul-2011.

[96] F. Danafar and M. Kalantari, "A Review of Natural Rubber Nanocomposites Based on Carbon Nanotubes," *J. Rubber Res.*, vol. 21, no. 4, pp. 293–310, Dec. 2018.

[97] S. Ata, C. Subramaniam, A. Nishizawa, T. Yamada, and K. Hata, "Highly Thermally Conductive Yet Flexible Composite of Carbon Fiber, Carbon Nanotube, and Rubber Obtained by Decreasing the Thermal Resistivity at the Interface between Carbon Fiber and Carbon Nanotube ," *Adv. Eng. Mater.*, vol. 19, no. 2, p. 1600596, Feb. 2017.

[98] P. A. Klonos, S. N. Tegopoulos, C. S. Koutsiara, E. Kontou, P. Pissis, and A. Kyritsis, "Effects of CNTs on thermal transitions, thermal diffusivity and electrical conductivity in nanocomposites: comparison between an amorphous and a semicrystalline polymer matrix," *Soft Matter*, vol. 15, no. 8, pp. 1813–1824, Feb. 2019.

[99] S. Araby, Q. Meng, L. Zhang, I. Zaman, P. Majewski, and J. Ma, "Elastomeric composites based on carbon nanomaterials," *Nanotechnology*, vol. 26, no. 11, p. 112001, Mar. 2015.

[100] P.-C. Ma, N. A. Siddiqui, G. Marom, and J.-K. Kim, "Dispersion and functionalization of carbon nanotubes for polymer-based nanocomposites: A review," *Compos. Part A Appl. Sci. Manuf.*, vol. 41, no. 10, pp. 1345–1367, Oct. 2010.

[101] T. Souier, M. Stefancich, and M. Chiesa, "Characterization of multi-walled carbon nanotube–polymer nanocomposites by scanning spreading resistance microscopy," *Nanotechnology*, vol. 23, no. 40, p. 405704, Oct. 2012.

[102] A. K. Geim, "Graphene: Status and prospects," *Science*, vol. 324, no. 5934. American Association for the Advancement of Science, pp. 1530–1534, Jun-2009.

[103] A. Li, C. Zhang, and Y. F. Zhang, "Thermal Conductivity of Graphene-Polymer Composites: Mechanisms, Properties, and Applications," *Polymers (Basel).*, vol. 9, no. 12, p. 437, Sep. 2017.

[104] B. Yin, J. Wang, H. Jia, J. He, X. Zhang, and Z. Xu, "Enhanced mechanical properties and thermal conductivity of styrene-butadiene rubber reinforced with polyvinylpyrrolidone-modified graphene oxide," *J. Mater. Sci.*, pp. 5724–5737, 2016.

[105] H. Yang, F. Cai, Y. Luo, X. Ye, C. Zhang, and S. Wu, "The interphase and thermal conductivity of graphene oxide/butadiene-styrene-vinyl pyridine rubber composites: A combined molecular simulation and experimental study," *Compos. Sci. Technol.*, vol. 188, p. 107971, Mar. 2020.

[106] W. Liang *et al.*, "Reduced Graphene Oxide Embedded with MQ Silicone Resin Nano-Aggregates for Silicone Rubber Composites with Enhanced Thermal Conductivity and Mechanical Performance," *Polymers (Basel).*, vol. 10, no. 11, p. 1254, Nov. 2018.

[107] B. Zhong *et al.*, "Immobilization of rubber additive on graphene for high-performance rubber composites," *J. Colloid Interface Sci.*, vol. 550, pp. 190–198, Aug. 2019.

[108] S. H. Song *et al.*, "High performance graphene embedded rubber composites," *RSC Adv.*, vol. 5, no. 99, pp. 81707–81712, Sep. 2015.

[109] V. B. Mohan, K. Lau, D. Hui, and D. Bhattacharyya, "Graphene-based materials and their composites: A review on production, applications and product limitations," *Compos. Part B Eng.*, vol. 142, pp. 200–220, Jun. 2018.

[110] M. W. Ahmad, K. Soren, B. Dey, M. S. Khan, and A. Choudhury, "Synergistic reinforcement effect of 3D graphene@multi-walled carbon nanotube hybrid nanofiller in enhancing the electrical, EMI-shielding, and mechanical properties of polyethersulfone," *Int. J. Polym. Anal. Charact.*, vol. 26, no. 8, pp. 754–771, Nov. 2021.

[111] H. S. Kim, H. S. Bae, J. Yu, and S. Y. Kim, "Thermal conductivity of polymer composites with the geometrical characteristics of graphene nanoplatelets," *Sci. Rep.*, vol. 6, no. 1, p. 26825, Jun. 2016.

[112] E.-C. Cho *et al.*, "Graphene-based thermoplastic composites and their application for LED thermal management," *Carbon N. Y.*, vol. 102, pp. 66–73, Jun. 2016.

[113] J. Song, L. Ma, Y. He, H. Yan, Z. Wu, and W. Li, "Modified graphite filled natural rubber composites with good thermal conductivity," *Chinese J. Chem. Eng.*, vol. 23, no. 5, pp. 853–859, May 2015.

[114] H. Fang, S.-L. Bai, and C. P. Wong, "'White graphene' – hexagonal boron nitride based polymeric composites and their application in thermal management," *Compos. Commun.*, vol. 2, pp. 19–24, Nov. 2016.

[115] Q. Cai *et al.*, "High thermal conductivity of high-quality monolayer boron nitride and its thermal expansion," *Sci. Adv.*, vol. 5, no. 6, Jun. 2019.

[116] X. Shen, Z. Wang, Y. Wu, X. Liu, Y.-B. He, and J.-K. Kim, "Multilayer Graphene Enables Higher Efficiency in Improving Thermal Conductivities of Graphene/Epoxy Composites," *Nano Lett.*, vol. 16, no. 6, pp. 3585–3593, Jun. 2016.

[117] D. Yang *et al.*, "Mussel-inspired modification of boron nitride for natural rubber composites with high thermal conductivity and low dielectric constant," *Compos. Sci. Technol.*, vol. 177, pp. 18–25, Jun. 2019.

[118] X. Wu, H. Liu, Z. Tang, and B. Guo, "Scalable fabrication of thermally conductive elastomer/boron nitride nanosheets composites by slurry compounding," *Compos. Sci. Technol.*, vol. 123, pp. 179–186, Feb. 2016.

[119] C. I. Idumah and A. Hassan, "Recently emerging trends in thermal conductivity of polymer nanocomposites," *Rev. Chem. Eng.*, vol. 32, no. 4, Jan. 2016.

[120] Z. Wang, Y. Lu, J. Liu, Z. Dang, L. Zhang, and W. Wang, "Preparation of nano-zinc oxide/EPDM composites with both good thermal conductivity and mechanical properties," *J. Appl. Polym. Sci.*, vol. 119, no. 2, pp. 1144–1155, Jan. 2011.

[121] Q. Mu, S. Feng, and G. Diao, "Thermal conductivity of silicone rubber filled with ZnO," *Polym. Compos.*, vol. 28, no. 2, pp. 125–130, Apr. 2007.

[122] A. Susanna *et al.*, "Catalytic effect of ZnO anchored silica nanoparticles on rubber vulcanization and cross-link formation," *Eur. Polym. J.*, vol. 93, pp. 63–74, Aug. 2017.

[123] C. Li *et al.*, "Electrically insulating ZnOs/ZnOw/silicone rubber nanocomposites with enhanced thermal conductivity and mechanical properties," *J. Appl. Polym. Sci.*, vol. 135, no. 27, p. 46454, Jul. 2018.

[124] Q. Wei, D. Yang, L. Yu, Y. Ni, and L. Zhang, "Fabrication of carboxyl nitrile butadiene rubber composites with high dielectric constant and thermal conductivity using Al2O3@PCPA@GO hybrids," *Compos. Sci. Technol.*, vol. 199, p. 108344, Oct. 2020.

[125] J. Li *et al.*, "Construction of interconnected Al2O3 doped rGO network in natural rubber nanocomposites to achieve significant thermal conductivity and mechanical strength enhancement," *Compos. Sci. Technol.*, vol. 186, p. 107930, Jan. 2020.

[126] D. B. Cordes, P. D. Lickiss, and F. Rataboul, "Recent Developments in the Chemistry of Cubic Polyhedral Oligosilsesquioxanes," *Chem. Rev.*, vol. 110, no. 4, pp. 2081–2173, Apr. 2010.

[127] W. Zhang and A. H. E. Müller, "Architecture, self-assembly and properties of well-defined hybrid polymers based on polyhedral oligomeric silsequioxane (POSS),"

Prog. Polym. Sci., vol. 38, no. 8, pp. 1121–1162, Aug. 2013.

[128] K. Tanaka and Y. Chujo, “Advanced functional materials based on polyhedral oligomeric silsesquioxane (POSS),” *J. Mater. Chem.*, vol. 22, no. 5, pp. 1733–1746, 2012.

[129] Lichtenhan, Pielichowski, and Blanco, “POSS-Based Polymers,” *Polymers (Basel).*, vol. 11, no. 10, p. 1727, Oct. 2019.

[130] M. D’Arienzo *et al.*, “Hybrid SiO 2 @POSS nanofiller: a promising reinforcing system for rubber nanocomposites,” *Mater. Chem. Front.*, vol. 1, no. 7, pp. 1441–1452, 2017.

[131] J. Gu, Y. Guo, Z. Lv, W. Geng, and Q. Zhang, “Highly thermally conductive POSS-g-SiCp/UHMWPE composites with excellent dielectric properties and thermal stabilities,” *Compos. Part A Appl. Sci. Manuf.*, vol. 78, pp. 95–101, Nov. 2015.

[132] X. Huang, C. Zhi, P. Jiang, D. Golberg, Y. Bando, and T. Tanaka, “Polyhedral Oligosilsesquioxane-Modified Boron Nitride Nanotube Based Epoxy Nanocomposites: An Ideal Dielectric Material with High Thermal Conductivity,” *Adv. Funct. Mater.*, vol. 23, no. 14, pp. 1824–1831, Apr. 2013.

[133] J. Gu, C. Liang, J. Dang, W. Dong, and Q. Zhang, “Ideal dielectric thermally conductive bismaleimide nanocomposites filled with polyhedral oligomeric silsesquioxane functionalized nanosized boron nitride,” *RSC Adv.*, vol. 6, no. 42, pp. 35809–35814, 2016.

[134] Z. Hu, T. Zhao, L. Dong, and Y. Zhang, “Polyhedral Oligosilsesquioxane-Modified Alumina/Aluminum Nitride/Silicone Rubber Composites to Enhance Dielectric Properties and Thermal Conductivity,” *J. Electron. Mater.*, vol. 51, no. 5, pp. 2308–2315, May 2022.

[135] R. Scotti *et al.*, “Shape controlled spherical (0D) and rod-like (1D) silica nanoparticles in silica/styrene butadiene rubber nanocomposites: Role of the particle morphology on the filler reinforcing effect,” *Polymer (Guildf).*, vol. 55, no. 6, pp. 1497–1506, Mar. 2014.

[136] M. Galimberti, S. Agnelli, and V. Cipolletti, “11 - Hybrid filler systems in rubber nanocomposites,” in *Woodhead Publishing Series in Composites Science and Engineering*, S. Thomas and H. J. B. T.-P. in R. N. Maria, Eds. Woodhead Publishing, 2017, pp. 349–414.

[137] B. Di Credico *et al.*, “Size-controlled self-assembly of anisotropic sepiolite fibers in rubber nanocomposites,” *Appl. Clay Sci.*, vol. 152, pp. 51–64, Feb. 2018.

[138] M. Shiva, S. S. Akhtari, and M. Shayesteh, “Effect of mineral fillers on physico-mechanical properties and heat conductivity of carbon black-filled SBR/butadiene rubber composite,” *Iran. Polym. J. (English Ed.*, vol. 29, no. 11, pp. 957–974, Nov. 2020.

[139] S. H. Song, “Synergistic Effect of Clay Platelets and Carbon Nanotubes in Styrene-Butadiene Rubber Nanocomposites,” *Macromol. Chem. Phys.*, vol. 217, no. 23, pp. 2617–2625, Dec. 2016.

[140] J. G. Seo, C. K. Lee, D. Lee, and S. H. Song, “High-performance tires based on graphene coated with Zn-free coupling agents,” *J. Ind. Eng. Chem.*, vol. 66, pp. 78–85, Oct. 2018.

[141] S. H. Song, “Graphene-Silica Hybrids Fillers for Multifunctional Solution Styrene Butadiene Rubber,” *J. Polym. Res.*, vol. 27, no. 6, p. 155, Jun. 2020.

[142] *Polymer Science and Engineering*. Washington, D.C.: National Academies Press, 1994.

[143] J. Gangwar, B. K. Gupta, S. K. Tripathi, and A. K. Srivastava, “Phase dependent thermal and spectroscopic responses of Al 2 O 3 nanostructures with different morphogenesis,” *Nanoscale*, vol. 7, no. 32, pp. 13313–13344, 2015.

[144] K. Wefers and C. Misra, “Oxides and hydroxides of aluminum. alcoa technical paper No. 19,” *Alum. Co. Am*, vol. 92, 1987.

[145] S. Lamouri *et al.*, “Control of the γ-alumina to α-alumina phase transformation for an optimized alumina densification,” *Boletín la Soc. Española Cerámica y Vidr.*, vol. 56, no. 2, pp. 47–54, Mar. 2017.

[146] J. P. Cheng *et al.*, “Influence of phase and morphology on thermal conductivity of alumina particle/silicone rubber composites,” *Appl. Phys. A*, vol. 117, no. 4, pp. 1985–1992, Dec. 2014.

[147] H. Yeo *et al.*, “Characteristic correlation between liquid crystalline epoxy and alumina filler on thermal conducting properties,” *Compos. Sci. Technol.*, vol. 141, pp. 99–105, Mar. 2017.

[148] H. S. Roh *et al.*, “Size-controlled synthesis of monodispersed mesoporous α-Alumina spheres by a template-free forced hydrolysis method,” *Dalt. Trans.*, vol. 40, no. 26, pp. 6901–6905, 2011.

[149] H. Yang, Y. Yan, and Z. Hu, “Synthesis of spherical α - alumina and its effect on the performances of phase change materials based on sodium acetate trihydrate,” *Mater. Res. Express*, vol. 6, no. 11, p. 115111, Oct. 2019.

[150] J. Wang, L. Ge, Z. Li, L. Li, Q. Guo, and J. Li, “Facile size-controlled synthesis of well-dispersed spherical amorphous alumina nanoparticles via homogeneous precipitation,” *Ceram. Int.*, vol. 42, no. 7, pp. 8545–8551, May 2016.

[151] J. Wang, D. Zhao, G. Zhou, C. Zhang, P. Zhang, and X. Hou, “Synthesis of nano-sized γ-Al2O3 with controllable size by simple homogeneous precipitation method,” *Mater. Lett.*, vol. 279, p. 128476, Nov. 2020.

[152] Z. Sun, B. Li, P. Hu, F. Ding, and F. Yuan, “Alumina ceramics with uniform grains prepared from Al2O3 nanospheres,” *J. Alloys Compd.*, vol. 688, pp. 933–938, 2016.

[153] A. K. Srivastava, *Oxide nanostructures: growth, microstructures, and properties*. CRC Press, 2014.

[154] W. Zhou, S. Qi, C. Tu, H. Zhao, C. Wang, and J. Kou, “Effect of the particle size of Al2O3 on the properties of filled heat-conductive silicone rubber,” *J. Appl. Polym. Sci.*, vol. 104, no. 2, pp. 1312–1318, Apr. 2007.

[155] Y. Ouyang, X. Li, F. Ding, L. Bai, and F. Yuan, “Simultaneously enhance thermal conductive property and mechanical properties of silicon rubber composites by introducing ultrafine Al2O3 nanospheres prepared via thermal plasma,” *Compos. Sci. Technol.*, vol. 190, p. 108019, Apr. 2020.

[156] J. Song, L. Wu, and Y. Zhang, “Thermal conductivity enhancement of alumina/silicone rubber composites through constructing a thermally conductive 3D framework,” *Polym. Bull.*, vol. 77, no. 4, pp. 2139–2153, Apr. 2020.

Chapter 2 - $SiO_2@Al_2O_3$ filler in SBR/BR matrix

2.1 - Introduction

As already described in the Introduction of the thesis, tires must satisfy fundamental safety, performance and environmental footprint features established by law. As an example, the stability at high velocity, loudness, wet grip and rolling resistance of tires are regulated by European legislations. [1] These characteristics strongly depend on compounds mechanical properties, and a correlation between a specific mechanical behaviour and the resulting macroscopic properties can be detected for most of them. For instance, the dynamical mechanical properties of tread compound at 0 °C and 70 °C can be correlated to wet grip performance and rolling resistance, respectively. [2] Thus, severe requirements on mechanical properties must be satisfied when nanocomposites for tire production are formulated, which essentially rely on the characteristics of rubber polymers and, more importantly, to the morphological and surface features of reinforcing filler. Besides improving mechanical properties, the choice of filler in rubber formulations for tires has to comply with other important characteristics of this peculiar application, such as the thermal dissipation, which could improve personal safety issues and for the durability of the material. In this context, commonly employed SiO_2 NPs cannot be satisfactory candidates, due to their low intrinsic thermal conductivity (~3.5 $W\ m^{-1}\ K^{-1}$), which is insufficient for an effective thermal management. Thus, ceramics or carbon-based phases having high λ values could be additionally utilized. As widely reported in Chapter 1, several alternatives can be considered, though for the specific application in tires a careful tradeoff among several parameters as performance, wide availability, low costs, stability and negligible toxicity, has to be pursued. The introduction of alumina filler in rubber composites for tires appear a valid option. The promising thermal transport features imparted by addition of thermally conductive Al_2O_3 particles to several different rubber matrices have been discussed in Chapter 1. However, very few example deal with tire applications and, usually, high loadings (> 20-30 v/v %) are required in order to obtain a significant increase of the heat transmission, leading to a degradation of the rubber mechanical features. Besides the concentration, the morphology and the surface features of the filler play a crucial role in deciding the final properties. In fact, the chemistry of alumina is significantly different compared to the ones of SiO_2 and silicate filler, envisaging compatibilization and segregation concerns upon incorporation in rubber matrix. As concerns on the dimensions, micro-size alumina particles were found to upgrade thermal conductivity, but not the mechanical strength. On the contrary, nano-alumina often does not significantly contribute to thermal conductivity enhancement, but it displays beneficial effects on other mechanical properties. A recent study of Vaisakh S.A. et al. [3] , reported on the beneficial effects of SiO_2/Al_2O_3 mixed filler with different size and shape on the thermal conductivity, strength, and tribology properties of epoxy composites (Fig. 2.1), envisaging a potential synergistic action among the filler. Although focused on epoxy matrix, this study resulted inspiring and prompted us to investigate the introduction of alumina particle, in conjunction with SiO_2, in elastomers exploited in tire tread formulation. In detail, the idea was to develop a novel filler where SiO_2 and Al_2O_3 NPs are not simply mixed together, but belong to the same functional structure, which combine both the reinforcement ability of silica and the thermal conductivity mainly governed by alumina.

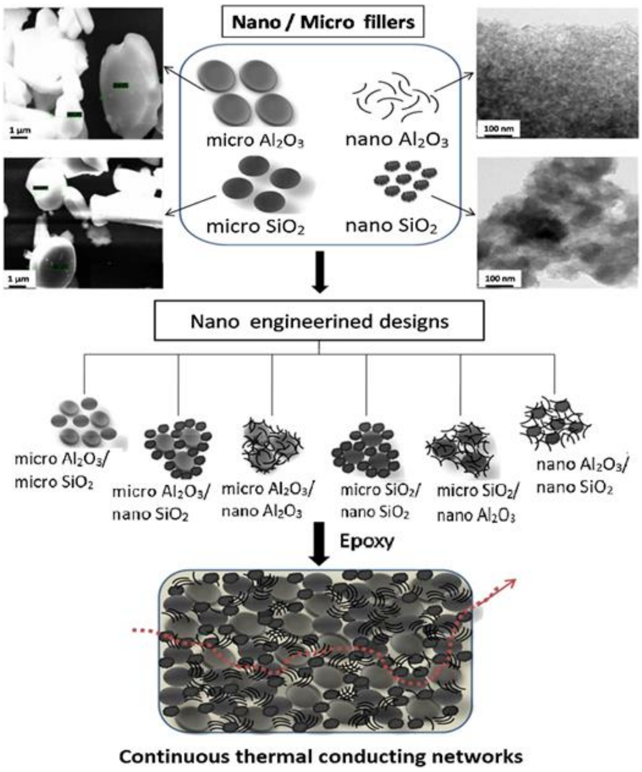

Figure 2.1 – Scheme summarizing the different mixed filler combinations utilized in epoxy composites according to [3].

To synthetise this filler, at first aluminium hydroxide was grown at the surface of silica NPs, and then converted into alumina phase by a thermal treatment ($SiO_2@Al_2O_3$). The material was then compositionally, structurally and morphologically characterized by ICP-OES, XRD, Solid State NMR and TEM analysis. $SiO_2@Al_2O_3$ NPs were used to prepare, by ex situ blending, styrene butadiene rubber (SBR) nanocomposites. The mechanical properties of SBR/$SiO_2@Al_2O_3$ nanocomposites were investigated in detail. Finally, the thermal conductivity of the composites was measured by MPTS analysis and the results connected to the morphological features of composites assessed by TEM.

2.2 - Preparation of $SiO_2@Al_2O_3$ NPs

Materials: precipitated commercial silica Zeosil® 1165 was obtained by Solvay, Aluminium Nitrate nonohydrate was acquired from Sigma Aldritch, Aluminium Sulfate exadecahydrate and Urea was acquired from Alfa Aesar.

The filler was prepared by following the synthetic route shown in figure 2.2, modifying a synthetic method present in literature for the preparation of nano alumina. [4]

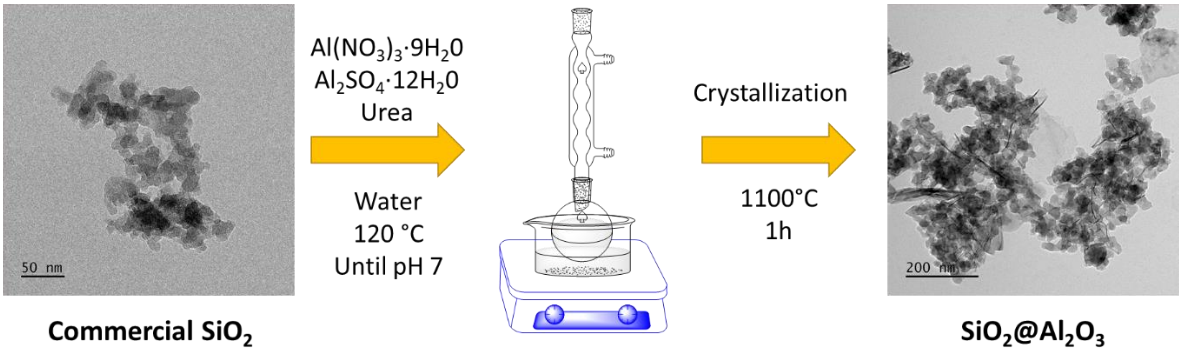

Figure 2.2 – Scheme of $SiO_2@Al_2O_3$ synthesis

In details, 4 g of the commercial silica was dispersed in 500 mL of water by sonication for 15 min. Then, in a 3 L round bottom flask 1.12 g of Al_2SO_4, 8.04 g of $Al(NO_3)_3$, and 15 g of urea were dissolved in 2 L of distilled water by magnetic stirrer. The amounts of precursors were selected in order to obtain 20 wt% on SiO_2. After dissolution, the silica suspension was added to the flask and heated at 120 °C in an oil bath for about 3h when pH reaches a value of 7. After cooling, the suspension was vacuum filtered and the obtained solid washed with water and dried at 70°C for 12 hours. Alumina crystallization was performed at 1100 °C for 1 hour in a muffle furnace.

2.3 - Structural and morphological characterization of $SiO_2@Al_2O_3$ filler

The quantification of the alumina grafted on SiO_2 NPs was evaluated by ICP-OES analysis. Due to the chemical stability of the alumina, the Al quantification was done on the filler precursor $SiO_2@Al(OH)_3$, to get the material solubilized (see appendix for the experimental conditions). The results the as produced filler contains 20 ± 3% in weight of alumina over SiO_2 NPs. The structural properties and the crystalline phases present in the filler after each reaction step were studied through XRD. At first, the behaviour of the commercial silica after the thermal treatment was assessed. As expected, SiO_2 NPs pass from an amorphous state (Fig. 2.3a, black line) to a crystalline form (Fig. 2.3a, red line) under the same thermal treatments used for alumina crystallization. However, SiO_2 crystallization is detrimental for the industrial application due to the health hazard correlated to crystalline silica. Remarkably the diffractogram of $SiO_2@Al_2O_3$ (Fig. 2.3b, blue line) does not show any peaks related to crystalline silica, and the broad reflection at about 22° of the amorphous silica is predominant in the diffractogram, suggesting that the growth of alumina prevents the silica crystallization. Besides, in the diffractogram of $SiO_2@Al_2O_3$ the peaks of the alumina γ phase are clearly present (attribution in Fig. 2.3b).

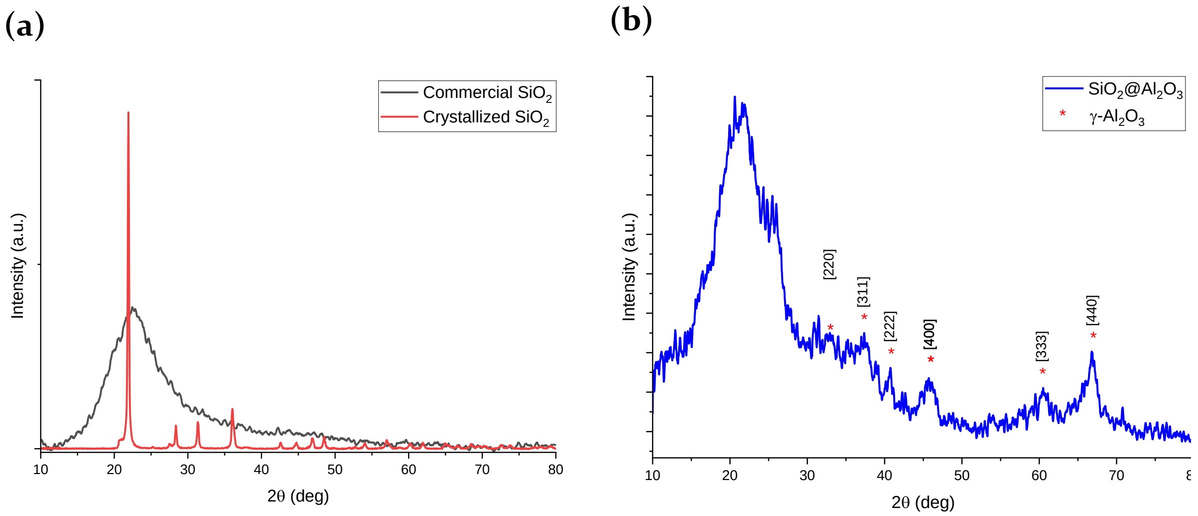

Figure 2.3 – XRD of (a) commercial SiO_2 (black line), commercial SiO_2 treated at 1100°C for 1h (red line) and (b) $SiO_2@Al_2O_3$ filler (blue line).

To study the interfacial interaction between SiO_2 and Al_2O_3 phases, ^{27}Al and ^{29}Si solid state NMR spectra were acquired (respectively Fig. 2.4 (a) and (b)). The ^{27}Al spectra of SiO_2@Al_2O_3 was further compared both to commercial alumina NPs (polydisperse size up to 200 nm, γ-phase) and alumina NPs synthetized in the same experimental conditions but in the absence of SiO_2. The ^{27}Al spectra of both pure Al_2O_3 samples result perfectly superimposable indicating the structural equivalence in terms of octahedral and tetrahedral Al sites, clearly visible at 7,7 and 59 pm, respectively (Fig. 2.4a). However, the different shape and intensity of the peak connected to the tetrahedral Al sites in SiO_2@Al_2O_3, as well as the shift to higher field, suggest the presence of a higher amount of these Al sites with a different chemical environment. In accordance with the literature [5, 6], it is possible to deconvolute the tetrahedral sites peak in two components at 62 and 50 ppm, that are respectively related to Al-O-Al (64.5%) and Al-O-Si (35.5%) bonds, possibly connected to the interaction between SiO_2 and Al_2O_3. Besides, the increase of the intensity of the tetrahedral Al sites, indicates that the Al-O-Si bonds force the Al and first Al neighbours to adopt the silica coordination mode, coherently proving the growth of Al_2O_3 on SiO_2 NPs. To further confirm the SiO_2 surface functionalization, ^{29}Si spectrum of SiO_2@Al_2O_3 was compared to that of bare commercial SiO_2 NPs (Fig. 4b). As expected, in the latter case, the signal of the typical Q^2, Q^3 and Q^4 components of silica located at -90.0 (1.8%), -100.3 (23.6%) and -110.5 (74.6%) ppm respectively, were observed. Instead, in the spectra of SiO_2@Al_2O_3, the amount of non-completely condensed units (surface units as Q^2 and Q^3) is reduced probably by the presence of alumina at the surface, which induces the formation Al-O-Si bonds, thus increasing the intensity of Q^4 signal [7, 8]. Consequently, ^{29}Si MAS spectrum corroborates the successful surface functionalization of the silica.

The morphology of the novel filler material has been investigated by TEM. From the images, it can be noticed that the commercial SiO_2 powder is constituted of aggregates with a dimension up to 200 nm of composed by small pseudo spherical nanometric particles with an average of size 20 nm (Fig. 2.5a and a'). At higher resolution no crystalline plane are visible for bare SiO_2 in agreement with XRD. Images of SiO_2@Al_2O_3 shows the presence of Al_2O_3 sheet like species surrounding SiO_2 aggregates (Fig. 2.5b). Their morphology is in accordance with the structure of boehmite precursor, that retains its morphology after crystallization. [9] Besides, an increase of the dimension of the SiO_2 aggregates up to the micrometric scale is observed, possibly due to the presence of alumina nano-sheets that link together the smaller aggregates. Higher magnification on the sheet confirms the presence of an ordered Al_2O_3 structure (Fig, 2.5b').

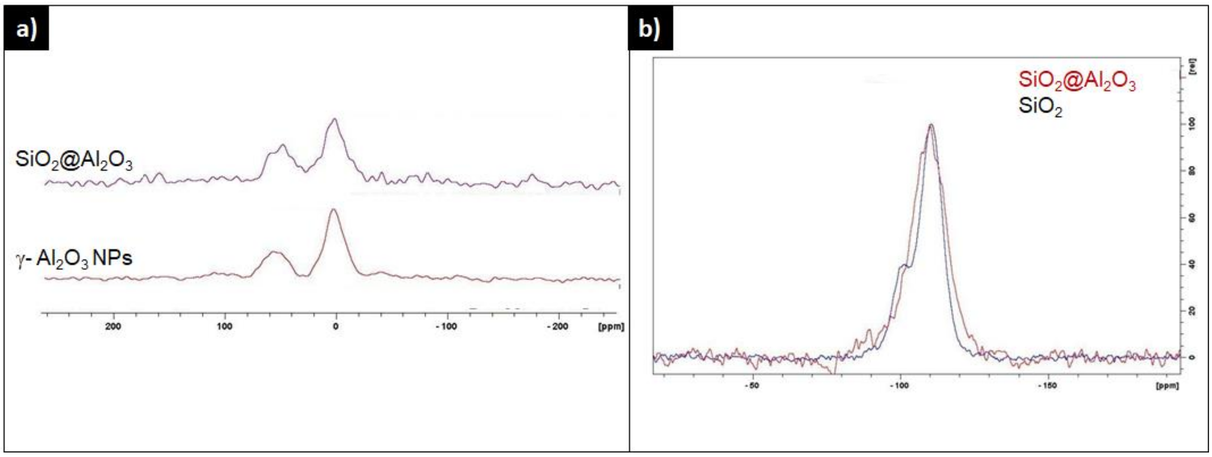

Figure 2.4 – (a) ^{27}Al Hahn-echo MAS NMR and (b) ^{29}Si MAS spectra of the commercial SiO_2 and $SiO_2@Al_2O_3$ filler

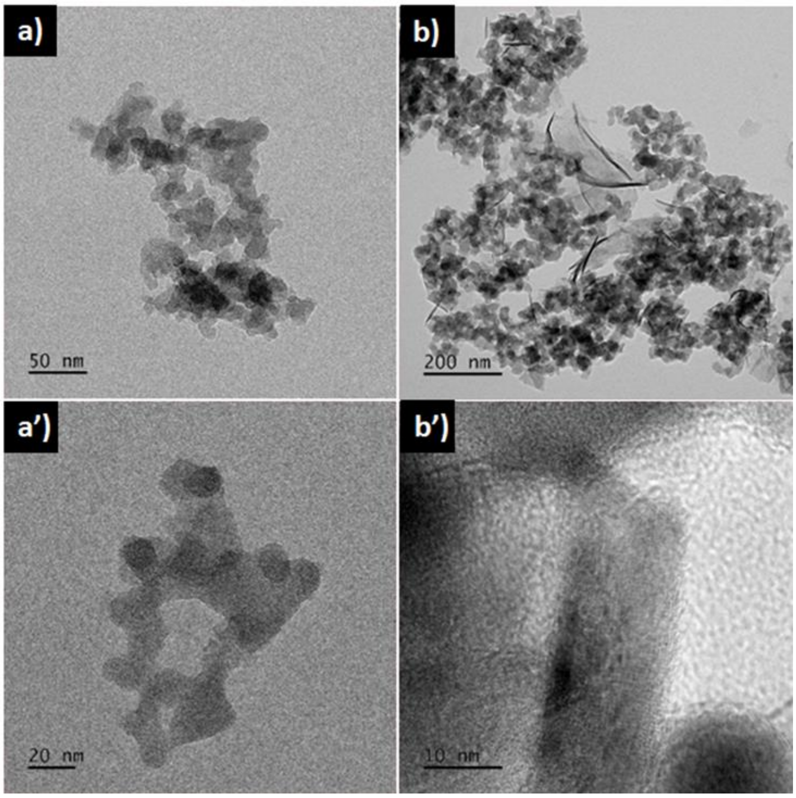

Figure 2.5 - TEM images of commercial SiO_2 (a, a') and $SiO_2@Al_2O_3$ filler (b, b')

2.4 - Preparation of SBR-BR composites

Materials: Sprintan SLR 4630 (Styrene Butadiene Rubber, SBR) supplied from Synthos Group, while Europrene Neocis BR60 (Butadiene Rubber, BR) from Versalis; bis(3-triethoxysilylpropyl)tetrasulphide (TESPT) from Aldrich; antioxidant N-(1,3-dimethylbutyl)-N-phenyl-p-phenylenediamine (6PPD) from Flexsys; stearic acid (Stearina TP8) from Undesa; N-cyclohexyl-2-benzothiazole sulfenamide (CBS) from Lanxess; sulphur from Redball Superfine; ZnO from Zincol Ossidi.

$SiO_2@Al_2O_3$ was tested as filler in a model tire compound produced by melt blending in a Brabender Plasti-Corder internal mixer (55 mL mixing chamber, 60 rpm rotor speed). The procedure consists in a first SBR and BR mastication step at 130 °C for 1 min followed by inclusion of the filler and TESPT and other 4 min mixing. Subsequently, the antioxidant 6PPD, the curing activator ZnO and stearic acid as co-activator was added and mixed for 2 min. The compound was allowed to rest for 24 hours and a second mixing was subsequently done. In this second step, the compound was masticated for 1 min and then mixed with sulphur as vulcanizing agent and CBS as curing accelerator for 2 min at low temperature (80°C) to prevent vulcanization. Compounds recipes are reported in Table 2.1. The composites will be labelled SBR-BR/SiO_2X and SBR-BR/$SiO_2@Al_2O_3$X, where X refers to the filler fraction in PHR. The vulcanization curves of the SBR-BR nanocomposites were obtained by vulcanizing rubber specimens through the rubber process analyzer (RPA, the details are reported in the Appendix) at 170 °C for a total time of 10 min with a frequency of 10 Hz. As concerns on static and compression tests, the curing was carried out utilizing a hydraulic press that worked at 170 °C and 100 bar. The vulcanization time was fixed for all the sample at 10 minutes. Two shapes of sample have been produced, square sheets of 1 mm of height and 11 cm of length for tensile tests and cylinder of 18 mm of diameter and 25 mm of height for DMA and MTPS analysis.

Table 2.1 – Recipes of the compounds produced by melt blending utilizing commercial SiO_2 or $SiO_2@Al_2O_3$ as filler

COMPONENT	PHR			
BR	30	30	30	30
SBR	70	70	70	70
Commercial SiO_2	**50**	**60**	0	0
$SiO_2@Al_2O_3$	0	0	**50**	**60**
TESPT	4	4.8	4	4.8
6PPD	2.5	2.5	2.5	2.5
ZnO	2	2	2	2
Stearic acid	1	1	1	1
CBS	3	3	3	3
Sulfur	1	1	1	1

2.5 - Characterization of the nanocomposites: mechanical analysis thermal conductivity

SBR-BR/$SiO_2@Al_2O_3$ composites have been mechanically characterized by Rubber Process Analyzer (RPA) and compression DMA. As a representative example, the curing curve of the composites containing 60 PHR of commercial SiO_2 or $SiO_2@Al_2O_3$ filler (i.e. SBR-BR/$SiO_2$60 and SBR-BR/$SiO_2@Al_2O_3$60) are shown in Fig. 2.6 (a).

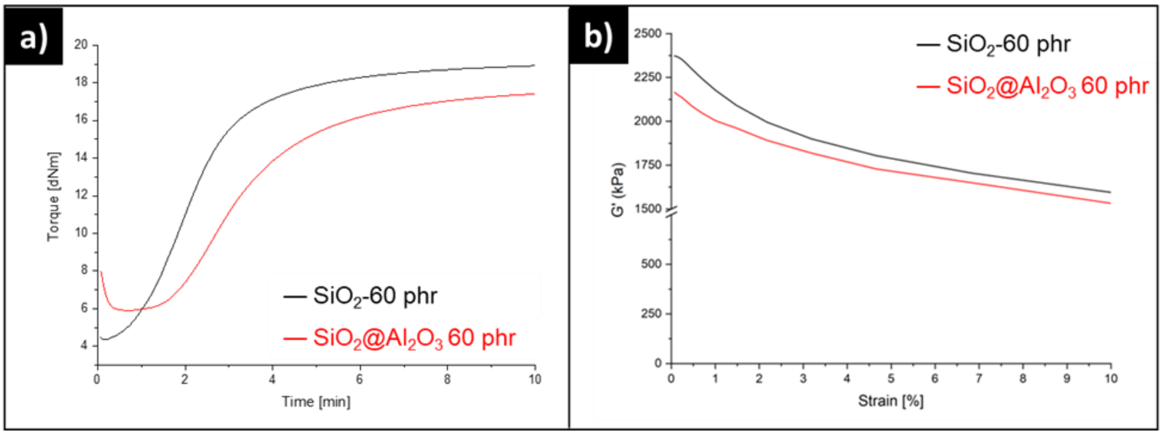

Figure 2.6 –Curing curves (a) and Storage Modulus (b) obtained from RPA of SBR-BR composites containing 60 PHR of commercial SiO_2 or $SiO_2@Al_2O_3$ filler.

Comparing the two samples, it can be noticed that the scorch time, the time in which the torque value starts to increase, is slightly higher when $SiO_2@Al_2O_3$ filler is used. In this case, the increase of the scorch time could allow to handle the composite at high temperature preventing the rapid beginning of the curing process, thus enhancing the processability of the composite at this temperature. In other words, higher scorch times increases the possible application of this material from an industrial point of view, as the homogeneous vulcanization requires a certain delay for the beginning of the curing. However, the rate of the vulcanization and the maximum torque of the compound containing the filler are slightly lower compared to the commercial silica. These results seem to suggest that the presence of alumina at the silica surface impacts on the complex vulcanization reactions decreasing the overall vulcanization efficiency. After vulcanization reaction, the dynamical mechanical analysis on the cured compound was then performed. The vulcanized rubber acts as a viscoelastic material. When this kind of material is deformed, a fraction of the given energy is elastically stored, while the remaining is dissipated (hysteresis loss). The mechanical behaviour of a viscoelastic material is described by two measurable properties, the storage modulus (G') and the loss modulus (G"), moreover the ratio between this modulus is called dissipative factor or tan δ and all together describe the macroscopic behaviour of the rubber under dynamic conditions. RPA allows to acquire these parameters by applying an oscillatory strain which induce a sinusoidal stress that is measured. Since the material is viscoelastic, the measured stress is not in phase with the strain. The stress can so be divided in two components, one in phase with strain and the other out of phase. These two components are associated with the two modulus G' and G". The resulting G' values for SBR-BR/SiO_2@$Al_2O_3$60 and SBR-BR/$SiO_2$60 are reported in Figure 2.6b. The storage modulus at low strain of the two composites is rather similar indicating that the introduction of alumina does not significantly hinder the reinforcement. Interestingly, the modulus loss increasing strain (i.e. Payne effect) of SBR-BR/SiO_2@$Al_2O_3$60 appears slightly decreased in comparison to that of the composite enclosing exclusively silica NPs. This result, together with the very similar G" values (not shown), indicates a better capability of the SiO_2@Al_2O_3 nanofiller in decreasing the hysterical losses, which may derive from the peculiar anisotropic morphology of alumina nanosheets promoting the formation of regions among the silica aggregates, where polymer chains may be partially confined. However, further investigations are needed in order to clarify this point.

To obtain further information on the SBR-BR/SiO_2@Al_2O_3 composites, compression DMA at different temperature (0, 23 and 70°C) and frequency (1, 10, 100 Hz) have been conducted. As examples the results for the compounds containing 60 PHR of commercial SiO_2 or SiO_2@Al_2O_3 are shown in Figure 2.7. The measurements were performed by pre-deforming the cylindrical sample and imparting a sinusoidal compression stress with selected frequency values, at different controlled and constant temperatures. In agreement with the RPA results, DMA shows that only small differences in the elastic modulus E' are present between the composites at each temperature and frequency tested (Fig. 2.7a, c). Interestingly, tan δ values for SBR-BR/SiO_2@Al_2O_3 result significantly lower than those of composites enclosing commercial silica NPs (Fig. 2.7 b, d), suggesting that the introduction of SiO_2@Al_2O_3 imparts a lower energy dissipation to the rubber matrix, in agreement with the better hysteretic behaviour retrieved in RPA (see Fig. 2.6b). As clearly evidenced in Figure 2.7, the moduli E' and E" are dependent from temperature and frequency. The temperature and frequency dependence is associated with the mobility of the polymer chains. In particular, an increase of temperature, as well as a decrease of frequency, leads to an increase of mobility. Above the glass transition (T_g), such mobility is a function of the distance from Tg , entanglements and crosslinks, which limit the translational motion of the chains at high temperature. [10] Consequently, a drop in elastic component of modulus E' is generally measured upon raising the temperature. In the present case the trend of E' as a function of temperature and frequency is similar for the reference silica compound and SBR-BR/SiO_2@Al_2O_3, as polymer matrix is the same. The major difference concerns hysteresis values, which are lower at all temperatures for the SBR-BR/SiO_2@Al_2O_3 compound: this could be interpreted in terms of the larger aggregates of the composite SiO_2@Al_2O_3 filler, which might increase the occluded rubber percentage. From the applicative point of view, a lower hysteresis at high temperature (70 °C) is desirable, being with a lower fuel consumption, but a lower hysteresis at low temperature (0-10°C) is potentially critical, being associated to the grip in wet conditions, so the compound with the new filler would need further tuning to be applied as a tread.

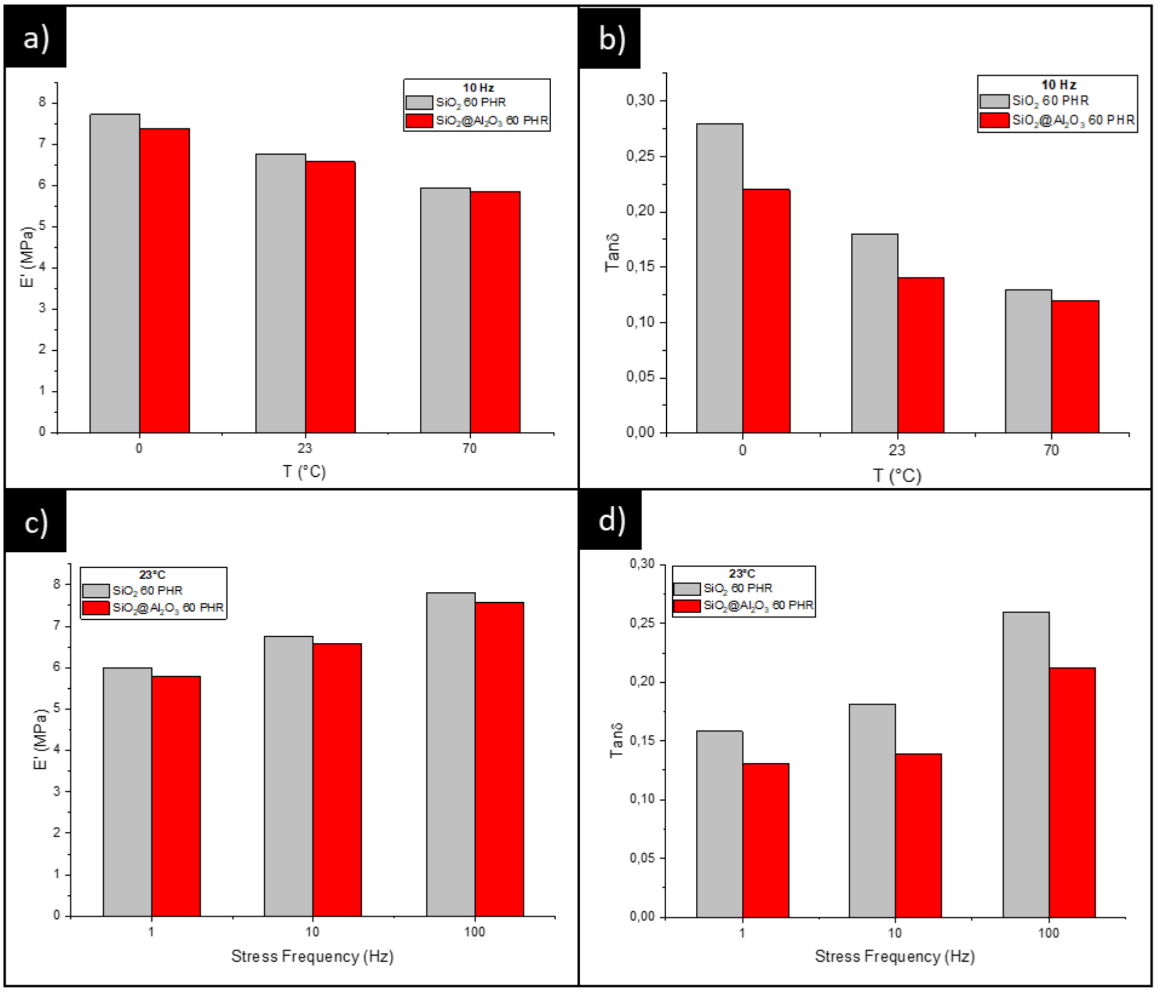

Figure 2.7 – Compression DMA measured elastic modulus (E’) and tanδ plotted as function of temperature (a, b) and stress frequency (c, d)

To further characterize the composites, tensile tests have been performed. A dogbone specimen was cut and subjected to a controlled tension until failure in an Instron instrument (see Appendix). In Table 2.2 the average values (3-56 samples, error below 5%) of the stress at 50, 100 and 300% of elongation respect to the initial length and the tensile strength for different composites are summarized. Substantial differences among the composites enclosing bare SiO_2 NPs and SiO_2@Al_2O_3 filler can be observed especially at larger deformations and in terms of tensile strengths. In particular, the introduction of alumina leads to lower stress at 300% deformation, which is associated to the polymer-filler network and might be explained by a lower reactivity with the silane of the composite filler; the lower stress and tensile strength values compared to those of reference compounds may indicate a bad macroscopical dispersion of SiO_2@Al_2O_3 in the rubber matrix, with the occurrence of some filler segregation regions which may make brittle the composites (see also TEM characterization of the SBR-BR/$SiO_2@Al_2O_3$). The high decrease of the tensile strength when SBR/$SiO_2@Al_2O_3$ is incorporated in SBR/BR matrix represents a weak point for the large-scale application of the formulation. Further trials are ongoing to improve this property.

Table 2.2 –Tensile test results.

	SBR-BR/ $SiO_2$50	**SBR-BR/ $SiO_2@Al_2O_3$50**	**SBR-BR/ $SiO_2$60**	**SBR-BR/ $SiO_2@Al_2O_3$60**
σ_50% (MPa)	1.10	1.31	1.48	1.09
σ _100% (MPa)	1.76	2.14	2.43	1.69
σ _300% (MPa)	7.68	**5.01**	10.03	**3.94**
Tensile Strength (MPa)	18.67	6.12	20.29	4.79

Finally, thermal conductivities of the composites have then been measured by an MTPS method and the results are shown in figure 2.8. It can be observed that, in general, the introduction of filler in the SBR-BR matrix leads to an increase of the λ value compared to the bare polymers. It is interesting to note that, when the $SiO_2@Al_2O_3$ filler is utilized, more significant enhancement can be observed in the thermal transport properties, with an upgrade of ~30% for SBR-BR/$SiO_2@Al_2O_3$60 in comparison to the reference composite enclosing exclusively 60 PHR of silica and of ~ 80% with respect to the neat polymer blend. Considering that the novel filler system contains about 20wt. of alumina, this means that just a little concentration of the thermal conductive material leads to a substantial improvement of the heat transfer in the composites. Although still preliminary, these data suggest that combining SiO_2 and Al_2O_3 with different aspect ratio in a singular multifunctional filler appears a promising strategy for attaining both good thermal transport and interesting mechanical features, even at relatively low loadings of thermal conductive materials. In order to investigate more in depth, the reasons of the improved performance imparted by $SiO_2@Al_2O_3$ to the rubber matrix, TEM/EDS investigation has been performed on SBR-BR/$SiO_2@Al_2O_3$ nanocomposites (Fig. 2.9). The experimental procedure adopted to prepare the sample specimens for the analysis is described in the Appendix of the thesis.

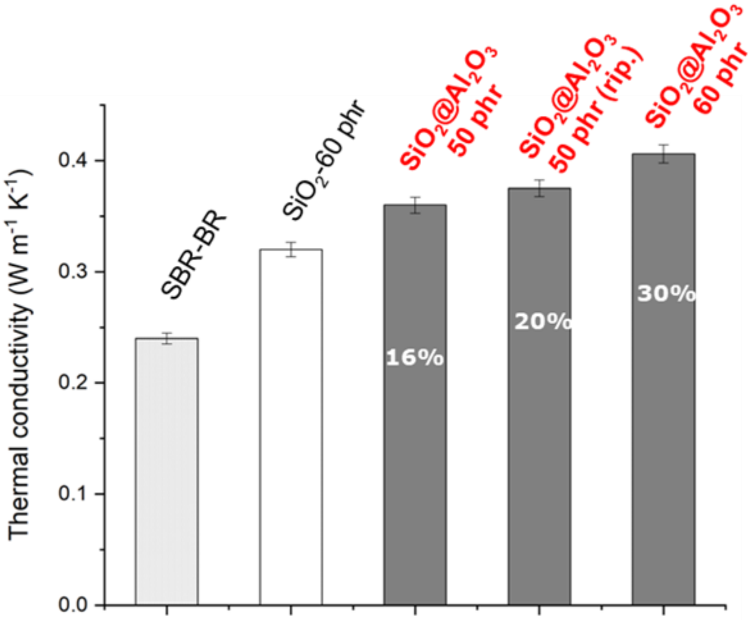

Figure 2.8 – Thermal conductivity results by MTPS method of bare SBR-BR and SBR-BR enclosing: 60 PHR of bare silica NPs; 50 and 60 PHR of $SiO_2@Al_2O_3$ filler. (rip.) stands for a repetition on another batch the same sample. The percentage reported in the bars is the increment with respect to the composite enclosing exclusively silica.

Micrometric or sub-micrometric interconnected filler aggregates can be observed at lower magnifications (Fig. 2.9a), Their dispersion in the rubber matrix appears rather homogeneous, even if regions with a poorer filler occurrence are clearly visible. Images collected at higher magnifications (Fig. 2.9b) reveal the presence of the sheet like structure typical of the $SiO_2@Al_2O_3$ filler, suggesting that the *ex-situ* blending procedure does not damage the peculiar morphology of alumina. The dark field image and, particularly, the corresponding Si and Al EDS map (Fig. 2.9c, d) allow to identify, besides several isolated agglomerates, some interconnected large areas where both Si and Al are detectable, implying that they are composed of $SiO_2@Al_2O_3$ particles. These unique morphological features may support the existence of some thermally conductive pathways, which can increase of the thermal transport of the composite, as demonstrated by mild enhancement of the λ value upon incorporation of $SiO_2@Al_2O_3$ in the SBR-BR matrix in comparison to SBR-BR/$SiO_2$60 (cfr. Fig. 2.8). Moreover, the TEM images seem to support the mechanical characterization results which, besides showing that alumina, despite its very different chemistry compared to silica filler, does not significantly hamper the reinforcement, highlight critical issues for SBR-BR/$SiO_2Al_2O_3$ composites as regards their static behaviour.

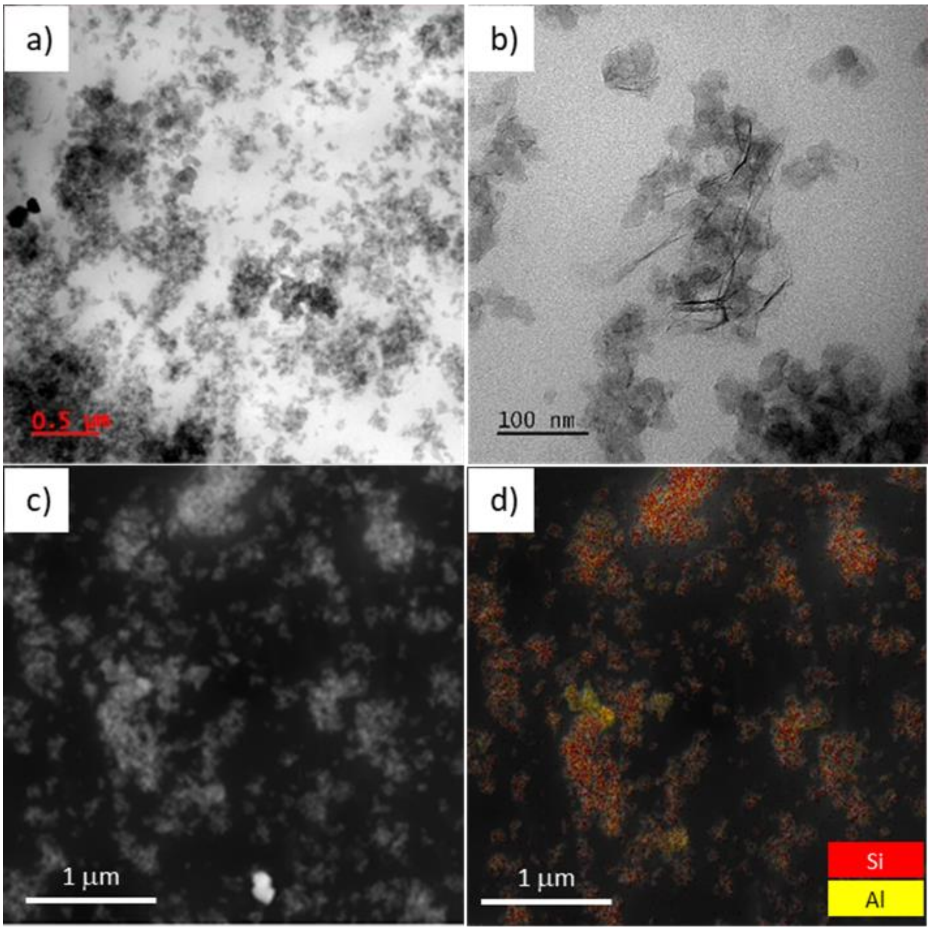

Figure 2.9 – (a, b) TEM images at different magnifications, (c) TEM dark field image and (d) corresponding EDS map for Si and Al of SBR-BR/SiO_2@$Al_2O_3$60 composite

In summary, a novel nanofiller, SiO_2@Al_2O_3, where silica NPs and alumina nanosheets belong to the same functional structure, has been developed by a simple and easy to scale-up method. Although tensile properties need to be improved, incorporation of the material in SBR-BR matrix imparts interesting dynamic-mechanical properties to the composites and a considerable decrease of the hysteresis, foreshadowing a potential application in tire tread formulation. Moreover, a mild but significant increase of the thermal conductivity (+30% in comparison to reference compound enclosing only silica NPs) has been detected in SBR-BR/SiO_2@Al_2O_3, envisaging the ambitious chance to tailor the thermal dissipation properties of tires.

2.6 - Bibliography

[1] E. Union, “Regulation (EU) 2020/740 of the European Parliament and of the Council of 25 May 2020 on the labelling of tyres with respect to fuel efficiency and other parameters, amending Regulation (EU) 2017/1369 and repealing Regulation (EC) No 1222/2009,” *Off. J. Eur. Union*, vol. 2019, no. 5, pp. 20–21, 1999.

[2] M.-J. Wang, “Effect of Polymer-Filler and Filler-Filler Interactions on Dynamic Properties of Filled Vulcanizates,” *Rubber Chem. Technol.*, vol. 71, no. 3, pp. 520–589, Jul. 1998.

[3] S. S. Vaisakh, A. A. Peer Mohammed, M. Hassanzadeh, J. F. Tortorici, R. Metz, and S. Ananthakumar, “Effect of nano-modified SiO 2 /Al 2 O 3 mixed-matrix micro-composite fillers on thermal, mechanical, and tribological properties of epoxy polymers,” *Polym. Adv. Technol.*, vol. 27, no. 7, pp. 905–914, Jul. 2016.

[4] H.-S. Roh *et al.*, “Size-controlled synthesis of monodispersed mesoporous α-Alumina spheres by a template-free forced hydrolysis method,” *Dalt. Trans.*, vol. 40, no. 26, p. 6901, 2011.

[5] M. Fedel, E. Callone, S. Diré, F. Deflorian, M.-G. Olivier, and M. Poelman, “Effect of Na-Montmorillonite sonication on the protective properties of hybrid silica coatings,” *Electrochim. Acta*, vol. 124, pp. 90–99, Apr. 2014.

[6] T. Takahashi, T. Ohkubo, K. Suzuki, and Y. Ikeda, “High resolution solid-state NMR studies on dissolution and alteration of Na-montmorillonite under highly alkaline conditions,” *Microporous Mesoporous Mater.*, vol. 106, no. 1–3, pp. 284–297, Nov. 2007.

[7] S. Greiser, G. J. G. Gluth, P. Sturm, and C. Jäger, “29 Si{ 27 Al}, 27 Al{ 29 Si} and 27 Al{ 1 H} double-resonance NMR spectroscopy study of cementitious sodium aluminosilicate gels (geopolymers) and gel–zeolite composites,” *RSC Adv.*, vol. 8, no. 70, pp. 40164–40171, 2018.

[8] J. Hiet, M. Deschamps, N. Pellerin, F. Fayon, and D. Massiot, “Probing chemical disorder in glasses using silicon-29 NMR spectral editing,” *Phys. Chem. Chem. Phys.*, vol. 11, no. 32, p. 6935, 2009.

[9] F. Rashidi, A. N. Kharat, A. M. Rashidi, E. Lima, V. Lara, and J. S. Valente, “Fractal Geometry Approach to Describe Mesostructured Boehmite and Gamma-Alumina Nanorods,” *Eur. J. Inorg. Chem.*, vol. 2010, no. 10, pp. 1544–1551, Apr. 2010.

[10] N. Lagakos, J. Jarzynski, J. H. Cole, and J. A. Bucaro, “Frequency and temperature dependence of elastic moduli of polymers,” *J. Appl. Phys.*, vol. 59, no. 12, pp. 4017–4031, Jun. 1986.

Chapter 3 - Al_2O_3@POSS filler in PB and SBR/BR matrix

3.1 - Introduction

As already mentioned in Chapter 1, Al_2O_3 represents an interesting choice to produce composite for tire application due to its low cost, chemical stability and non-toxicity and good intrinsic thermal conductivity. Moreover, alumina has been extensively studied as filler in silicon rubber, thus dependence of mechanical, thermal conductivity and electrical features from of crystal phase, morphology and surface properties are known. However, both scientific and technological problems must be solved when alumina is included in polymers to produce composites with λ values comparable with the theoretical prediction. Generally, the main concerns are associated with: i) the interfacial adhesion between the fillers and the matrix that influence the phonon scattering and thus the interfacial thermal resistance; ii) the inhomogeneous fillers distribution in the matrix, which hinders the generation of thermal conductive pathways and leads to an increase of the interfaces and contact thermal resistance. To overcome these issues, extremely high Al_2O_3 loadings (even higher than 50-60 v/v %) are usually needed to increase thermal conduction, generating severe drawbacks in terms of mechanical properties and processability of the composites. Furthermore, when dealing with tire industry, it must be considered that the superficial chemistry of Al_2O_3 is different from the commonly used filler like silica, silicate or carbon black. With the aim of producing an Al_2O_3-rubber composites with both good thermal conductivity and mechanical properties, a filler based on Al_2O_3 modified at the surface with polyhedral silsesquioxane (POSS) was produced. A similar system was already investigated in Milano Bicocca research group, in particular OctaMethacrylPOSS (POSS) units functionalized SiO_2 (i.e. SiO_2@POSS hybrid filler) was utilized to make rubber composites for tire application. The composites showed significant reinforcement and decreased energy loss under strain. [1, 2] In the present work, the extension to a different functional filler was successfully achieved. Alumina nanoparticles (NPs) functionalized with POSS (Al_2O_3@POSS), combine the optimal compatibilization and thermomechanical properties conveyed by silsesquioxane with the thermal conductivity of alumina. The two-step synthesis consists of a first silanization step with a methacrylsilane (MPTMS) and subsequently the POSS grafting was performed by a radicalic reaction utilising dicumylperoxide (DCP) as initiator. The use of this initiator permits to anchor the POSS nanocages preserving in the hybrid structure unreacted methacryl groups which are fundamental for creating interaction with the polymeric matrix. The as produced filler was structurally, surface, and morphologically characterized by X-ray diffraction analysis (XRD), attenuated total reflection Fourier transform infrared spectroscopy (ATR-FTIR), ^{13}C and ^{29}Si solid-state Nuclear Magnetic Resonance (NMR) and Transmission Electron microscopy (TEM). TGA was used as quantitative analysis to estimate the functionalization degree. Al_2O_3@POSS was then used as filler in polybutadiene (PB) matrix to produce composites by an easy solution-blending methodology. The choice of a simple binary system allows us to reveal the role played by the POSS units. The composites were characterized by solid-state NMR, scanning electron microscopy (SEM) and dynamic mechanical thermal analysis (DMTA) to study their structure, morphology and mechanical properties, while Laser Flash Analysis (LFA) was used to determine the thermal transport features.

3.2 - Preparation of Al_2O_3@POSS NPs

Materials: Nanometric aluminium oxide “NanoArc”, Toluene and Dicumyl peroxide (DCP) was acquired from Alfa Aesar, MPTMS was obtained from Sigma Aldritch and POSS-MA from Hybrid Plastics.

Al_2O_3@POSS filler was prepared according to a double-step functionalization procedure shown in Scheme 3.1.

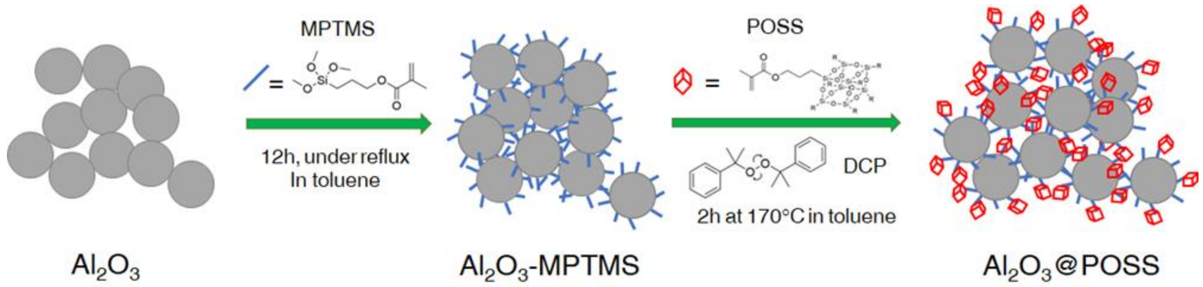

Scheme 3.1 - Experimental procedure for the preparation of Al_2O_3@POSS filler

Firstly, the commercial Al_2O_3 NPs (1.00 g) were dispersed in 25.0 mL of toluene by ultrasonication (2 min) in a two-neck round-bottom flask, the mixture was then taken in reflux conditions. MPTMS (0.304 g) were added to the dispersion and kept under reflux conditions for 12 hours. The mixture was finally centrifuged at 9000 rpm for 15 min and washed twice with toluene and ethanol (EtOH) and dried at 120 °C for 12h. The as obtained nanoparticle was called Al_2O_3-MPTMS. In the second step, Al_2O_3-MPTMS NPs were suspended in 50 mL of toluene and then POSS (0.1000 g) was introduced in the solution. Successively, a small amount of DCP (4 wt.% with respect to Al_2O_3-MPTMS) was added and the suspension was refluxed for 2h. Finally, the obtained Al_2O_3@POSS powders were filtered, washed several times with toluene and finally with EtOH, and dried in oven at 120 °C in air for 12 h.

3.3 - Structural, morphological and surface characterization of alumina-based fillers

The crystalline phases of commercial Al_2O_3 NPs were determined by XRD (Fig. 3.1).

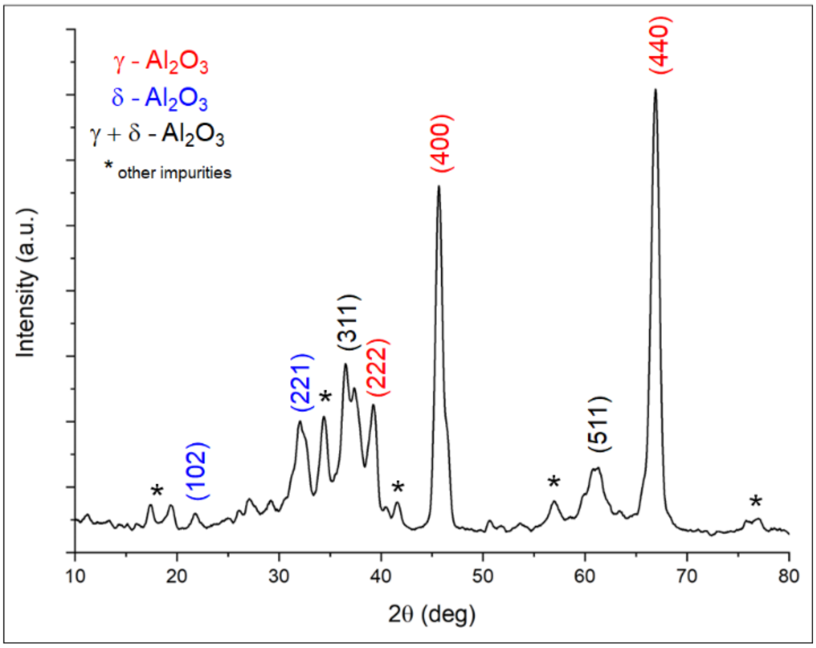

Figure 3.1 – XRD pattern of commercial Al_2O_3 nanoparticles.

The diffraction pattern shows the presence of two different crystalline structures, γ and δ alumina (JCPDS card [3] no. 29-0063 and JCPDS card no. 46-1215, respectively). The presence of other reflections could be related to impurities. The NPs phase composition was evaluated by profile fitting, revealing that the sample is composed of ~88% of γ-Al_2O_3 and ~12 % of δ-Al_2O_3.

To preliminary prove the effective functionalization of the NPs firstly with MPTMS and, in turn, with POSS, FT-IR spectra were acquired.

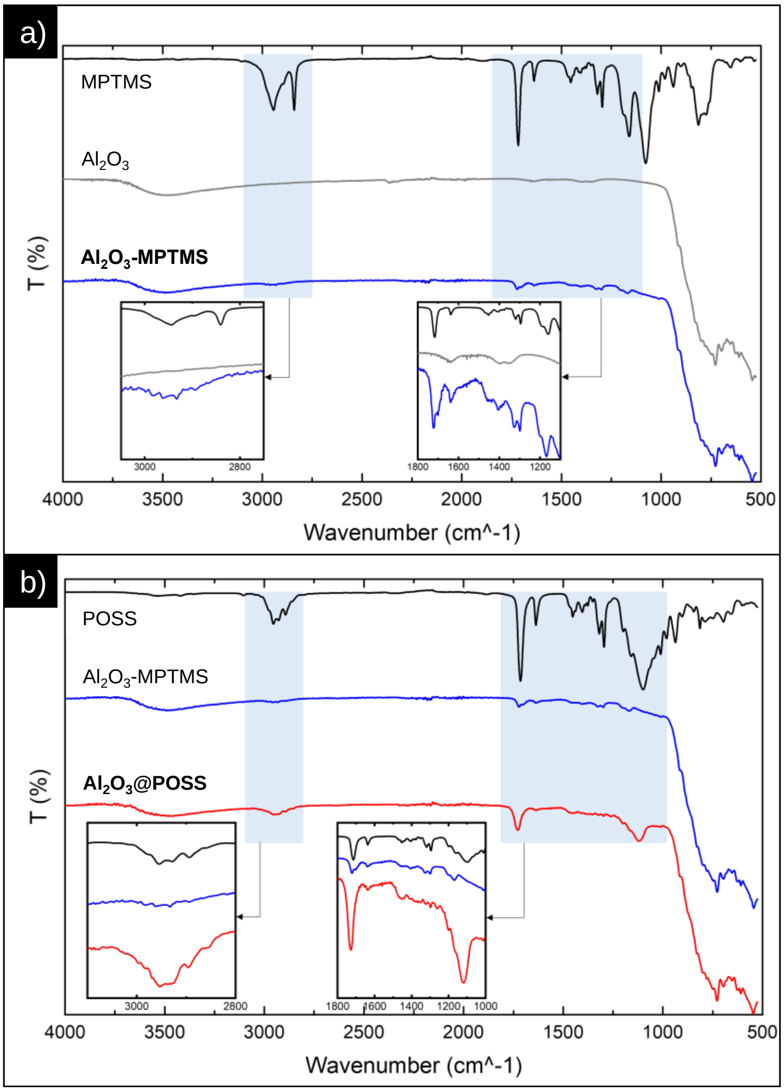

Figure 3.2 – FT-IR spectra of: (a) MPTMS (black line), pristine Al_2O_3 (grey line) and Al_2O_3-MPTMS (blue line); (b) pure POSS (black line), Al_2O_3-MPTMS (blue line) and Al_2O_3@POSS (red line); the insets show the magnifications of the spectral regions related to the functional groups of MPTMS (top) and of the POSS units (bottom).

Figure 3.2a presents the comparison between the spectra of the reagents and the final product. MPTMS spectrum a (black line) accordingly to literature presents the following peaks: at 2945 and 2840 cm^{-1} of the silane C–H stretching; at 1454 cm^{-1} of the methylene C–H bending; the 1320 and 1160 cm^{-1} bands attributed to the –C–CO–O– skeletal vibration; at 1080 cm^{-1} Si–O–C stretching; the carbonyl vibration band at 1715 cm^{-1} and finally the weak stretching band at 1639 cm^{-1} of C=C bond. The spectra of bare alumina (grey line) show the presence of a broad band at ~3498 cm^{-1} that could arise due to the probable presence of Al–OH bonds in the materials. Moreover, the peak at 1650 cm^{-1} (right inset Figure 3.2a) of H–O–H bending of weakly bound molecular water is clearly visible. The bands below 900 cm^{-1} are typical of alumina and are correlated to Al–O–Al bending and Al–O stretching modes. Other weak bands may be attributed to the presence of some undesired impurities in the commercial Al_2O_3 NPs. [4] The spectra of the product obtained after silanization (Al_2O_3-MPTMS, blue line) confirm the presence of MPTMS bonded to alumina surfaces. In fact, the peaks at 2840 cm^{-1} of the methylene C–H bending (left inset Figure 3.2a), at 1720 and 1639 cm^{-1} ascribed to C=O and C=C stretching, and the –C–CO–O– skeletal vibration bands typical of MPTMS (right inset Fig. 3.2a) are clearly detectable. FTIR spectra of the second step reactants and of Al_2O_3@POSS reaction product are reported in Figure 3.2b. The spectra of the alumina functionalized with MPTMS and POSS (blue and red line, respectively) results similar, since the organic functional groups of the MPTMS and POSS are essentially the same. Noticeably, in Al_2O_3@POSS spectra (right inset Figure 3.2b), beyond the higher intensity of the stretching modes of C=O at 1710 cm^{-1} and C=C at 1640 cm^{-1} related to the methacrylic groups, the presence of an intense band at 1090 cm^{-1} distinctive of the Si–O stretching vibration of the POSS cage, indicates the anchoring of POSS units on the filler surface.

Quantitative estimation of the functionalizing agents grafted on alumina NPs was obtained by TGA analysis. In Figure 3.3 the thermal profiles of the bare Al_2O_3 and the functionalized Al_2O_3-MPTMS and Al_2O_3@POSS NPs are presented. As expected, in bare alumina (back curve) only a small weight loss at about 400°C can be detected. This loss was associated to the condensation of superficial Al-OH and consequent production of water. The amount of functionalizing agent was calculated by the net loss in weight between 150 and 1000°C. For MPTMS calculations contribution of unbonded OH was determined and subtracted from weight loss, while for POSS both unbonded OH and MPTMS contribution was withdrawn. Additionally, the number of functionalizing molecules per nm^2 (Σ = molecules nm^{-2}) was assessed assuming that the functionalizing agent is equally distributed on the alumina surface and using the BET surface area provided by the supplier (SSA_{BET} = 35 m^2 g^{-1}). The results are shown in Table 3.1.

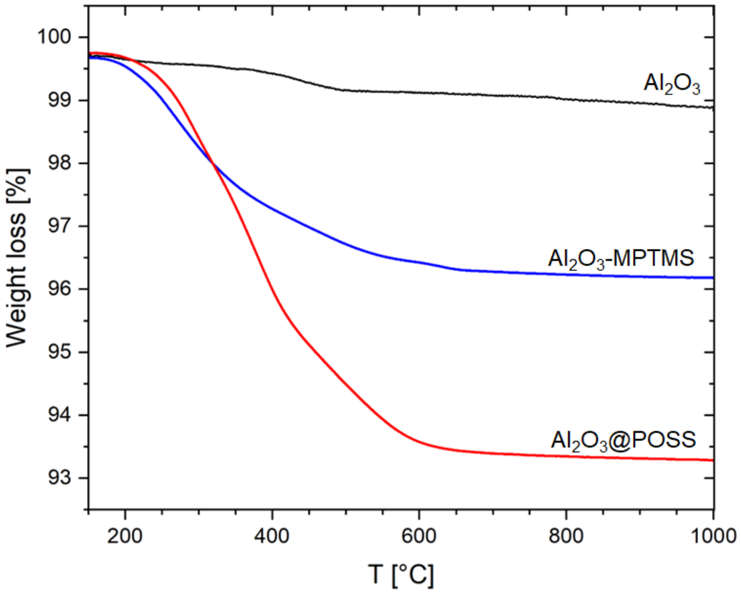

Figure 3.3 – TGA curves of bare Al_2O_3 (black line), Al_2O_3-MPTMS (blue line) and Al_2O_3@POSS (red line)

Table 3.1- Surface density of functional molecules on Al_2O_3-MPTMS and Al_2O_3@POSS

Sample	Functionalizing Agent	Net weight loss (wt. %)	M_w (g mol^{-1})	Grafted amount (mmol g^{-1})	Σ (molecules nm^{-2})
Al_2O_3-MPTMS	MPTMS	2.13	248.4	$1.41 \cdot 10^{-4}$	2.7
Al_2O_3@POSS	POSS	5.04	1434.0	$4.17 \cdot 10^{-5}$	0.8

Solid state NMR spectra was also conducted in order to have a further proof of functionalization. Figure 3.4a show the ^{29}Al spectra of Al_2O_3, Al_2O_3-MPTMS and Al_2O_3@POSS powder. All the samples show two resonances peaks. The main peak centred at 7.7 ppm is assigned to octahedral Al sites (Al(VI)) and the minor component at about 59 ppm is attributed to tetrahedral Al atoms. [5, 6] The ratio between Al(IV) and Al(VI) is 28:72 for all the spectra. Thus, the spectra result entirely superimposable, confirming that the functionalizing methods do not alter the Al-O structure. CPMAS ^{29}Si NMR investigation (Figure 3.4b), outlined remarkable difference between the different functionalized alumina NPs. In Al_2O_3-MPTMS spectrum it is possible to see the T1, T2 and T3 units due to the presence of the organosilane at δ -45.5, -54.7 and -64.3

ppm respectively. The simultaneous presence of T2 and T1 units indicates that the condensation degree of the silane on alumina surface is low. A small amount of Q units centred at -99.0 ppm arise due to the declared contamination present in the commercial alumina. The Al_2O_3@POSS spectrum displays instead the presence of signals ascribable to almost fully condensed T3 units at -66.3 ppm (i.e. POSS units) and a really small amount of T2 units.

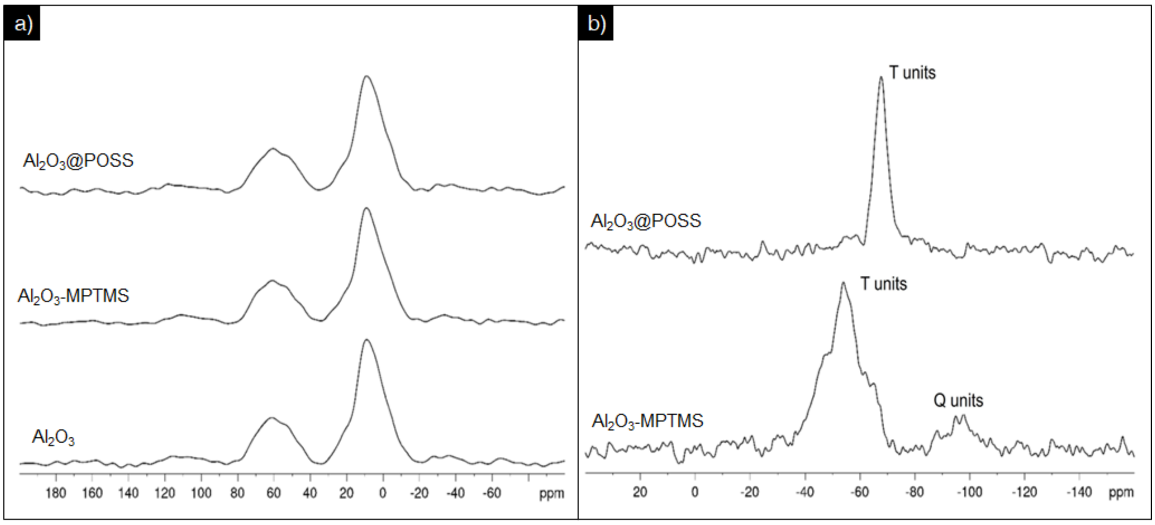

Figure 3.4 – a) ^{27}Al Hahn-echo MAS NMR spectra of Al_2O_3, Al_2O_3-MPTMS and Al_2O_3@POSS; b) ^{29}Si CPMAS spectra of Al_2O_3-MPTMS and Al_2O_3@POSS.

To gain potential information on the interactions among the acrylate functions of MPTMS and POSS, ^{13}C CPMAS NMR investigation was performed (Figure 3.5). The liquid NMR spectrum of the pristine MPTMS and the corresponding labelling is also reported for comparison. In Al_2O_3-MPTMS and Al_2O_3@POSS spectra a downshift of peak 7 (Si-CH_2-) confirms the condensation of MPTMS; moreover, the absence of the resonance peak at 50ppm of OCH_3 indicates a full hydrolyzation of the silane. Focusing on Al_2O_3-MPTMS sample, the presence of 1*a* and *2a* in the 60-40 ppm and the downfield component of the broad resonance *4* confirm the partial dimerization of MPTMS. Therefore, both dimerized and free methacrylate groups can be easily identified due to the broadness of the environmental sensitive C=O signal. In Al_2O_3@POSS the carbon peaks reveal the presence of a high polymerized methacrylate groups. Anyway, signals related to unreacted methacrylate functionalities are present, in particular, the peaks *1*, *2* and *2a*, and also the downfield shift of *4*. Furthermore, the all the resonance peaks of the spectrum result broad, indicating that the POSS functionalized alumina is a system more rigid compared with MPTMS one.

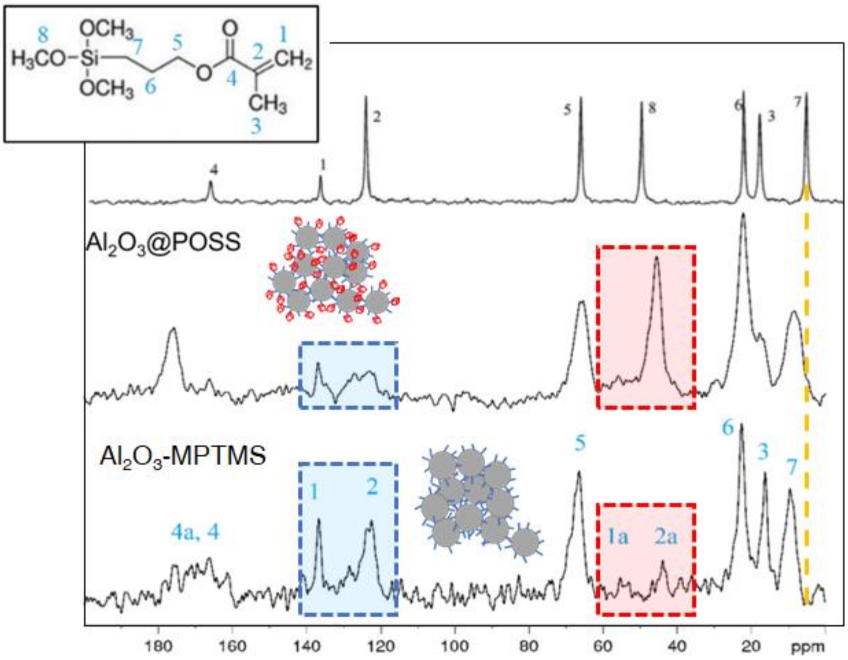

Figure 3.5 – ^{13}C CPMAS NMR spectra of Al$_2$O$_3$-MPTMS and Al$_2$O$_3$@POSS.
For comparison, the liquid NMR spectrum of the pristine MPTMS is also reported (top).

In summary, solid-state NMR confirms the surface functionalization of alumina with POSS and proves the presence of available methacrylate groups desirable for the cross-linking reaction with the matrix.

The morphology of neat alumina and POSS functionalized NPs was assessed by TEM (figure 3.6). From images it is possible to see that commercial alumina is made of polydisperse spherical nanoparticles with a diameter that ranges from 20 to 150 nm. At higher magnification nanocrystal facets and sharp edges are clearly visible. After functionalisation with the POSS units, the degree of aggregation increased and the surface of the NPs seemed less defined than in neat alumina. This behaviour could be attributed to the effective functionalization of the alumina surface. Indeed, the presence of POSS on the alumina surface, due to interactions driven by the condensation among the methacrylic terminations, leads to the aggregation of the NPs and the formation of a covering polymeric shell.

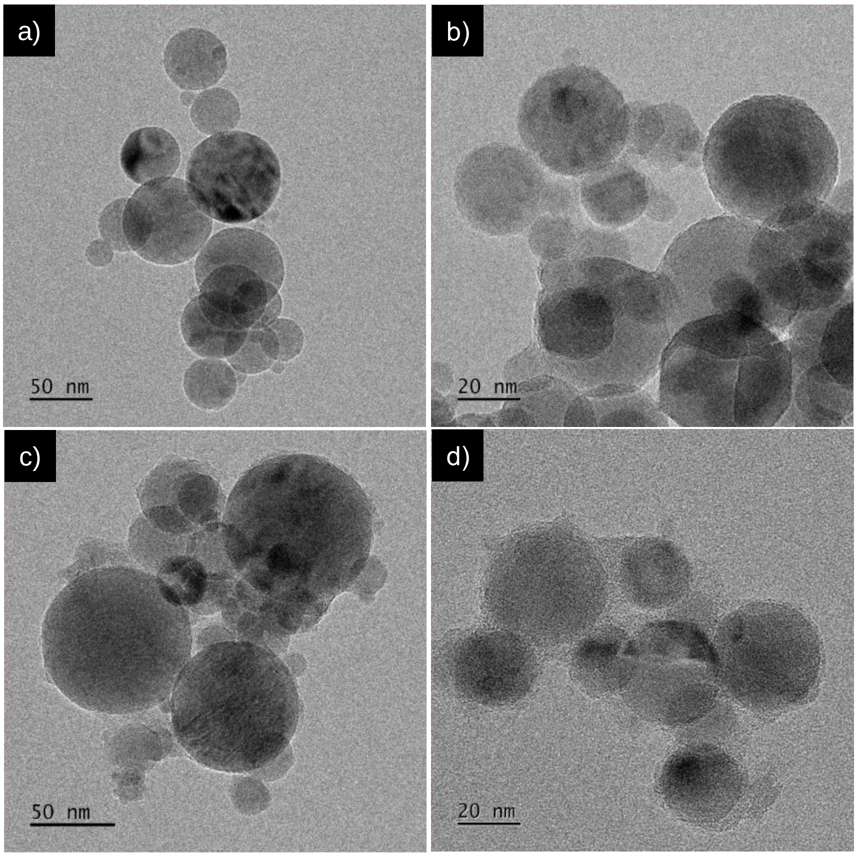

Figure 3.6 – TEM images of Al_2O_3 (a, b) and Al_2O_3@POSS (c, d) nanoparticles.

3.4 - Preparation of PB/Al_2O_3 composites

Materials: Toluene was acquired from Alfa Aesar, high molecular weight cis polybutadiene an azobisisobutirronitrile (AIBN) obtained from Sigma Aldritch.

To create composites, bare, MPTMS and POSS functionalized alumina NPs was introduced in PB at various loading (10, 30, 40, 50 wt. %, corresponding to 2.57, 9.24, 13.67, 19.19 v/v %,). The production procedure is shown in Scheme 3.2. Typically, 2 g of PB is dissolved in 20 mL of toluene at 65°C, subsequently a filler dispersion in toluene and 0,02g of AIBN as crosslinking agent was added. The solution was then stirred at 65°C for 6h under nitrogen flow. The as obtained solutions was casted in pre-heated Teflon Petri and the solvent was allowed to evaporate under aspiration hood and finally the samples were heated at 70 °C for 9 h under vacuum. The obtained composites are films with an average thickness of 280–300 μm.

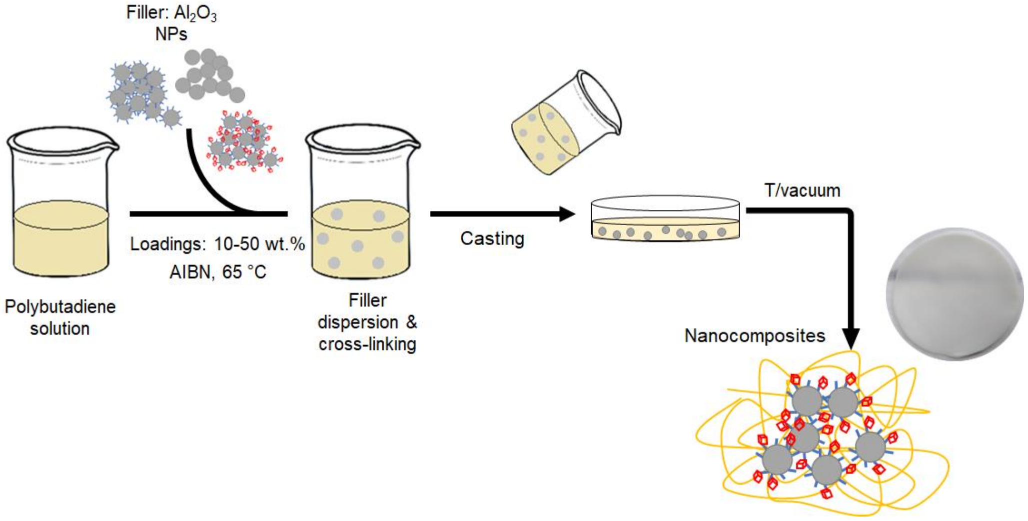

Scheme 3.2 - Experimental procedure for the preparation of PB/alumina composites by *solution* blending.

The nanocomposites are labeled as PB/XAl_2O_3Y where X refers to the loading of the filler (X= 10, 30, 40, 50 wt. %) and Y denotes the alumina surface functionalization (-MPTMS, @POSS). Unfilled PB material was also producing utilizing same composite production procedure. FTIR and solid-state NMR was utilized to characterize the composites.

3.5 - Spectroscopic and morphological characterization of nanocomposites

FTIR spectra of PB, Al_2O_3@POSS and PB/40Al_2O_3@POSS are shown as illustrative example in Figure 3.7. The spectra have been divided in three spectral regions for a better visualization of the bands. At the high wavenumbers the typical PB associated peaks are present: in particular, at ~3005 cm^{-1} the =C–H stretching; at ~2940 cm^{-1} and ~2850 cm^{-1}, respectively, the asymmetrical and symmetrical C–H stretching vibration of methylene groups. The introduction of the filler does not significantly affect the spectral features of the PB in the composite. More significant modifications in the spectra can be observed at lower wavenumbers (Fig. 3.7B-C). In particular, the thermal crosslinking in the presence of Al_2O_3@POSS leads to the generation of new signals at ~1695 cm^{-1} and ~1722 cm^{-1}, together with a decrease in the intensity of the absorption band at 1654 cm^{-1} relatable to the stretching C=C of PB chains (Fig. 3.7B). These new features can be tentatively associated to the self-polymerization of the POSS methacrylic groups. At the lower wavenumber, a broad band at ~ 1100 cm^{-1} can be attributed to the Si–O stretching of the POSS cages and below 800 cm^{-1} the signal of alumina is dominant.

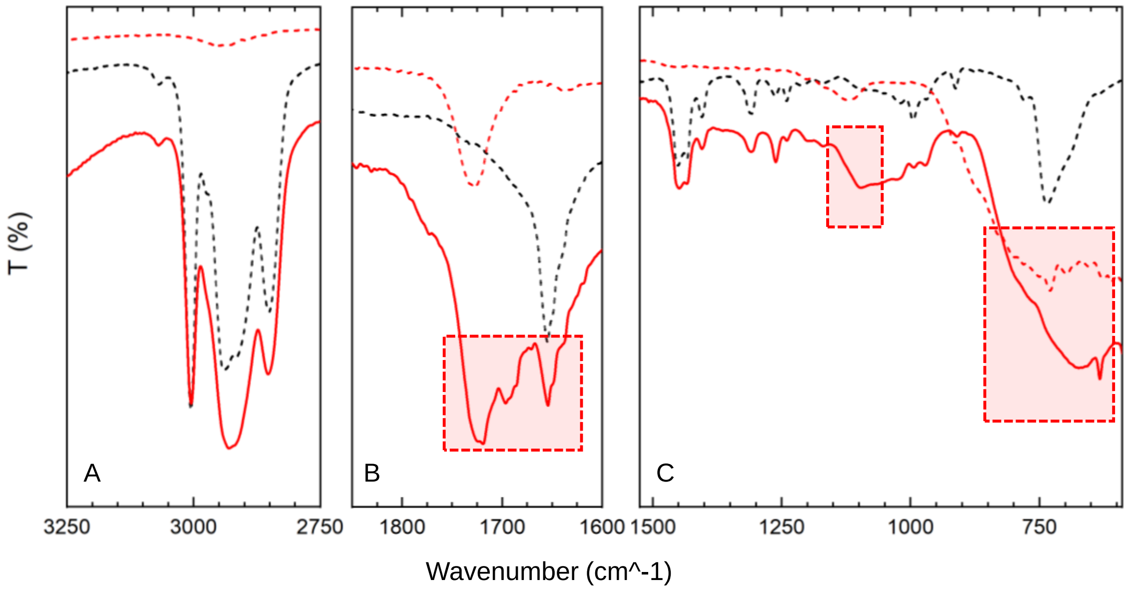

Figure 3.7 – FTIR spectra of Al_2O_3@POSS (red-dotted line), homopolymerized PB (black-dotted line) and PB/40Al_2O_3@POSS (red line) in the a) 2750-3250 cm^{-1}, b) 1600-1850 cm^{-1} and c) 590-1525 cm^{-1} spectral regions.

Investigation on the influence of alumina functionalization on the distribution in the PB matrix was carried out by SEM-EDS analysis. SEM micrographs and the corresponding Al elemental mapping images of PB/40Al_2O_3, PB/40Al_2O_3-MPTMS and PB/40Al_2O_3@POSS are reported in figure 3.8. As visible, surface functionalization strongly affects the filler distribution in the matrix. Bare alumina, due to its polar surfaces, forms inhomogeneous dispersion in the matrix and tends to aggregate forming aggregates up to micrometric size. This is much clearly visible from Al EDS elemental map (Fig. 3.8a'). Alumina functionalization with both MPTMS and POSS improves filler distribution (Fig. 3.8b, c), due to the change of the alumina superficial properties that leads to a better affinity with the PB matrix. However, a key difference can be noticed between the fillers. In fact, in PB/40Al_2O_3-MPTMS, alumina is arranged sub-micrometric or nanometric groups, which are only partially connected. While in PB/40Al_2O_3@POSS nanometric aggregates with a homogeneous distribution and well interconnected are formed, moreover, from SEM-EDS images it is possible to see that a continuous filler network is formed (Fig. 3.8c, c'). This distinctive feature could be exploited for the formation of thermally conductive pathways resulting in an increase of the thermal conductivity of the composites.

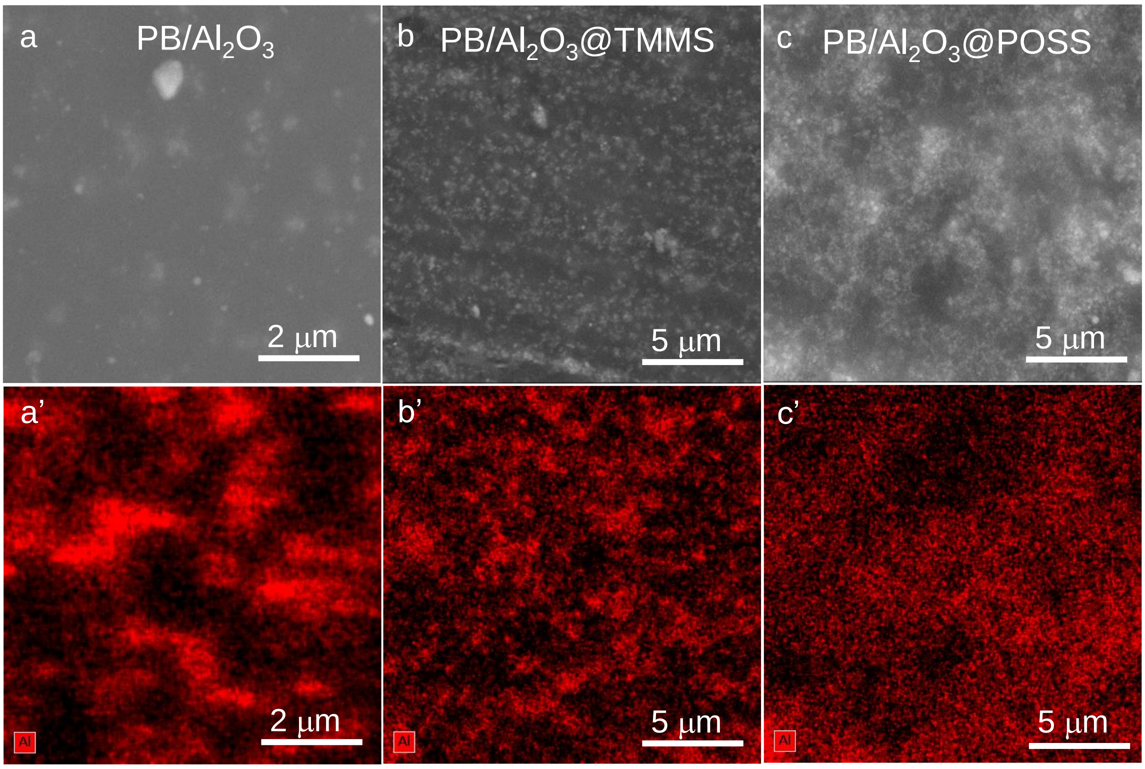

Figure 3.8 – SEM micrographs and corresponding EDS elemental maps of Al for PB/40Al_2O_3, PB/40Al_2O_3-MPTMS and PB/40Al_2O_3@POSS nanocomposites.

Furthermore, to study the effect of filler inclusion on PB, ^1H solid state NMR relaxation experiments were conducted on the composites. Figure 3.9 shows the resulting proton spectra. Resonance at 2.1 and 5.4 ppm can be attributed to the methylene and methine group of PB respectively. Interestingly broadening of the signals appear when alumina is functionalized suggesting that a difference in spin-spin (T_2) and spin-lattice in the rotating frame ($T^H_{1\rho}$) relaxation times arise when different nanofiller is included in PB. The values of the calculated relaxation time are summarized in Table 3.2. The results of the relaxation experiments show that bare alumina causes an expected higher $T^H_{1\rho}$ and T_2 values proving the stiffening of the polymer chains. On the contrary, the functionalized filler generates a strong reduction of the relaxation times, corresponding to interaction between the organic groups onto the surface of alumina and the polymer chains of the PB that lead to conformational reorganization of the backbones. [7]

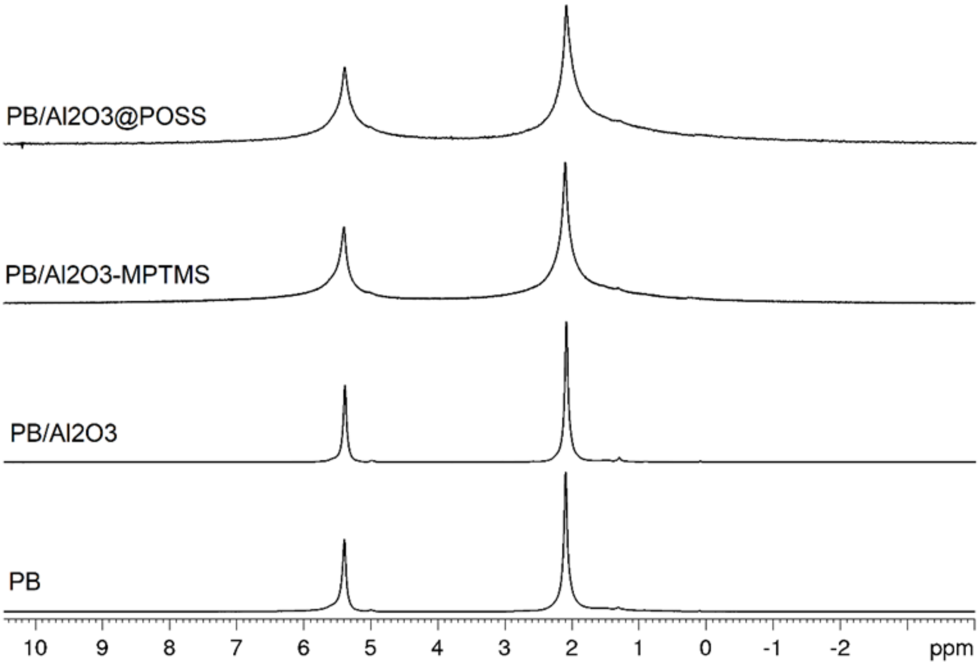

Figure 3.9 - ^{1}H MAS spectra of PB and PB/alumina composites

Table 3.2 - Resonance linewidth and relaxation time constants $T^H_{1\rho}$ and T_2 obtained from the analysis of the proton spectra and related magnetization curve trends for all the composites.

		PB	PB/40Al_2O_3	PB/40Al_2O_3-MPTMS	PB/40Al_2O_3@POSS
LW (Hz)	-CH_2-	24.0	20.2	60.4	78.9
	=CH-	25.5	19.3	56.2	81.2
$T^H_{1\rho}$ (ms)	-CH_2-	41.2	57.5	16.5	11.8
	=CH-	38.9	52.6	16.8	11.7
T_2 (ms)	-CH_2-	25.5	29.9	16.2	12.6
	=CH-	24.5	29.4	16.1	13.1

The effect of chain reorganization is prominent in POSS functionalized alumina respect to MPTMS-ones, due to the presence of a higher number of organic groups that can interact with the PB leading to an improvement of the filler/polymer interactions. This results at molecular level collaborates the hypothesis done from SEM-EDS images and effectively explains the dispersion of the filler in the matrix.

3.6 - Functional properties of the nanocomposites: thermal transport properties and dynamic mechanical analysis

The thermal transport properties of the composites were evaluated by LFA. Figure 3.10 summarizes the results of the analysis for PB/Al_2O_3, PB/Al_2O_3-MPTMS and PB/Al_2O_3@POSS. In detail, thermal diffusivity (α) is plotted as a function of the filler volume fraction (Fig. 3.10a).

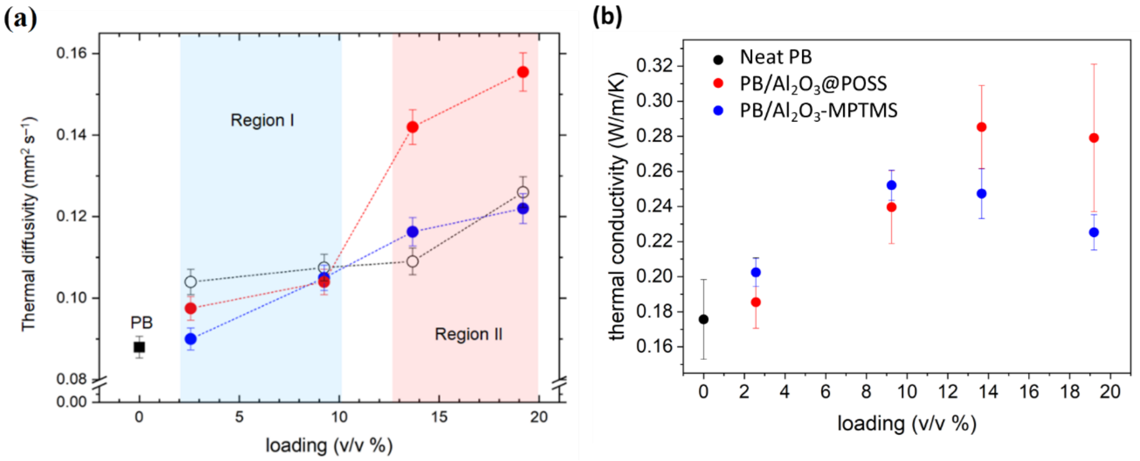

Figure 3.10 – Thermal diffusivity (a) and thermal conductivity (b) of PB filled with unmodified and functionalized Al_2O_3

Two different regions can be identified. In the Region I (< 10 v/v %), only slight changes in values can be displayed for PB/Al_2O_3 nanocomposites, while an appreciable decrease of α respect to bare alumina is visible when Al_2O_3-MPTMS and Al_2O_3@POSS are used as filler. This behaviour could be correlated to the better interaction between the functionalized alumina and the matrix that leads to the occurrence of homogeneous and random dispersion of the filler as already discussed in SEM-EDS images. Increasing the filler volume fraction up to Region II, significant differences in α emerge when POSS is used as functionalizing agent. In fact, while for PB/Al_2O_3 and PB/Al_2O_3-MPTMS α values are almost the same, a remarkable enhancement in thermal transport can be observed for PB/Al_2O_3@POSS nanocomposites (+60-70% with respect to PB/Al_2O_3 and PB/Al_2O_3-MPTMS and +90% compared to homopolymerized PB). Again, an explanation to this phenomenon can be found in the morphological features of the nanocomposite and to the ability of the Al_2O_3@POSS NPs to create interconnected aggregates and, thus, thermal conductive pathways which enhance the thermal diffusivity of the composites already at relative low filler loadings.

Thermal conductivity was calculated by the equation (1):

$$\lambda = \alpha \cdot \rho \cdot C_p \tag{1}$$

where r is the density measured by He pycnometer and C_p is the specific heat capacity of the composites measured by differential scanning calorimetry (DSC). High error bars on the determination of the Cp, due to the small amount of the samples analysed, lead to an increase of the uncertainties in the thermal conductivity values (Fig. 3.10b). However, higher λ values are retrieved for PB/Al_2O_3@POSS composites with respect to PB/Al_2O_3-MPTMS, confirming the ability of the POSS nanounits in improving the thermal transport. In summary, POSS functionalization, besides assuring the compatibility between filler and polymer host, allows a homogeneous distribution and a continuous networking of the alumina NPs. This positively influences heat transport of the nanocomposites leading to the raise of the thermal diffusivity even at low filler loadings.

Producing Al_2O_3-rubber composites with simultaneous satisfactory thermal conductivity and mechanical properties is a challenging target. Supported by the good thermal diffusivity evidenced in PB/Al_2O_3@POSS nanocomposites, DMTA analysis were performed to study the mechanical properties of the nanocomposites. The results of temperature sweep analysis shown as the trend of the storage modulus (E') and the loss modulus (E") for the neat PB and the PB-50Al_2O_3, PB-50Al_2O_3-MPTMS, and PB-50Al_2O_3@POSS composites are summarized in Figure 3.11. Noticeably, for all the samples the E' decrease with increasing of the temperature with a fast drop between -110 and -90°C where the glass transition takes places. The glass transition temperature (T_g) is associated with the peak temperature of E" graph and shift to higher values when filler is introduced in the matrix, passing from -104°C for neat PB to ~ -101°C for the nanocomposites. This small but evident shift could be caused by difference on the crosslink density or due to the confinement effect of the nanofillers on the matrix (Fig. 3.11a). While the filler functionalization does not influence the T_g, the absolute values of

E' and E" show a strongly dependence on the filler functionalization (Fig. 3.11a). In fact, introduction of alumina NPs in PB leads to an increase of both the moduli values, more remarkably for Al_2O_3@POSS. Moreover, for PB/Al_2O_3-MTPMS and PB/Al_2O_3@POSS, the stiffness of the materials is retained also above the glassy state, as observable from the inset of Figure 3.11a. The same trend can be noticed for E" (Fig. 3.11b) and confirms the more homogeneous dispersion of the nanofiller after the functionalization. To prove the improved filler/matrix adhesion other analysis are required.

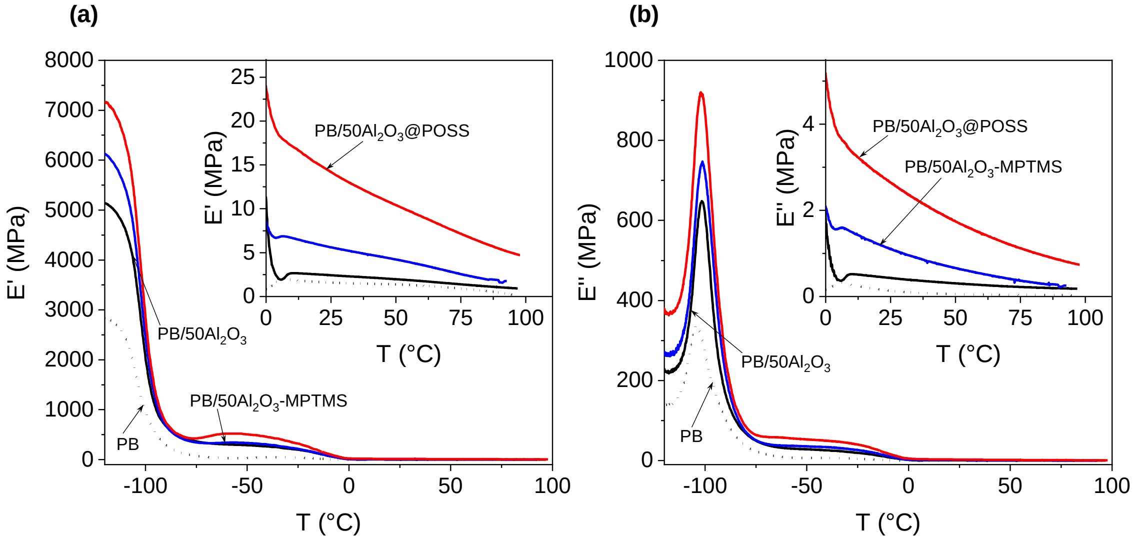

Figure 3.11– Trend of the storage (a) and complex (b) modulus of homopolymerized PB, PB/40Al_2O_3, PB/40Al_2O_3-MPTMS and PB/40Al_2O_3@POSS nanocomposites.

Overall, the results of DMTA analysis confirm that the addition of functionalized alumina NPs not only promotes an increase in the thermal transport properties but also an improvement in the mechanical features of the composites, thus making them promising candidates for real applications.

3.7 - A versatile strategy: extension to alumina nanorods

Filler morphology is one of the key aspects that affect the enhancement of the thermal conductivity of polymer nanocomposites. High aspect ratio fillers generally have the advantage of reaching percolation threshold at lower loadings in comparison to 0D nanomaterials, providing also higher λ values, due to their improved ability to form thermally conductive pathways. [8, 9] In the light of these considerations, the POSS modification protocol developed for commercial alumina NPs has been extended to elongated α-alumina particles (α-Al_2O_3), obtained by hydrothermal synthesis.

Hereafter the synthesis, characterization and functionalization of α-Al_2O_3 with POSS nanounits, as well as their exploitation in the preparation of thermally conductive polybutadiene nanocomposites, will be comprehensively described.

3.7.1 - Hydrothermal synthesis of α -Al_2O_3 nanorods

Materials: Aluminium Nitrate nonohydrate was acquired from Sigma Aldritch, Urea was acquired from Alfa Aesar and used as received.

Alumina nanorods were prepared according to a previously reported experimental synthesis. [10] In a typical procedure, 7,5 $Al(NO_3)_3 \cdot 9H_2O$ and 3,6 g urea were mixed with 20 mL distilled water. After 30 min of stirring, the resulting solution was transferred into a Teflon-lined stainless autoclave (45 cm^3 capacity). The autoclave was sealed and maintained in an electric oven at 120 °C for 24 h, and then cooled to room temperature naturally. The product was carefully collected by centrifugation and washed with distilled water and then dried at room temperature. To get the final α–alumina the precursor was calcined for 4 h at 1200 °C (ramp of 3°C/min) in a muffle furnace (Scheme 3).

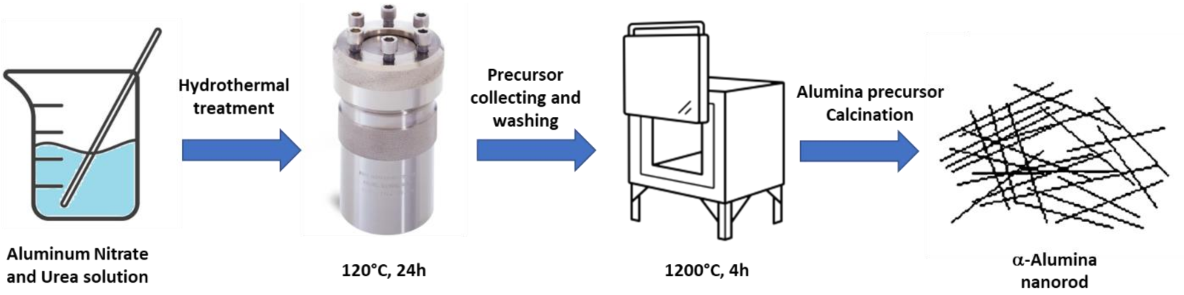

Scheme 3.3 – Experimental procedure of the α-alumina nanorods synthesis

3.7.2 - Structural, morphological and surface characterization of α-alumina nanorod fillers

The structural features of the materials obtained from hydrothermal synthesis and after calcination have been assessed by XRD (Fig. 3.12). The precursor have a Dawsonite like structure ($NaAl(CO_3)(OH)_2$), but Na^+ is substituted with NH_4^+ (i.e. $(NH_4)Al(CO_3)(OH)_2$) (Fig. 3.12, left side). Due to the difference in the radius of this cations, a shift of the peaks respect to dawsonite structure is present. After calcination, the diffractogram shows the characteristic pattern of α-alumina (JCPDS card no. 42-1468) and no other different phases are detectable (Fig. 3.12, right side)

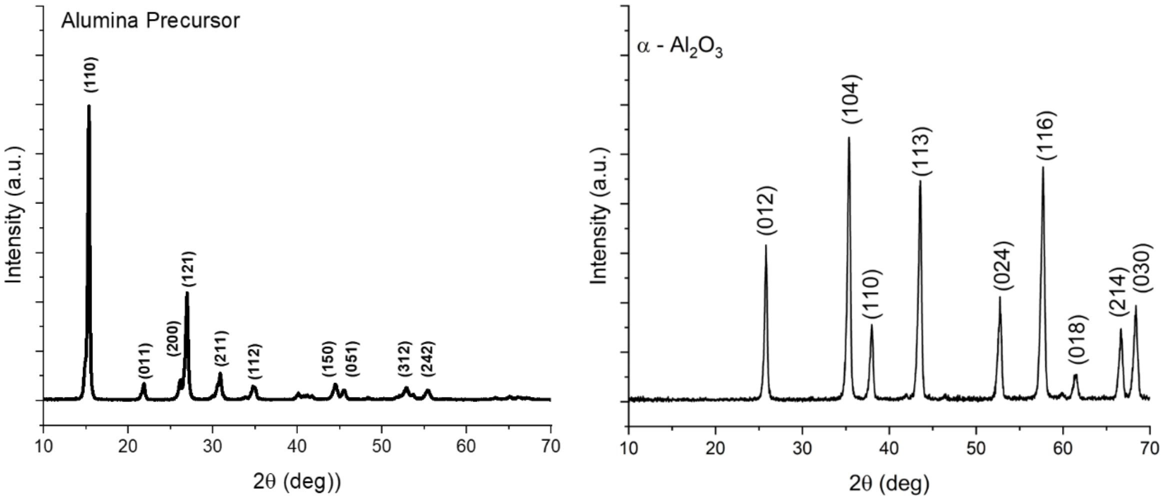

Figure 3.12 – XRD of hydrothermally synthetized alumina precursor and α-alumina nanorod

The morphology of the alumina nanorods was TEM (Fig. 3.13). Elongated structures with micrometric length, width of ~ 200 nm and aspect ratio > 10 are clearly visible in the images (Fig. 3.13a). At a higher resolution, besides some necking among the particles, clearly defined edges can be detected (Fig. 3.13a’). After surface modification with POSS nanounits, no relevant morphological changes can be detected (Fig. 3.13b) However, NPs boundaries appear less defined than in naked nanorods (Fig. 3.13b’), suggest the presence of POSS domains at the alumina surface.

First evidence of the occurred functionalization of alumina nanorods both with MPTMS and POSS was obtained from FTIR spectra (Fig. 3.14). The spectra are similar to ones retrieved for the commercial alumina NPs. The presence of peaks attributable to the functionalizing agents in the α-Al_2O_3-MPTMS and α-Al_2O_3@POSS indicate the effective functionalization of the α-Al_2O_3 nanorod. The quantitative determination of the amount of grafted functionalizing agents was performed by TGA analysis (Figure 3.15). The results, shown in Table 3.4, are rather similar to those obtained for commercial alumina NPs.

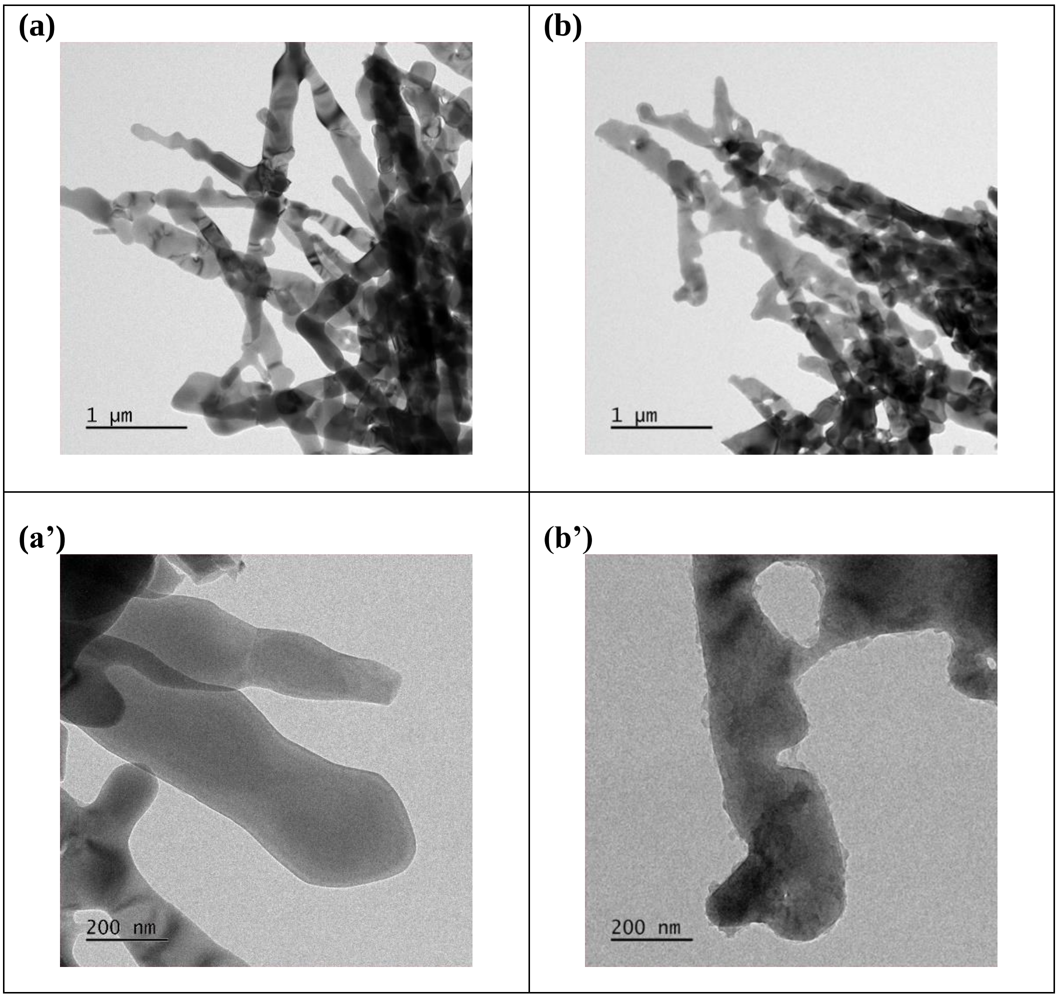

Figure 3.13 –TEM images of α-Al_2O_3 (a, a’) and α-Al_2O_3@POSS (b, b’)

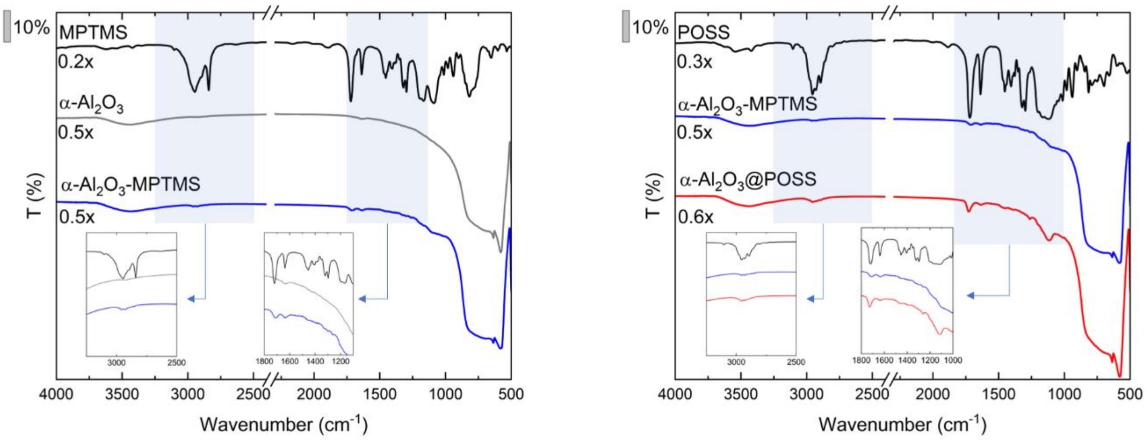

Figure 3.14 – FT-IR spectra of: (a) MPTMS (black line), pristine α-Al_2O_3 (grey line) and α–Al_2O_3-MPTMS (blue line); (b) pure POSS (black line), α-Al_2O_3-MPTMS (blue line) and α-Al_2O_3@POSS (red line); the insets show the magnifications of the spectral regions related to the functional groups of MPTMS (top) and of the POSS units (bottom).

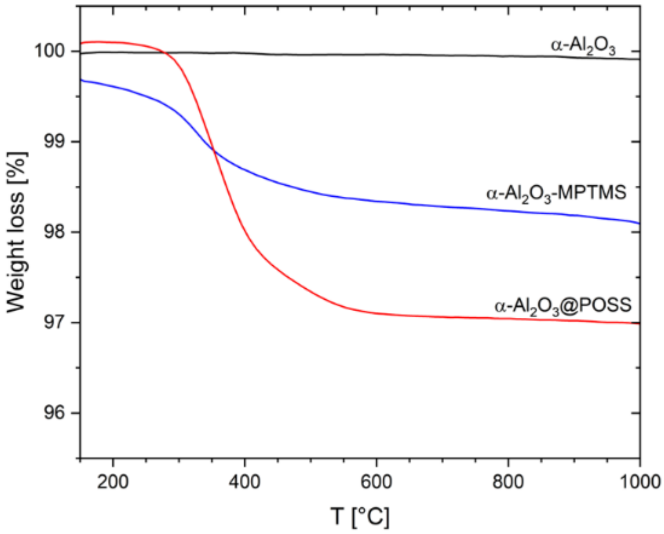

Figure 3.15 – TGA curves of bare α-Al_2O_3 (black line), α-Al_2O_3-MPTMS (blue line) and α-Al_2O_3@POSS (red line)

Table 3.4- Surface density of functional molecules on α-Al_2O_3-MPTMS and Al_2O_3@POSS

Sample	Functionalizing Agent	Net weight loss (wt. %)	M_w (g mol^{-1})	Grafted amount (mmol g^{-1})
α-Al_2O_3-MPTMS	MPTMS	1.64	248.4	$1.33 \cdot 10^{-4}$
α–Al_2O_3@POSS	POSS	3.04	1434.0	$4.79 \cdot 10^{-5}$

3.7.3 - Nanocomposites preparation and characterization

Following the same procedure used for commercial alumina NPs, different concentrations (20, 30, 40 and 50 wt%) of bare α-Al_2O_3 α-Al_2O_3-MPTMS and α-Al_2O_3@POSS particles have been incorporated into PB to produce composites with an average thickness of 500–650 μm.

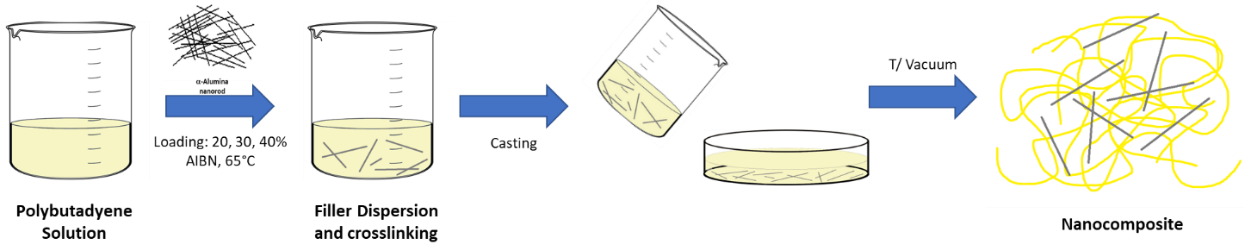

Scheme 3.5 – Experimental procedure for the preparation of PB/α-alumina composites by solution blending.

Hereafter, the different nanocomposites will be labeled PB/α-Xal$_2$O$_3$Y where X refers to the different percentage of filler (X= 20, 30, 40, 50 wt. %), while Y denotes the different surface functionalization (-MPTMS, @POSS).

The influence of alumina nanorods incorporation on the polymer matrix, was initially assessed by FTIR. In detail, Figure 16 shows the spectra of PB, α–Al$_2$O$_3$@POSS and of select corresponding nanocomposites. As already described for the systems enclosing commercial alumina NPs, the introduction of the filler does not significantly affect the spectral features of the PB in the composite, and the more relevant modifications in the spectral features can be observed at lower wavenumbers, i.e. decrease in the intensity of the absorption band at 1654 cm^{-1} relatable to the stretching C=C of PB chains associated to the self-polymerization of the POSS methacrylic groups. At very lower wavenumbers, the broad band at at ~ 1100 cm^{-1} of the Si–O stretching of the POSS cages and the signal of alumina below 800 cm^{-1} are dominating the spectra.

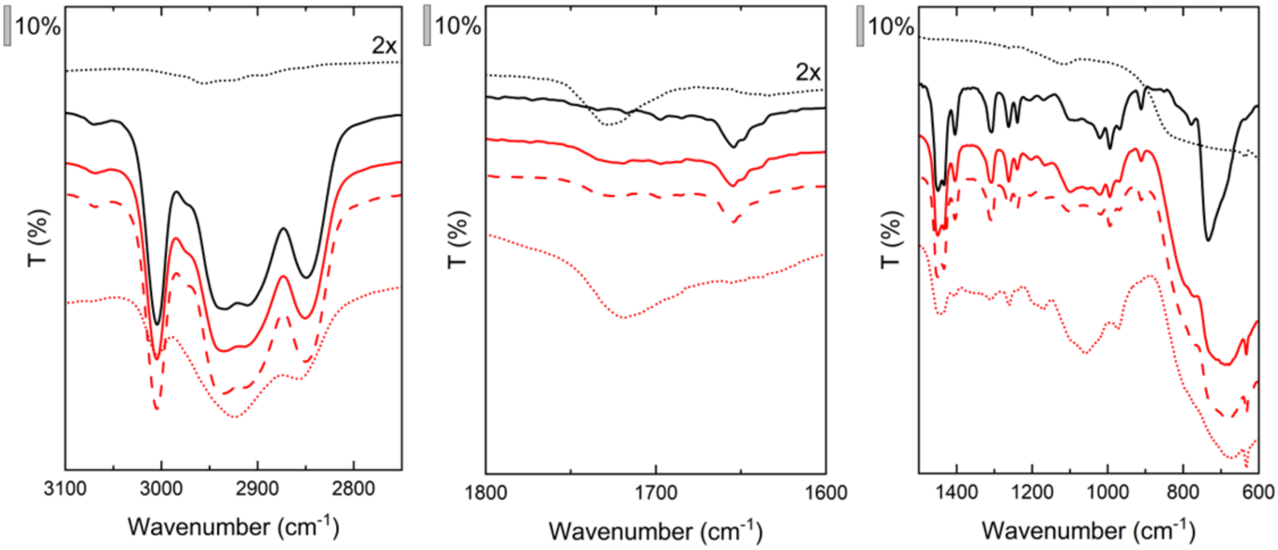

Figure 3.16 – FTIR spectra of α-Al$_2$O$_3$@POSS (black-dotted line), homopolymerized PB (black-line), PB/20α-Al$_2$O$_3$@POSS (red line), PB/30α-Al$_2$O$_3$@POSS (red-dashed line) and PB/40α-Al$_2$O$_3$@POSS (red-dotted line) in the a) 2750-3100 cm^{-1}, b) 1600-1800 cm^{-1} and c) 600-1500 cm^{-1} spectral regions.

The PB/α-Al$_2$O$_3$@POSS composites were also characterized by SEM (Fig. 3.17). The images shows that good dispersion of the filler is achieved especially at low loading (Fig 3.17a). At a higher loading (Fig. 3.17b), the filler aggregation increases together with a certain degree of interconnection between the elongated particles. From the cross-section of the two composites (Fig. 3.17a' and b') an orientation of the filler could be stated especially for PB/20α-Al$_2$O$_3$@POSS composite. This behaviour could be associated to the solution blending methodology, in which filler may possibly reorganize during solvent evaporation.

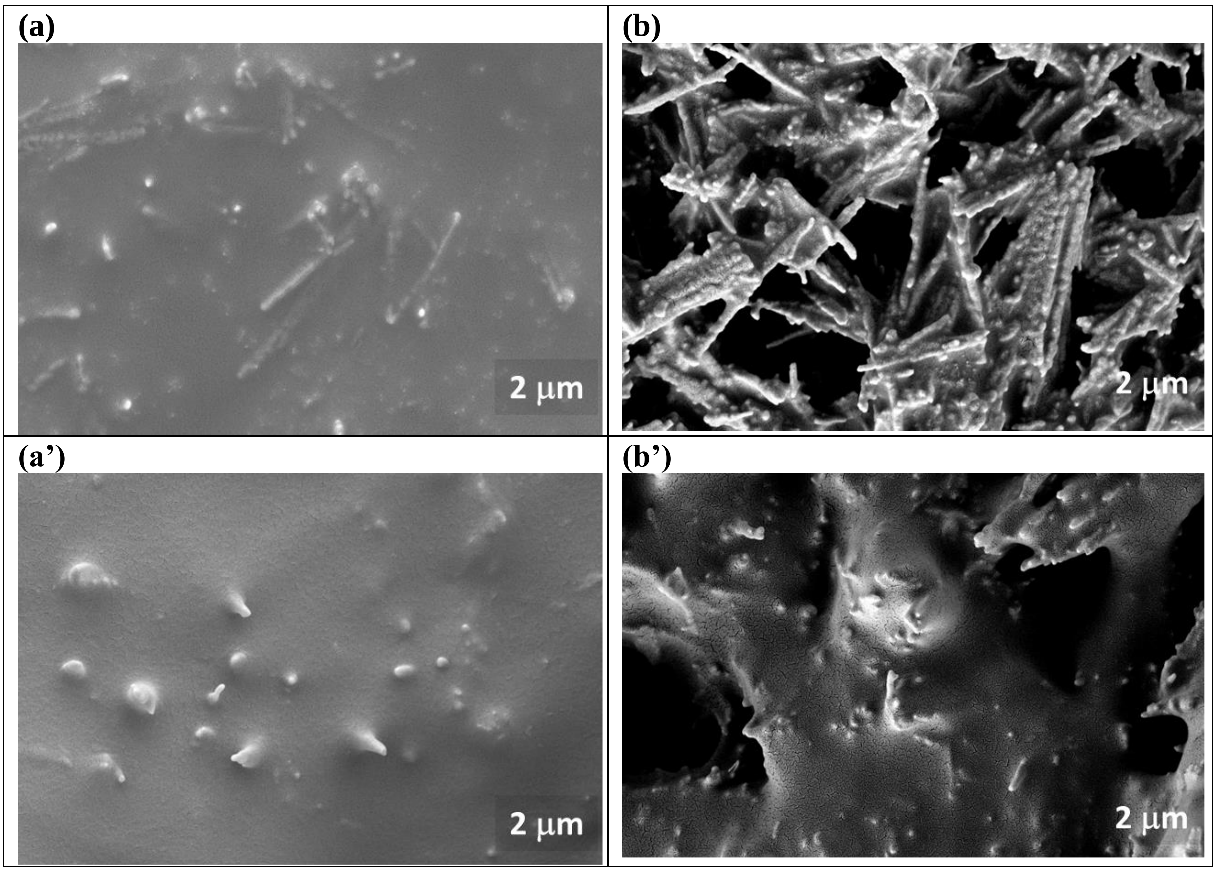

Figure 3.17 – SEM images of a) PB/20α-Al$_2$O$_3$@POSS and b) PB/40α-Al$_2$O$_3$@POSS nanocomposites and their lateral cross sections (a', b')

3.7.4 – Preliminary thermal conductivity measurements on PB/α-Al$_2$O$_3$@POSS

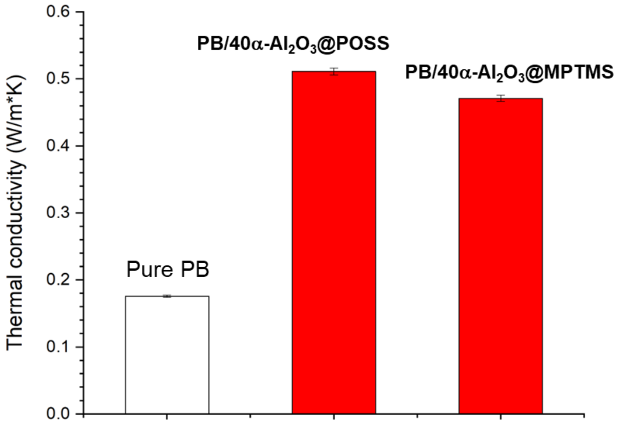

Figure 3.18 – thermal conductivity of neat PB, PB/40α-Al$_2$O$_3$@MTPMS and PB/40α-Al$_2$O$_3$@POSS composites

The thermal transport properties of PB/α–Al_2O_3@POSS composites was just preliminary evaluated by LFA. Figure 3.18 shows the results of the analysis for PB/40α-Al_2O_3@MTPMS and PB/40α-Al_2O_3@POSS composites. It can be easily observed that the introduction of a volume fraction of 13 v/v% the hybrid filler produces a very remarkable increase of the λ, much higher than that of neat PB and compared to the value retrieved at the same filler concentration for composite enclosing Al_2O_3@POSS constituted by smaller and almost spherical γ-alumina NPs (see Fig. 3.10b). These results suggest that the tailoring of both crystalline phase and morphology of the conductive filler allows to "take the best" from the intrinsic thermal conductivity of Al_2O_3 and from the anisotropic features of the particles, which allow, even at a very low loadings, the production of continuous and effective thermal conductive pathways in the rubber matrix. Further analysis are in progress on these samples.

In summary, Al_2O_3@POSS hybrid filler where alumina particles and POSS units belong to the same functional structure, appear promising candidates for upgrading both the thermal transport and the mechanical properties of rubber composites for tires.

In fact, the peculiar hybrid structure of the hybrid filler, where a shell of POSS nanounits decorate the alumina surface, besides assuring the compatibility between filler and polymer host, allows a homogeneous distribution and a continuous networking of the alumina NPs. This positively influences heat transport, providing thermal conductive pathways and leading to the raise of the thermal diffusivity even at low filler loadings, with a potential reduction of filler utilization in rubber composite formulations.

3.8 - Bibliography

[1] M. D'Arienzo *et al.*, "Hybrid SiO 2 @POSS nanofiller: a promising reinforcing system for rubber nanocomposites," *Mater. Chem. Front.*, vol. 1, no. 7, pp. 1441–1452, 2017.

[2] M. Redaelli *et al.*, "On the key role of SiO2@POSS hybrid filler in tailoring networking and interfaces in rubber nanocomposites," *Polym. Test.*, vol. 65, pp. 429–439, Feb. 2018.

[3] S. Gates-Rector and T. Blanton, "The Powder Diffraction File: a quality materials characterization database," *Powder Diffr.*, vol. 34, no. 4, pp. 352–360, Dec. 2019.

[4] P. Tarte, "Infra-red spectra of inorganic aluminates and characteristic vibrational frequencies of AlO4 tetrahedra and AlO6 octahedra," *Spectrochim. Acta Part A Mol. Spectrosc.*, vol. 23, no. 7, pp. 2127–2143, Jul. 1967.

[5] M. Fedel, E. Callone, S. Diré, F. Deflorian, M.-G. Olivier, and M. Poelman, "Effect of Na-Montmorillonite sonication on the protective properties of hybrid silica coatings," *Electrochim. Acta*, vol. 124, pp. 90–99, Apr. 2014.

[6] T. Takahashi, T. Ohkubo, K. Suzuki, and Y. Ikeda, "High resolution solid-state NMR studies on dissolution and alteration of Na-montmorillonite under highly alkaline conditions," *Microporous Mesoporous Mater.*, vol. 106, no. 1–3, pp. 284–297, Nov. 2007.

[7] S. Borsacchi *et al.*, "Rubber-Filler Interactions in Polyisoprene Filled with In Situ Generated Silica: A Solid State NMR Study," *Polymers (Basel).*, vol. 10, no. 8, p. 822, Jul. 2018.

[8] N. Burger, A. Laachachi, M. Ferriol, M. Lutz, V. Toniazzo, and D. Ruch, "Review of thermal conductivity in composites: Mechanisms, parameters and theory," *Prog. Polym. Sci.*, vol. 61, pp. 1–28, Oct. 2016.

[9] X. Huang, P. Jiang, and T. Tanaka, "A review of dielectric polymer composites with high thermal conductivity," *IEEE Electr. Insul. Mag.*, vol. 27, no. 4, pp. 8–16, 2011.

[10] J. Li, W. Li, X. Nai, S. Bian, X. Liu, and M. Wei, "Synthesis and formation of alumina whiskers from hydrothermal solution," *J. Mater. Sci.*, vol. 45, no. 1, pp. 177–181, 2010.

Chapter 4 - Coupling thermal conductivity & self-healing in rubber nanocomposites: Al_2O_3@POSS and Al_2O_3@ZnO in XNBR matrix as cases of study

4.1 - Introduction

According to Eurostat, the statistical office of the European Union, Europe is producing about 2,5 billion tonnes of waste every year. (Fig. 4.1a) Although municipal wastes affect less than 10% on that amount, the impact on nature is visible and complex. Due to this European Union (EU) parliament introduced stricter limits in order to reduce the amount of dangerous chemicals in waste and production processes, banning certain chemicals and keeping pollutants away from recycling. From 2018 EU is trying to reach ambitious goals on recycling, packaging waste and landfill to promote the shift towards a more sustainable model known as the *circular economy*. [1] Circular economy in contrast with linear economy, is a model of production and consumption in which life cycle of a product is extended by sharing, leasing, reusing, repairing, renovating and recycling. This model implies to reduce waste by reintroducing the materials that compose the object at the end of its life in the economy, creating further value and reducing the volume of raw materials needed (Fig. 4.1b).

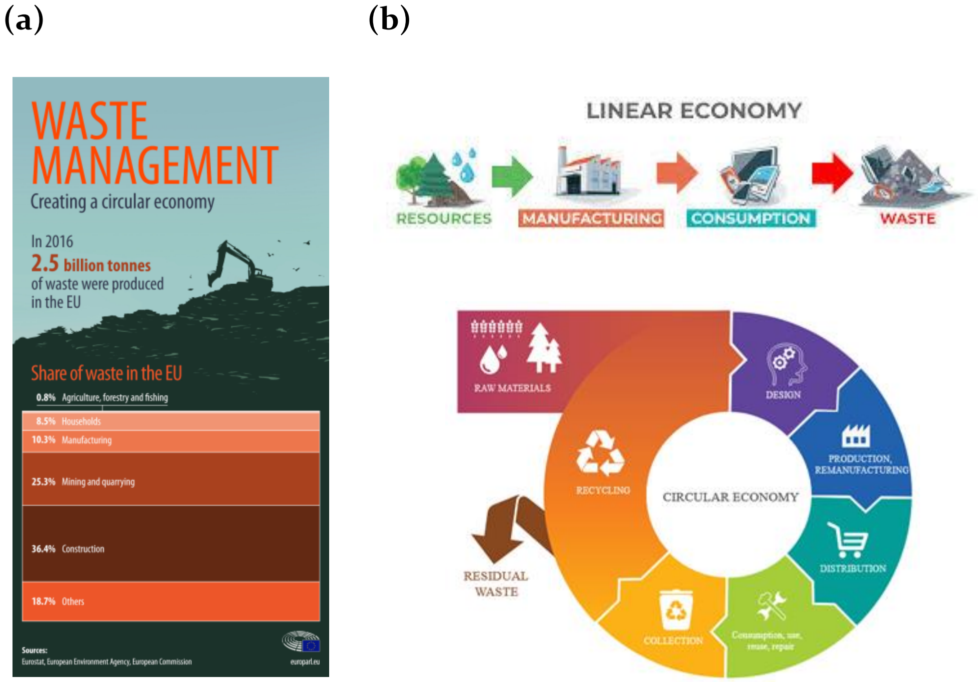

Figure 4.1 – (a) Eurostat analysis of European waste; (b) linear and circular economy models

In this context, smart materials which are capable of automatic healing and restoration of damage after suffering external damage appear promising alternatives to fulfil the reduction of waste production as well as the principles of circular economy. [2–5] Inspired by the energy dissipation and self-healability of sacrificial bonds in nature, several recent research efforts have been devoted to the incorporation of these sacrificial bonds into synthetic and natural polymers for imparting both mechanical strength and self-healing ability. [6–9] To design self-healing polymer composites, non-covalent interactions, such as H-bonding, metal-ligand coordination, π-π stacking, van der Waals, ion-dipole, hydrophobic and host-guest interactions, which exhibit a reversible association-dissociation mechanism, have been exploited. However, this often results in poor mechanical performance. [10–12] Self-healing polymer composites have been applied in many fields and several attempt were also directed to tire application [13]. However, in conventional natural or synthetic rubber composites, the presence of a stable covalently bonded network hinders the restoring upon damage and therefore they usually do not show self-healing. Therefore, a synergistic alliance between robust mechanical properties and virtuous self-healing ability remains a challenging task in order to upgrade the tire durability and, consequently, its safety. The healing ability of polymer composites mainly depends on: (i) the filler dispersion in the matrix, and (ii) the filler-polymer interfacial interactions. The former governs the segmental dynamics and the displacement of polymer chains, while the latter defines the strength and conformational relaxations of the polymer chains. [14–16] Connected to these parameters, three key concepts guarantee self-healing in polymer composites [17]: i) localization, ii) temporality and iii) mobility. Localization is correlated with the scale and position of the damage. Damages in fact can be macro or microscopic but can arise also at molecular level (i.e. breakage of the material network [18]). Temporality and mobility are two correlated concepts. Temporality indicates the time gap that occurs between the damage and the repair events. This parameter is strictly correlated to the mobility of the material. In fact, it can be assumed that, when a damage is produced, the healing agents need to flow to the damaged site to repair it. High mobility material will promote the diffusion of the healing agent to the damage area and thus the reformation of the broken bonds, allowing faster reparation. Self-healing materials can be classified depending on the healing mechanism in two families, extrinsic and intrinsic. In extrinsic self-healing materials, the healing process is activated by an external agent dispersed in the matrix, generally as capsules. In opposition, in intrinsic self-healing materials, reversible bonds are already present and thus can be restored after the damaging event. [18] Whether intrinsic or extrinsic a self-healing composite should be capable of repairing molecular, micro and macro-scale damages via a transient local increase in the mobility of the polymer chains.

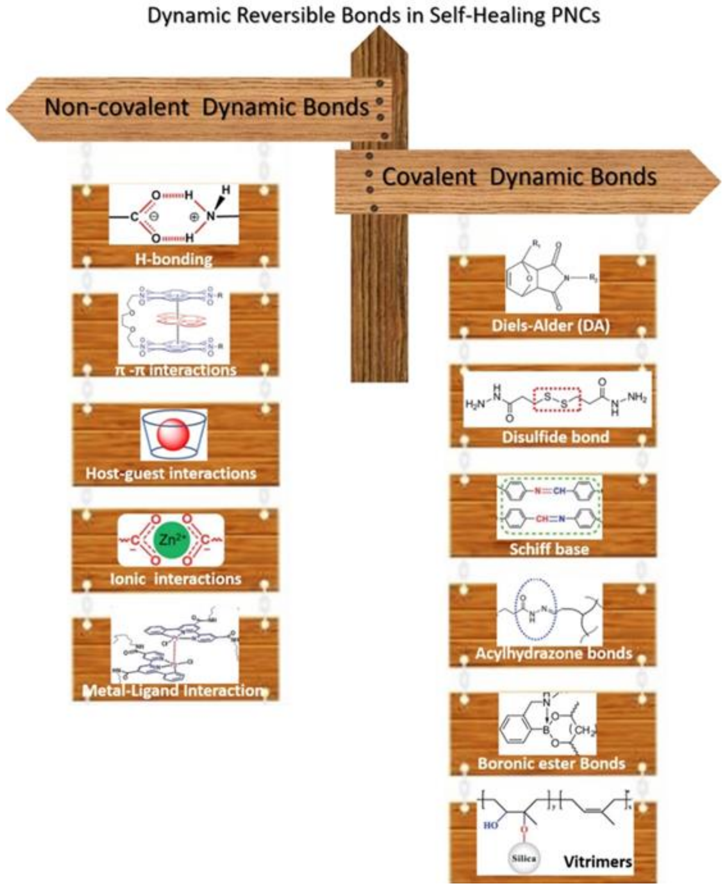

Figure 4.2 – Scheme of the main interactions and or reactions in self-healing materials

The intrinsic self-healing mechanism can be grouped into two broad classes according to the involvement of reversible supramolecular interactions or dynamic covalent bonding (Fig. 4.2). [2] Specifically, non-covalent interactions, such as H bonding, and metal-ligand coordination (see Fig. 4.2), have been exploited in the present thesis to develop reversible networks. The matrix chosen has been a carboxylated nitrile rubber (XNBR), which is a synthetic co-polymer of acrylonitrile (ACN), butadiene and acrylic acid. This kind of rubber has good resistance to oils and diluted acids and bases. Properties of the rubber can be modulated and strictly depend on the ACN content. Introduction of carboxylic groups leads to an increase of tensile and tear modulus and abrasion resistance, but reduction in compression set, water resistance and resilience properties. [19] Due to these properties XNBR is widely used in automotive and aeronautical application for (i.e., hoses and seals) but also in protective gloves for nuclear industry and to produce moulded materials, shoes, adhesives, sponges and expanded foams, sealants and floor mats. XNBR is interesting for the design of self-healing material, since the CN and the COOH groups can be exploited to produce weak and thus dynamic bonds useful for self-healing mechanisms. [20] With this background in mind and considering that, as mentioned in the Introduction, the mitigation of tires overheating effects entails also the problem of a permanent damage of the composites, we pursued the ambitious goal of developing/exploiting filler systems able not only to improve the thermal transport but also to induce self-healing effects in XNBR composites, in order to extend the service-life, the sustainability and the safety of the tires. The first material utilized has been Al_2O_3@POSS hybrid filler (cfr. Chapter 3). The high number of carbonylic groups belonging to the methacrylic terminations of POSS units has been employed to provide H-bond interactions with the carboxylic groups of the XNBR rubber [21]. Although 10 times weaker compared to carbon-carbon (C–C) bonds (~345 kJ mol^{-1}) [22], the H-bonding is strongest among the noncovalent interactions, thus conferring satisfactory mechanical strength and self-healing properties to polymer composites. [23–26] An innovative filler material based on Al_2O_3 and ZnO (i.e. Al_2O_3@ZnO) was also developed to impart remarkable λ and self-healing capability to XNBR, simultaneously. In this case, the possibility to generate ionic dynamic interactions in the rubber matrix by inducing the formation of electrostatic ZnO clusters or ionomers has been exploited [27]. In fact, it was demonstrated that, at a molecular scale, Zn^{2+} ions can form ionic interaction with the carboxylic groups of the XNBR. Anyway, usually not all the ZnO is solubilized in the rubber, thus ionic clusters are formed, where rubber interact with the aggregate (Fig. 4.3). The novel Al_2O_3@ZnO filler was obtained by the modification of a synthetic procedure previously developed in our group. [28] The filler was characterized by TEM, ICP-OES and DRS analysis. Both Al_2O_3@POSS and Al_2O_3@ZnO were then utilized to produce XNBR composites, which were comprehensively characterized in terms of mechanical, self-healing and λ properties.

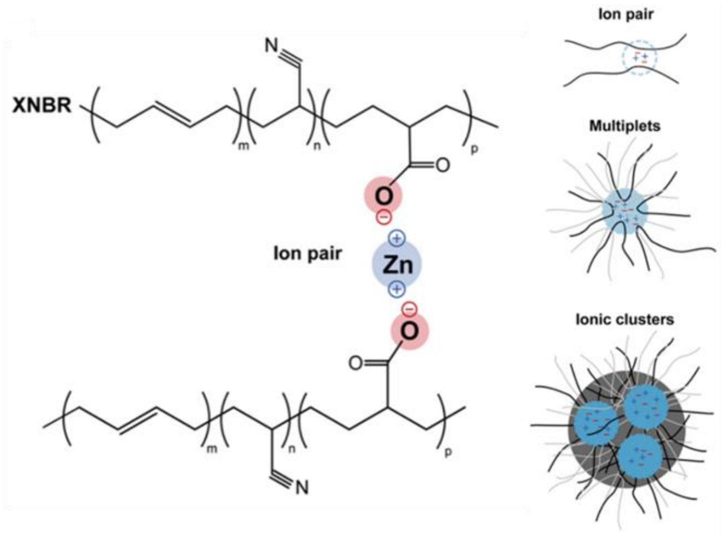

Figure 4.3 – Scheme of ionic interactions between XNBR and ZnO. [27]

4.2 - Preparation and Characterization of Al_2O_3@POSS

The filler was prepared and characterized according to the procedures reported in Chapter 3.

4.3 Preparation of Al_2O_3@ZnO

Materials: Alumina nanorods were synthetized following the procedure described in Chapter 3; Zinc acetate dihydrate ($Zn(CH_3COO)_2{\cdot}2H_2O$), sodium hydroxide (NaOH), ethanol (EtOH) was purchased from Sigma Aldrich.

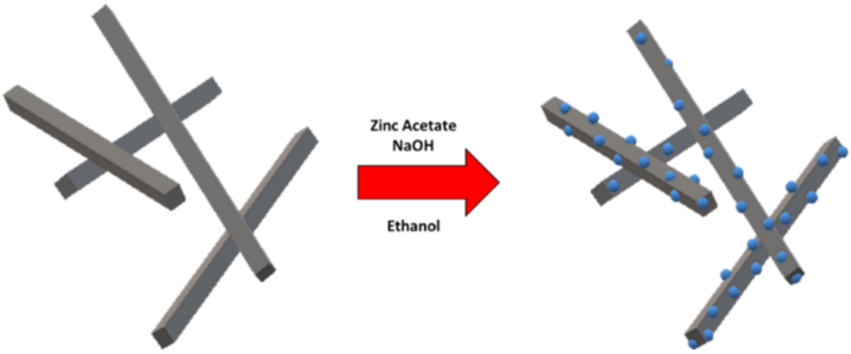

Figure 4.4 – scheme of the synthesis of Al_2O_3@ZnO filler

Al_2O_3@ZnO was synthesized firstly preparing a 0,1 M solution of NaOH in 70 mL of EtOH in a two neck round bottom flask. To this solution was then added 0,33 g of $Zn(CH_3COO)_2{\cdot}2H_2O$ and heated at 65°C for 20 minutes. Lately, 1 g of Al_2O_3 was added and the suspension continuously stirred for additional 20 minutes at 65 °C. After cooling the suspension was vacuum filtered and the solid washed with ethanol, dried and stored. To increase the amount of ZnO in the filler the product of the reaction was subjected to another cycle of the ZnO deposition. The samples obtained after the first and the second cycle of ZnO grafting have been labelled as Al_2O_3@ZnO_I and Al_2O_3@ZnO_II, respectively. A simplified scheme of the reaction procedure is reported in Figure 4.4.

4.4 - Compositional, morphological and spectroscopic characterization of Al_2O_3@ZnO filler

The amount of ZnO grafted on the surface of alumina nanorods was determined by ICP-OES. The analysis revealed the initial presence of 6.3 wt. % ZnO (Al_2O_3@ZnO_I). After the second cycle of the reaction, the amount of ZnO grown on the surface of alumina nanorods increases and reaches the 11 wt. % (Al_2O_3@ZnO_II).

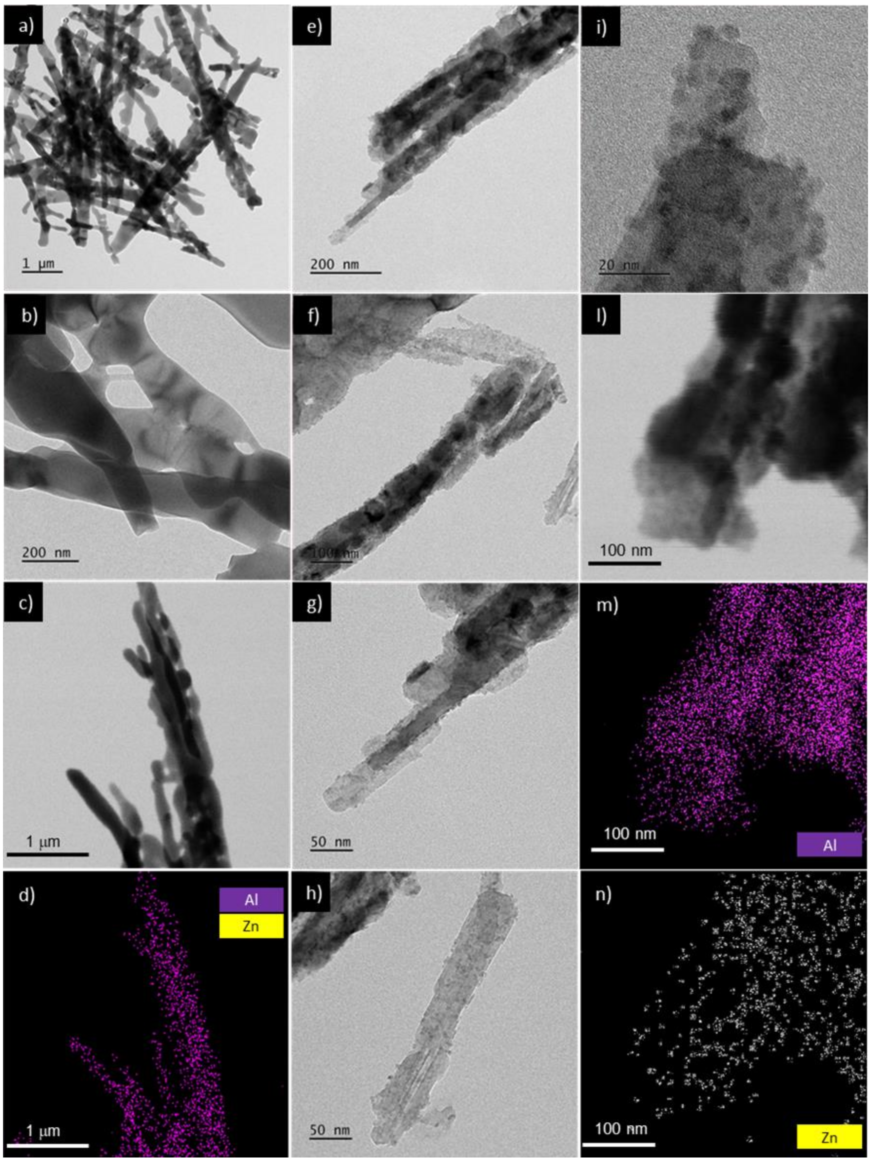

Figure 4.5 – TEM images ad different magnifications of: a-b) alumina nanorods, (e-i) Al_2O_3@ZnO_II. Dark field images and corresponding EDS elemental maps of Al and Zn in: c-d) Al_2O_3 nanorods and l-n) Al_2O_3@ZnO_II

The morphological features of the novel Al_2O_3@ZnO filler were investigated by TEM analysis and compared to those of bare alumina nanorods (Fig. 4.5). As already described in Chapter 3, hydrothermal Al_2O_3 nanorods present elongated structures with micrometric length, width of ~ 200 nm and aspect ratio > 10 (Fig. 4.5a). At a higher resolution, clearly defined edges can be observed (Fig. 4.5b), while EDS elemental analysis on a selected area (Fig. 4.5c) reveals the exclusive presence of Al (Fig. 4.5d) and O (not shown). Upon grafting of ZnO (sample Al_2O_3@ZnO_II), the surface boundaries of nanorods appear less defined (Fig. 4.5e, f) and, at higher magnifications, the presence of tiny NPs becomes detectable (Fig. 4.5g, h). In particular, figure 4.5i highlights the growth onto the crystalline alumina surfaces of amorphous and spherical ZnO NPs with an average diameter of 5 nm. EDS elemental map (Fig. 4.5l-n) allowed to distinguish the presence of Al and Zn, confirming the successful decoration of alumina nanorods with ZnO. Similar images have been obtained for Al_2O_3@ZnO_I, though with a minor occurrence of ZnO NPs covering the Al_2O_3 surface.

To further prove the presence of ZnO a UV-DRS analysis was carried out on both Al_2O_3@ZnO_I and Al_2O_3@ZnO_II samples. The material shows the typical reflectance spectra (Fig. 4.6a), with a maximum of light adsorption centered at 370 nm, with just minimal differences between the material after 1 or 2 deposition cycles. Kubelka-Munk analysis of the data (Fig. 4.6b) shows an energy blue-shift of band gap energy (E_g = 3.48 eV) compared with the conventional value retrieved for bulk ZnO (Eg = 3.37 eV), in agreement with the small and amorphous ZnO NPs dimensions revealed by TEM for these systems. These results match well with our previous investigation on mesoporous silica NPs decorated by ZnO. [28, 29]

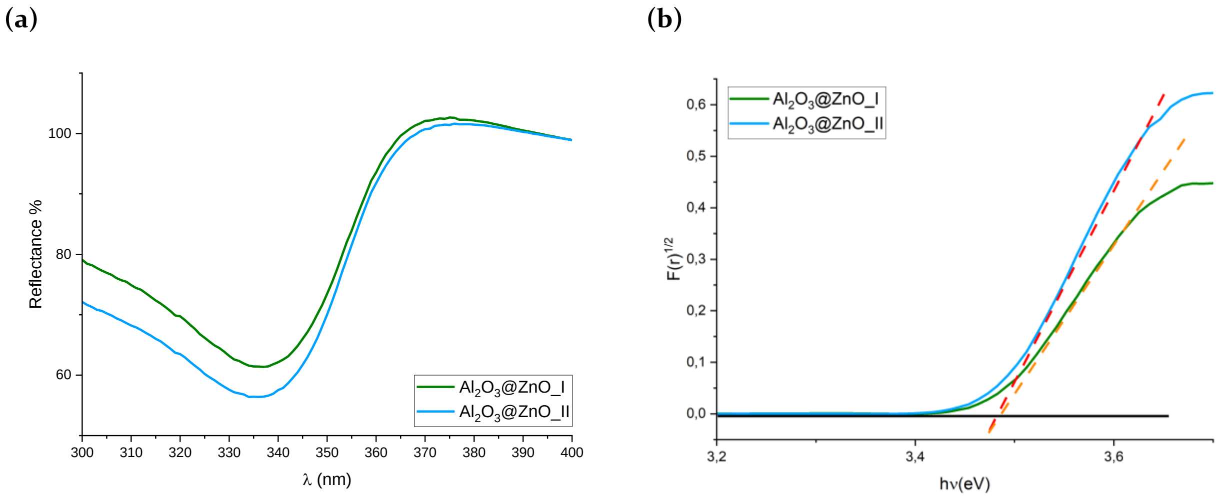

Figure 4.6 – (a) UV diffuse reflectance spectra vs wavelength of Al_2O_3@ZnO materials and (b) Kubelka-Munk analysis

4.5 - Al_2O_3@POSS compounds preparation and functional characterization

Materials: Krynac® X 750, XNBR with 27% of ACN content and 7% of carboxyl groups was supplied by Arlanxeo; $FeCl_3*6H_2O$ was acquired from Alfa Aesar.

The Al_2O_3@POSS nanocomposites were prepared in a two-roll rubber mill water chilled. Firstly 108 g of XNBR were masticated for 4 minutes and subsequently 20 g of commercial alumina NPs or Al_2O_3@POSS were introduced in the rubber. This amount allows to attain a loading of 15 wt. % of filler in the composite. Finally, 5,4 g of $FeCl_3*6H_2O$ (corresponding to 5 PHR) were introduced as crosslinking agent. In fact, this salt activates the crosslinking reaction through coordination of Fe^{3+} ions by CN groups of XNBR. [30] A reference compound without alumina filler was also produced for comparison. The mixing time was of about 30 minutes for all the compounds. The composites have been labelled as XNBR, XNBR/15%_Al_2O_3, XNBR15%_Al_2O_3@POSS corresponding to the unfilled, the commercial alumina and the Al_2O_3@POSS filled composites, respectively. In order to study the curing behaviour of the composites curing curves at 170°C for 6 minutes have been obtained in a rheometer (see experimental details and explanation in Appendix). The curves reported in Figure 4.7 show that $FeCl_3$ effectively acts as curing agent and the higher torque values obtained for XNBR/15%_Al_2O_3 and XNBR/15%_Al_2O_3@POSS compared to neat XNBR may suggest that effectively alumina filler is acting as a reinforcing agent. Moreover, it is important to notice that curing curves do not achieve a plateau, but the torque steadily increases along the curing time. This is a known behaviour in ionically crosslinked rubbers. [27, 31, 32] From these curves the t_{90} value, i.e. the optimum time required for reaching 90% of the maximum achievable torque or network density at the given temperature, was determined. As expected, the t_{90} only differ between the unfilled and the filled composite, suggesting that functionalization does not affect the curing process. Moreover, maximum torque results to be higher for the bare alumina suggesting the occurring of different interaction between the filler and the matrix. [33]

The composites were cured in a hot press at 170°C for the respective t_{90} values using a squared mold with length of 11 cm and thickness of 2 mm. For the determination of λ a squared sample with 4 cm of length and a thickness of 5 mm was necessary. In order to achieve a homogeneous curing, in such a sample the curing time was equal to t_{90} +3 minutes.

Table 4.1 – maximum torque and t90 of the reference and alumina filled composites

Sample	**Maximum Torque** (dNm)	**t_{90}** (min)
XNBR	5.30	46
XNBR_15%Al_2O_3	8.05	42
XNBR_15%Al_2O_3@POSS	6.94	41

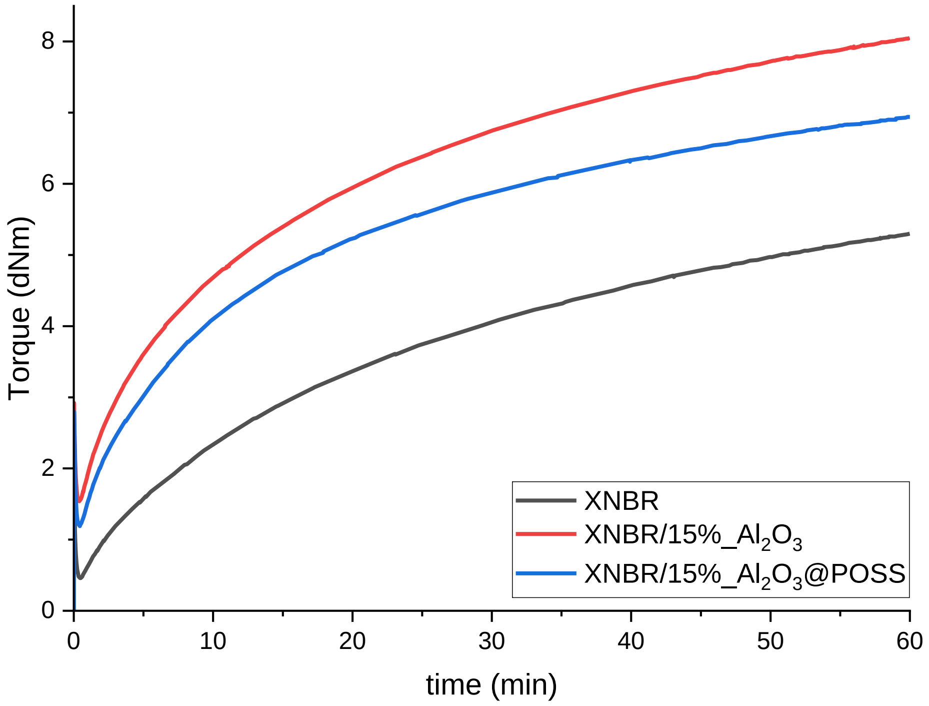

Figure 4.7 – Curing curves of XNBR (black), XNBR/15%_Al_2O_3 (red), XNBR/15%_Al_2O_3@POSS (blue).

The crosslink density (n) of the cured samples was then evaluated with a swelling technique. Briefly, for each compound, 5 pieces of the cured rubber were weighted (m_1) and submerged in toluene for 72 hours. After this time, the wet pieces were weighted again (m_2), then completely dried and re-weighted (m_3). The 3 masses were used in the Flory–Rehner equation to calculate the crosslink density of the composites. Results are summarized in Figure 4.8. The n value suggests that introduction of alumina effectively increases the crosslink density of the composite independently from the surface functionalization. This is clearly correlated to the interaction between alumina surface and the CN or COOH groups of the rubber. Despite OH groups are lower in functionalized alumina; crosslink density value appears almost similar to that of bare particles. This behaviour suggests that other kind of interactions are arising, hopefully the desired H-bond interactions among methacryl POSS termination and rubber carboxylic groups.

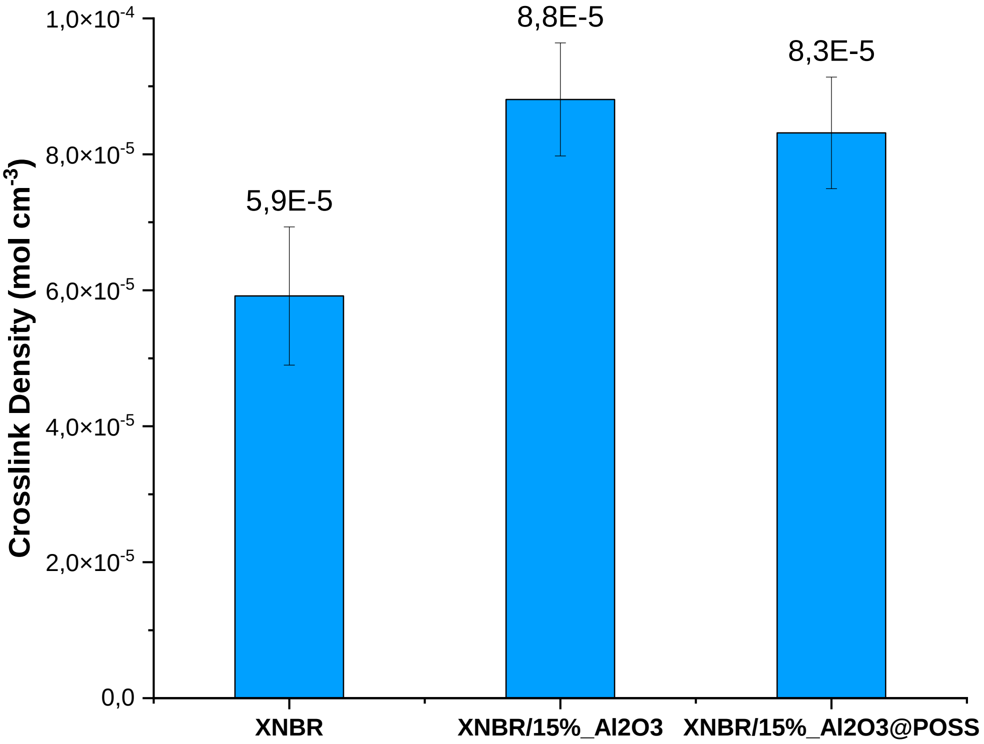

Figure 4.8 – Average crosslink density obtained by Flory–Rehner equation for XNBR, XNBR/15%_Al_2O_3 and XNBR/15%_Al_2O_3@POSS

Thermal conductivity of the composites was measured by the use of a FOX50 heat flowmeter instrument (see details in Appendix). The results of the measurements are shown in table 4.2 and indicate that the inclusion of bare commercial alumina in XNBR substantially does not affect the λ of the composite, while a noticeable increase of thermal transport (+ 54 %) is achieved when even small loadings (i.e. 15 wt. %) of Al_2O_3@POSS are used as filler. As already observed for PB in chapter 3, POSS functionalization, besides assuring the compatibility between filler and polymer host, allows a homogeneous distribution and a continuous networking of the alumina NPs. This may upgrade the heat transport also in XNBR leading to a raise of the thermal diffusivity even at low filler concentrations.

Table 4.2 – Thermal Conductivity of XNBR, XNBR/15%_Al_2O_3 and XNBR/15%_Al_2O_3@POSS measured by FOX50 instrument.

	XNBR	XNBR/15%_Al_2O_3	XNBR15%_Al_2O_3@POSS
λ ($W\ m^{-1}\ K^{-1}$)	0.1852	0.1865	0.2007
Error	±0.0002	±0.0003	±0.0001

Self-healing properties of XNBR/15%_Al_2O_3@POSS were evaluated firstly producing rectangular shaped specimens of cured rubber and then cutting them in two parts, to induce a damage. The two parts were then put in a rectangular mold and pressed at 60°C and 200 bar for 24h to drive the healing process (Fig. 4.9a).

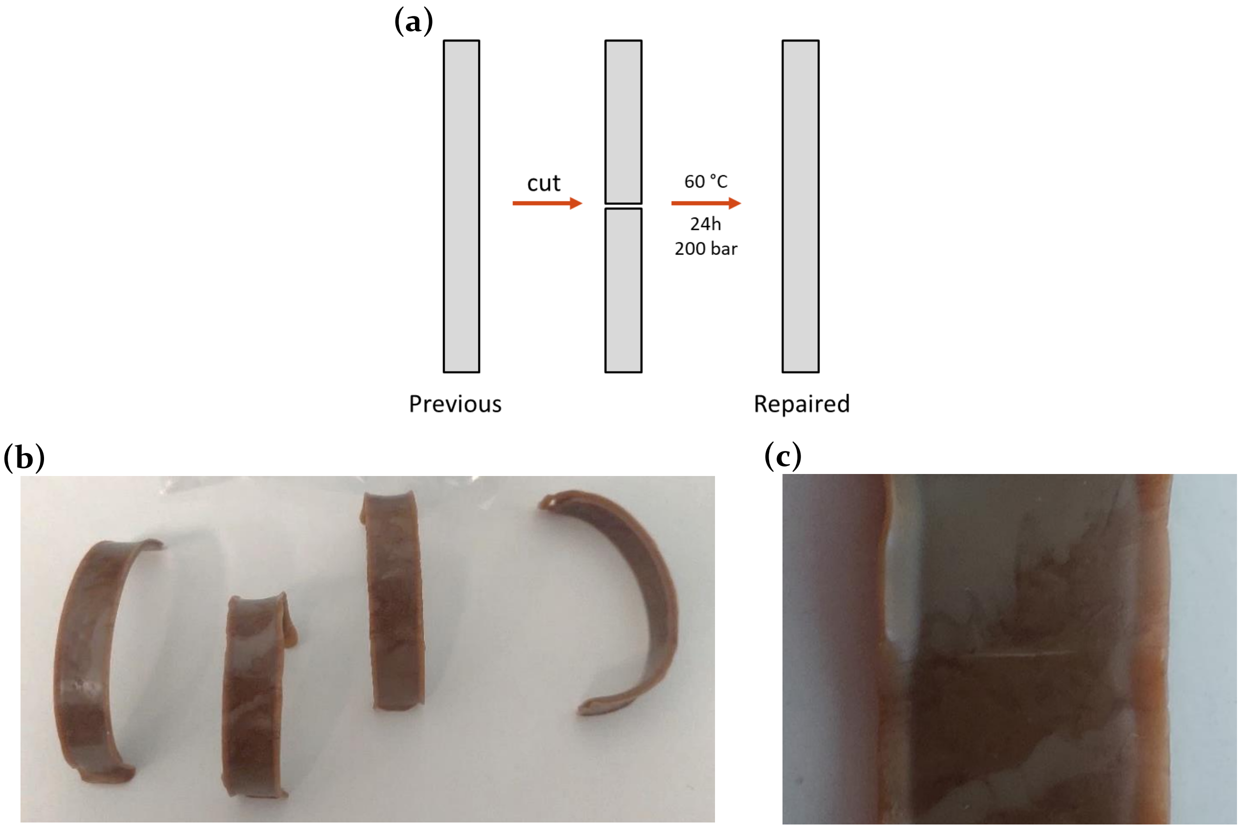

Figure 4.9 – (a) Scheme of healing procedure; pictures of (b) the self-standing samples and (c) a magnification on the cut after the healing thermal treatment

The tensile strength before and after the healing treatment was assessed and the healing efficiency ($\eta\%_{SH}$) was calculated by the following equation (1):

(1)
$$\eta\%_{SH} = \frac{Tensile\ Strength_{Healed}}{Tensile\ Strength_{Pristine}} * 100$$

At least three samples for each compound were analyzed and the average tensile strength (σ) values was calculated. In this case, the treated self-standing samples (Fig. 4.9b) result to be only partially healed as more clearly visible in Figure 4.9c. Accordingly the calculated $\eta\%_{SH}$ resulted slightly lower than 60%. These results, besides supporting a certain degree of self-repairing capability imparted by Al_2O_3@POSS to the XNBR matrix, indicate that an increased filler concentration is probably required in order to guarantee a satisfactory self-healing behavior. Moreover, the bending of the sample after the healing treatment could generate internal stresses and network inhomogeneities that may affect the mechanical properties and the self-healing features of the material. Further investigation will be done to shed light on this point.

4.6 - Al_2O_3@ZnO compounds preparation and functional characterization

Materials: Krynac® X 750, XNB with 27% of ACN content and 7% of carboxyl groups was supplied by Arlanxeo; micrometric ZnO was obtained from Sigma Aldrich.

The XNBR/Al_2O_3@ZnO composites formulations were developed in order to have a constant concentration of ZnO, equal to 10 PHR (Table 4.2). Typically, XNBR was initially masticated in two roll mill and then filler and ZnO were added. Compounding time was fixed to about 20 minutes.

Table 4.2 – Formulations of Al_2O_3 and Al_2O_3@ZnO XNBR filled composites

SAMPLE	XNBR/ ZnO	XNBR/ZnO/ 10_Al_2O_3	XNBR/ZnO/ 10_Al_2O_3@ZnO_I	XNBR/ZnO/ 30_Al_2O_3@ZnO_I	XNBR/ZnO/ 10_Al_2O_3@ZnO_II
RUBBER	**PHR**				
XNBR	100	100	100	100	100
FILLER	**PHR**				
Al_2O_3		10			
Al_2O_3@ZnO_I			10	30	
Al_2O_3@ZnO_II					10
CURING AGENT	**PHR**				
ZnO	10	10	9.37	7.70	8.92

The curing curves of the composites were measured at 160°C and the t_{90} values were obtained. As visible from table 4.3, the t_{90} values become smaller when the Al_2O_3@ZnO filler is included in the formulation. This could be correlate to the nanometric size of ZnO supported on the alumina surface that is more reactive than the micrometric commercial one, and is capable of accelerating the curing process.

Table 4.3 – t_{90} of the references and ZnO/alumina filled composites

Sample	**t_{90}** (min)
XNBR/10ZnO	10
XNBR/10ZnO/10Al_2O_3	9
XNBR/10ZnO/10Al_2O_3@ZnO_I	7
XNBR/10ZnO/30Al_2O_3@ZnO_I	8
XNBR/10ZnO/10Al_2O_3@ZnO_II	8

Composites were cured for their respective t_{90} in a hot press working at 200 bar. Crosslink density was then determined, following the same procedure described before. Results are shown in Figure 4.10 and indicate a very poor variation of the cross-link density upon incorporation of the filler in XNBR.

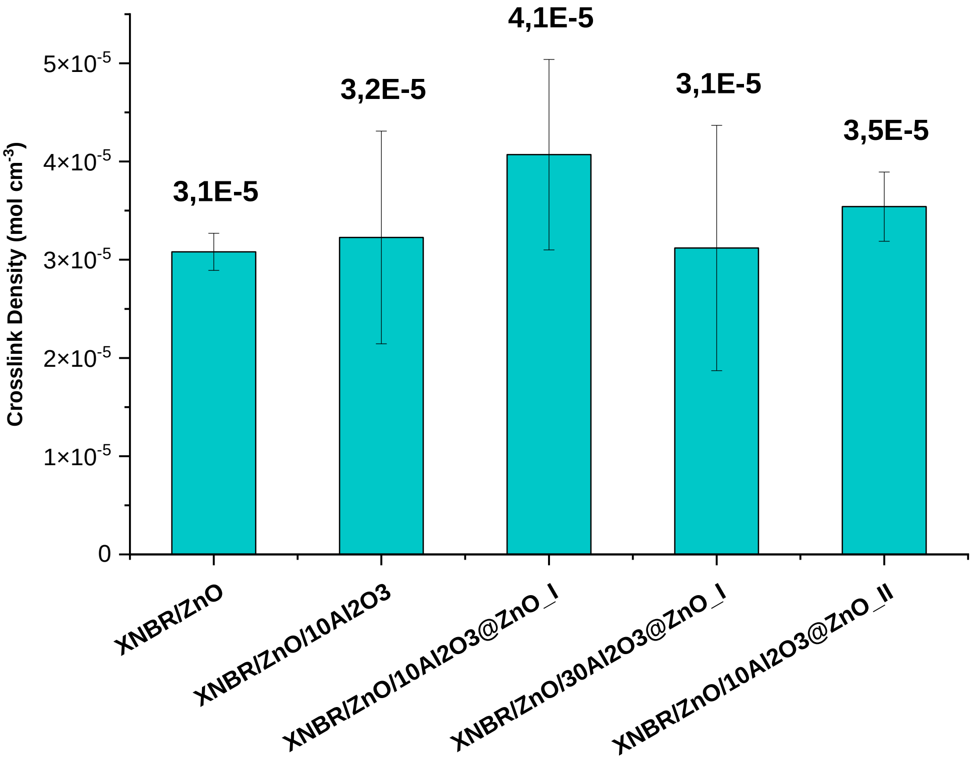

Figure 4.10 – Crosslink density value of Al_2O_3 and Al_2O_3@ZnO XNBR filled composites

As previously described, tensile strength (σ) before and after the healing treatment was measured on at least three samples for each compound and the retrieved average values are summarized in Figure 4.11, with the corresponding $\eta\%_{SH}$ reported in Table 4.4.

Table 4.4 – Values of tensile strength of the composites before and after healing treatment, and relative healing efficiency.

Sample	**σ (MPa)**	**η%$_{SH}$**
XNBR/ZnO	7,3	96%
XNBR/ZnO_SH	7	
XNBR/ZnO/10Al$_2$O$_3$	6	183%
XNBR/ZnO/10Al$_2$O$_3$_SH	11	
XNBR/ZnO/10Al$_2$O$_3$@ZnO_I	7	143%
XNBR/ZnO/10Al$_2$O$_3$@ZnO_I _SH	10	
XNBR/ZnO/30Al$_2$O$_3$@ZnO_I	9	178%
XNBR/ZnO/30Al$_2$O$_3$@ZnO_I _SH	16	
XNBR/ZnO/10Al$_2$O$_3$@ZnO_II	7	114%
XNBR/ZnO/10Al$_2$O$_3$@ZnO_II _SH	8	

Before the healing procedure, all the samples possess almost a similar tensile strength, which ranges between 6 and 9 MPa, suggesting that filler inclusion does not affect the tensile properties of XNBR. Upon the thermally induced self-repairing reaction, a very similar behavior can be observed for XNBR/ZnO and XNBR/ZnO/10Al$_2$O$_3$@ZnO_II, suggesting the suitability of this filler system in providing Zn(II) centers able to activate reversible ionic interactions with the carboxylic groups of XNBR chains.

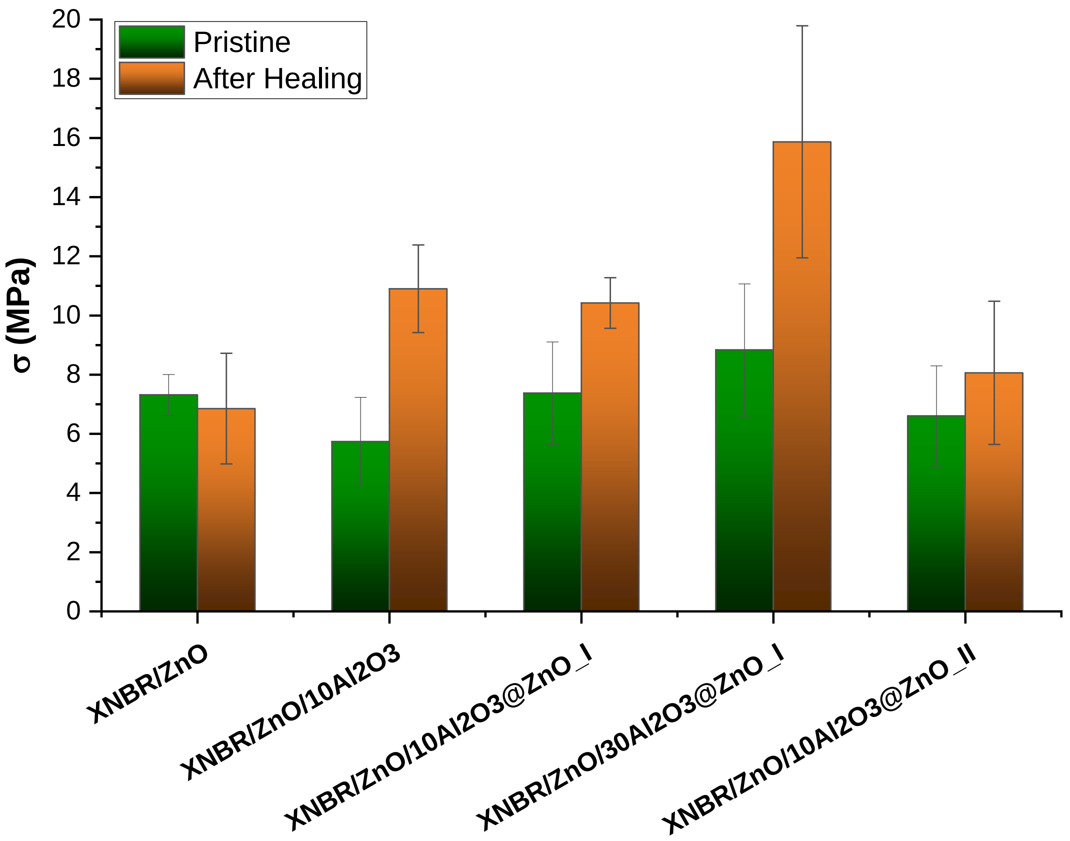

Figure 4.11– Average tensile strength of XNBR composites filled with Al$_2$O$_3$ and Al$_2$O$_3$@ZnO before and after healing treatment.

As the amount of ZnO grafted at the surface of alumina nanorods decreases (i.e. XNBR/ZnO/10Al_2O_3@ZnO_I and XNBR/ZnO/30Al_2O_3@ZnO_I composites) or becomes nil like in XNBR/ZnO/10Al_2O_3, the healing efficiency display values much higher than 100% (highlighted in red in Table 4.4), indicating the occurrence of other side-phenomena besides healing. These results might be interpreted referring to the curing curves reported in Figure 4.7, which show that, specifically in presence of bare alumina, the torque does not reach a plateau, while it gradually increases with time. This unavoidably modifies the mechanical properties of the composites. We may assume that also for both XNBR/ZnO/10Al_2O_3 and XNBR/ZnO/10Al_2O_3@ZnO_I a similar behavior occurs. In fact, without ZnO grafted at the surface of Al_2O_3 nanorods, the interaction with rubber seems to involve exclusively this latter filler, notwithstanding the presence of commercial ZnO particles in the formulation. These considerations suggest that a high degree of surface decoration with ZnO NPs in Al_2O_3@ZnO is essential to avoid overcuring effects and provide remarkable self-healing ability, simultaneously.

Thermal conductivity was measured by the heat flow meter method and the results are shown in Table 4.5. Data prove that alumina introduction is beneficial for the thermal conductivity of the composites with the best result in terms of λ improvement (+ 62%) achieved enclosing in XNBR 30 PHR of Al_2O_3@ZnO_I.

Table 4.5 – λ values of XNBR composites filled with Al_2O_3 and Al_2O_3@ZnO

Sample	**XNBR/ ZnO**	**XNBR/ZnO/ 10Al_2O_3**	**XNBR/ZnO/ 10Al_2O_3@ZnO_I**	**XNBR/ZnO/ 30Al_2O_3@ZnO_I**	**XNBR/ZnO/ 10Al_2O_3@ZnO_II**
λ ($W\ m^{-1}\ K^{-1}$)	**0,1894**	**0,20176**	**0,2056**	**0,2360**	**0,1995**
Error	±0,002	±0,008	±0,004	±0,0010	±0,004

In summary, the whole results reported in this Chapter, though preliminary, envisage the real chance of imparting enhanced self-healing and thermal transport properties to elastomers utilized in automotive industry. This can be accomplished by a careful modification of the alumina surface through POSS units or ZnO NPs, which activate selective healing mechanisms without hindering the intrinsic thermal conductivity of Al_2O_3.

Unquestionably, further in-depth studies on the effect of filler concentration and on the healing reaction mechanism must be performed to complete the picture described, together with a careful morphological characterization of the composites.

4.7 - Bibliography

[1] P. Toia and A. Cavazzini, “Draft Report on the New Circular Economy Plan,” vol. 2207, no. July 2006, pp. 1–10, 2010.

[2] M. A. Sattar and A. Patnaik, “Design Principles of Interfacial Dynamic Bonds in Self-Healing Materials: What are the Parameters?,” *Chem. – An Asian J.*, vol. 15, no. 24, pp. 4215–4240, Dec. 2020.

[3] M. Nakahata, Y. Takashima, H. Yamaguchi, and A. Harada, “Redox-responsive self-healing materials formed from host–guest polymers,” *Nat. Commun.*, vol. 2, no. 1, p. 511, Sep. 2011.

[4] Y. Shi, M. Wang, C. Ma, Y. Wang, X. Li, and G. Yu, “A Conductive Self-Healing Hybrid Gel Enabled by Metal–Ligand Supramolecule and Nanostructured Conductive Polymer,” *Nano Lett.*, vol. 15, no. 9, pp. 6276–6281, Sep. 2015.

[5] R. P. Wool, “Self-healing materials: a review,” *Soft Matter*, vol. 4, no. 3, p. 400, 2008.

[6] Q. Zhang *et al.*, “An Elastic Autonomous Self-Healing Capacitive Sensor Based on a Dynamic Dual Crosslinked Chemical System,” *Adv. Mater.*, vol. 30, no. 33, p. 1801435, Aug. 2018.

[7] D. Döhler, P. Michael, and W. H. Binder, “CuAAC-Based Click Chemistry in Self-Healing Polymers,” *Acc. Chem. Res.*, vol. 50, no. 10, pp. 2610–2620, Oct. 2017.

[8] Z. Zhang *et al.*, “Eco-Friendly, Self-Healing Hydrogels for Adhesive and Elastic Strain Sensors, Circuit Repairing, and Flexible Electronic Devices,” *Macromolecules*, vol. 52, no. 6, pp. 2531–2541, Mar. 2019.

[9] D. Fan *et al.*, “Surface Engineering of Porous Carbon for Self-Healing Nanocomposite Hydrogels by Mussel-Inspired Chemistry and PET-ATRP,” *ACS Appl. Mater. Interfaces*, vol. 11, no. 41, pp. 38126–38135, Oct. 2019.

[10] S. Dong, “B. 95 Zheng, Y. Yao, C. Han, J. Yuan, M. Antonietti, F. Huang,” *Adv. Mater*, vol. 25, pp. 6864–6867, 2013.

[11] M. Guo, L. M. Pitet, H. M. Wyss, M. Vos, P. Y. W. Dankers, and E. W. Meijer, “Tough Stimuli-Responsive Supramolecular Hydrogels with Hydrogen-Bonding Network Junctions,” *J. Am. Chem. Soc.*, vol. 136, no. 19, pp. 6969–6977, May 2014.

[12] H. Qiao *et al.*, “Multiple Weak H-Bonds Lead to Highly Sensitive, Stretchable, Self-Adhesive, and Self-Healing Ionic Sensors,” *ACS Appl. Mater. Interfaces*, vol. 11, no. 8, pp. 7755–7763, Feb. 2019.

[13] J. Araujo-Morera, M. Hernández Santana, R. Verdejo, and M. A. López-Manchado, “Giving a Second opportunity to tire waste: An alternative path for the development of sustainable self-healing styrene–butadiene rubber compounds overcoming the magic triangle of tires,” *Polymers (Basel).*, vol. 11, no. 12, p. 2122, 2019.

[14] B. K. Khatiwada and F. D. Blum, “Tightly Bound PMMA on Silica Has Reduced Heat Capacities,” *Langmuir*, vol. 35, no. 35, pp. 11482–11490, Sep. 2019.

[15] A.-C. Genix, G. P. Baeza, and J. Oberdisse, “Recent advances in structural and dynamical properties of simplified industrial nanocomposites,” *Eur. Polym. J.*, vol. 85, pp. 605–619, Dec. 2016.

[16] A. Alizadeh Sahraei, A. H. Mokarizadeh, D. George, D. Rodrigue, M. Baniassadi, and M. Foroutan, “Insights into interphase thickness characterization for graphene/epoxy nanocomposites: a molecular dynamics simulation,” *Phys. Chem. Chem. Phys.*, vol. 21, no. 36, pp. 19890–19903, 2019.

[17] S. van der Zwaag and E. Brinkman, *Self healing materials: pioneering research in the Netherlands*. IOS Press, 2015.

[18] B. J. Blaiszik, S. L. B. Kramer, S. C. Olugebefola, J. S. Moore, N. R. Sottos, and S. R. White, “Self-Healing Polymers and Composites,” *Annu. Rev. Mater. Res.*, vol. 40, no. 1, pp. 179–211, Jun. 2010.

[19] D. Threadingham, W. Obrecht, W. Wieder, G. Wachholz, and R. Engehausen, “Rubber, 3. Synthetic Rubbers, Introduction and Overview,” in *Ullmann’s Encyclopedia of Industrial Chemistry*, Weinheim, Germany: Wiley-VCH Verlag GmbH & Co. KGaA, 2011.

[20] L. Ibarra, A. Rodríguez, and I. Mora-Barrantes, “Crosslinking of unfilled carboxylated nitrile rubber with different systems: Influence on properties,” *J. Appl. Polym. Sci.*, vol. 108, no. 4, pp. 2197–2205, May

2008.

[21] P. Song and H. Wang, “High-Performance Polymeric Materials through Hydrogen-Bond Cross-Linking,” *Adv. Mater.*, vol. 32, no. 18, p. 1901244, May 2020.

[22] O. J. G. M. Goor, S. I. S. Hendrikse, P. Y. W. Dankers, and E. W. Meijer, “From supramolecular polymers to multi-component biomaterials,” *Chem. Soc. Rev.*, vol. 46, no. 21, pp. 6621–6637, 2017.

[23] Y. Wang, D. T. Pham, and C. Ji, “Self-healing composites: A review,” *Cogent Eng.*, vol. 2, no. 1, p. 1075686, Dec. 2015.

[24] C. L. Lewis, K. Stewart, and M. Anthamatten, “The Influence of Hydrogen Bonding Side-Groups on Viscoelastic Behavior of Linear and Network Polymers,” *Macromolecules*, vol. 47, no. 2, pp. 729–740, Jan. 2014.

[25] L. Yang, X. Tan, Z. Wang, and X. Zhang, “Supramolecular Polymers: Historical Development, Preparation, Characterization, and Functions,” *Chem. Rev.*, vol. 115, no. 15, pp. 7196–7239, Aug. 2015.

[26] L. Cao, D. Yuan, C. Xu, and Y. Chen, “Biobased, self-healable, high strength rubber with tunicate cellulose nanocrystals,” *Nanoscale*, vol. 9, no. 40, pp. 15696–15706, 2017.

[27] S. Utrera-Barrios *et al.*, “An effective and sustainable approach for achieving self-healing in nitrile rubber,” *Eur. Polym. J.*, vol. 139, p. 110032, Oct. 2020.

[28] A. Susanna *et al.*, “ZnO nanoparticles anchored to silica filler. A curing accelerator for isoprene rubber composites,” *Chem. Eng. J.*, vol. 275, pp. 245–252, Sep. 2015.

[29] A. Susanna *et al.*, “Catalytic effect of ZnO anchored silica nanoparticles on rubber vulcanization and cross-link formation,” *Eur. Polym. J.*, vol. 93, pp. 63–74, Aug. 2017.

[30] J. Huang, Z. Gong, T. Peng, L. Cao, and Y. Chen, “Design of thermoplastic vulcanizates induced by metal-ligand coordination towards enhanced mechanical properties and shape memory behavior,” *Compos. Commun.*, vol. 22, p. 100444, Dec. 2020.

[31] S. Utrera-Barrios *et al.*, “Understanding the Molecular Dynamics of Dual Crosslinked Networks by Dielectric Spectroscopy,” *Polymers (Basel).*, vol. 13, no. 19, p. 3234, Sep. 2021.

[32] I. Mora-Barrantes, M. A. Malmierca, J. L. Valentin, A. Rodriguez, and L. Ibarra, “Effect of covalent cross-links on the network structure of thermo-reversible ionic elastomers,” *Soft Matter*, vol. 8, no. 19, p. 5201, 2012.

[33] M. Faghihi and A. Shojaei, “Properties of alumina nanoparticle-filled nitrile-butadiene-rubber/phenolic-resin blend prepared by melt mixing,” *Polym. Compos.*, vol. 30, no. 9, pp. 1290–1298, Sep. 2009.

Chapter 5 - Other attempts: Graphitic materials in SBR/BR matrix

5.1 - Introduction

As already mentioned in Chapter 1, carbon fillers like CNTs, carbon fibres, graphene, and graphite are extensively used to increase the thermal conductivity of polymer composites [1–8]. In fact, λ values of this materials results to be high (100-4000 W m^{-1} K^{-1}), anyway their heat conductivity is highly anisotropic and, as a result, strongly dependent on the direction of the heat propagation. [9] Thus, if on one side these materials allow the production of highly conductive composites by filler alignment, on the other side, their application in systems where anisotropic thermal conductivity is essential, like in tires, raises some concerns. Moreover, since a consistent volume fraction in the matrix is usually required, delamination or peeling phenomena which sacrifice the composite processability and finally damage the composites may occur, besides an increase of the costs of formulations. In this scenario, graphite can be a cost-effective alternative. Owing to its high theoretical intrinsic thermal conductivity (500-1000 W m^{-1} K^{-1}) and the platelet like morphology, it has been already applied in silicone rubber nanocomposites. [10] In particular, expanded graphite (EG), also known as exfoliated graphite and constituted of layers with wide surface area and high aspect ratio, has shown to provide, when included in polymer, outstanding thermal and electrical conductivity as well as good mechanical properties. [11] Due to these properties, EG attracts a lot of interest in terms of industrial-scale composites. However, the use of graphite entails its compatibilization/dispersion and interfacial adhesion with the rubber matrix, in order to avoid segregation and peeling effects and very few studies in the literature report the exploitation of graphite platelets in rubber composites for tires. Very recently, Khan et al. [13, 14] reported on milled graphite nanoparticles having a porous structure and consisting of stacked and randomly oriented planes with a large number of defect sites, which can be easily oxidized, silanized and incorporated in a polymer matrix, remarkably improving their thermo-mechanical behaviour. Although focused on epoxy nanocomposites, these studies suggest a facile and economical approach to potentially replace the use of graphene at industrial scale. Moreover, the results envisage the importance of the silanization of the graphite surface in order to provide a suitable platform not only for compatibilization with rubber chains but also for further modification/derivatization of the carbon-based filler. In this context, another very recent investigation of Cao et al. [15] stimulated our attention. The authors produced a novel hybrid filler based on surface silanized SiO_2 NPs grafted on graphene oxide sheets (GO) to develop natural rubber (NR)-based high-performance tire-treads (Fig. 5.1). Besides the good compatibilization properties with natural rubber, the SiO_2/GO filler imparted increasing storage modulus and energy dissipation capability to the final master batch, while decreasing loss factor and elongation at break with increasing GO content. Fabrication of tire-tread enclosing just 10 PHR of the NR composite leads to remarkable wear resistance and decreased rolling resistance properties, foreshadowing a promising utilization of this filler system.

Figure 5.1 – Schematic representation on the preparation and exploitation in tire tread fabrication of SiO_2/GO hybrid filler

Along the same line, Song et al. recently prepared hybrid fillers based on silica nanoparticles decorating graphene nanosheets for the preparation of SBR nanocomposites for tire. [16] Their mechanical properties, thermal and electrical conductivities, even at low filler loadings (i.e. 5 PHR), resulted significantly higher than those of similar SBR nanocomposites enclosing silica decorating carbon black, graphite and rGO, prepared by the same procedure (See Chapter 1). Moreover, the tread compounds enclosing this filler showed lower rolling resistance and highly improved grip, corroborating the great potentiality of surface modifying carbon-based filler with silica NPs for tire engineering. Although referred to graphene, these studies prompted us to try to extend the described approach also to exfoliated graphite. With this aim, three graphitic materials and a graphene with different characteristics have been supplied and enclosed in SBR-BR rubber composites, evaluating their ability to impart enhanced dynamic mechanical and thermal conductivity properties. Successively, a specific graphite was utilized for developing a novel SiO_2/graphite hybrid filler (i.e. EG@SiO_2), which was incorporated in SBR-BR to produce composites, whose thermal transport properties has been preliminary determined.

5.2 - Info on the supplied graphite and graphene nanomaterials

The materials have been supplied by Imerys S.A and Avanzare S.L. companies. According to the producer, Timrex® is a high aspect ratio graphite specifically engineered to enhance the λ of polymers using low filler loadings. No further information about the dimensions of this graphite is given by the manufacturer. Two graphite nanoplatelets (NPls) and a highly reduced graphene oxide, here referred as graphene, were instead supplied by Avanzare S.L. The information provided by the producer about these materials are reported in Table 5.1.
All the materials were characterized by SEM and XRD. Subsequently they were introduced at low loadings in tire model compounds and characterized by means of DMA and thermal conductivity.

Table 5.1 – Relevant information supplied by Avanzare on their graphitic materials

Material	Lateral size	Thickness	BET	Average n_{layer}
av-PLAT_40	40 μm	10 nm	22 $m^2\ g^{-1}$	< 30
av-PLAT_7	7.2 μm	3 nm	70 $m^2\ g^{-1}$	5 - 10
Graphene	70 μm	< 1 nm	416 $m^2\ g^{-1}$	< 3

5.3 - Commercial graphitic materials characterization

Representative SEM images collected on the commercial Timrex® and Avanzare graphitic materials are reported in Figure 5.2.

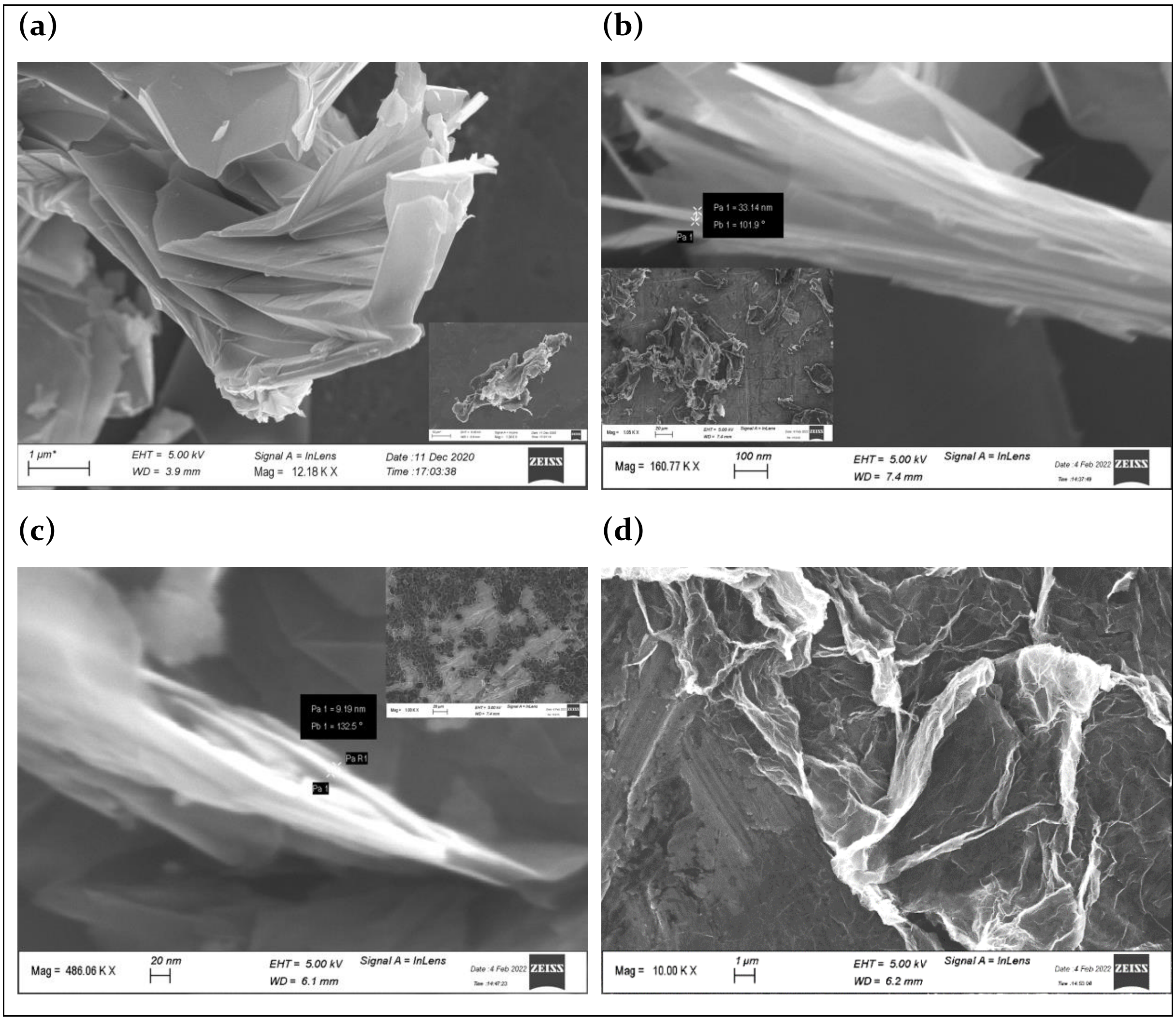

Figure 5.2 – SEM images of (a) graphite Timrex®, (b) av-PLAT_40, (c) av-PLAT_7 and (d) graphene.

From the images, except for the graphene in which the morphological parameters are hard to identify, for the other graphitic materials, the lateral size and the platelet dimension have been measured. Timrex® graphite resulted formed of platelets with a thickness of 10/15 nm that strongly aggregate leading to the formation micrometric structure of stacked platelets. Moreover, the platelets are irregular morphology with a lateral size of about 40 μm. the av-PLAT_40 graphite have a platelet morphology similar to Timrex® one, but the lateral sizes result to be more polydisperse within 25 and 40 μm range. Differences are present also on the thickness, in fact, the platelets have a thickness of about 30/40 nm and the aggregates in the hundreds of nm. Av-PLAT_7 have the smallest lateral size of about 10 μm, a thickness of 10 nm and the platelet results to be quietly regular. Graphene deposited on the stub forms aggregate structure that does not permit to evaluate its lateral size, anyway it is still possible to see the sheet like morphology and the really small thickness of this material.

XRD characterization revealed the presence for all the materials, except for graphene, of the (002) peak typical of graphite *P*6₃/*mmc* space group, which appear rather larger for the av-PLAT_7 sample due to its reduced particle size (see Fig. 5.2c). The peak position and full width at half maximum (FWHM) allowed the calculation of the interplanar spacing, which correlates with the layer stacking distance (L_c) and the number of the layers of the three graphitic materials. (Table 5.3) [17] As a first observation, the retrieved interplanar distances are compatible with those of true graphytic structures, confirming that the materials are in an hexagonal crystal structure. [18] Thickness values are in accordance with those estimated by SEM images for the Timrex® and av-PLAT_7 graphites, while appear lower for the av-PLAT_40.

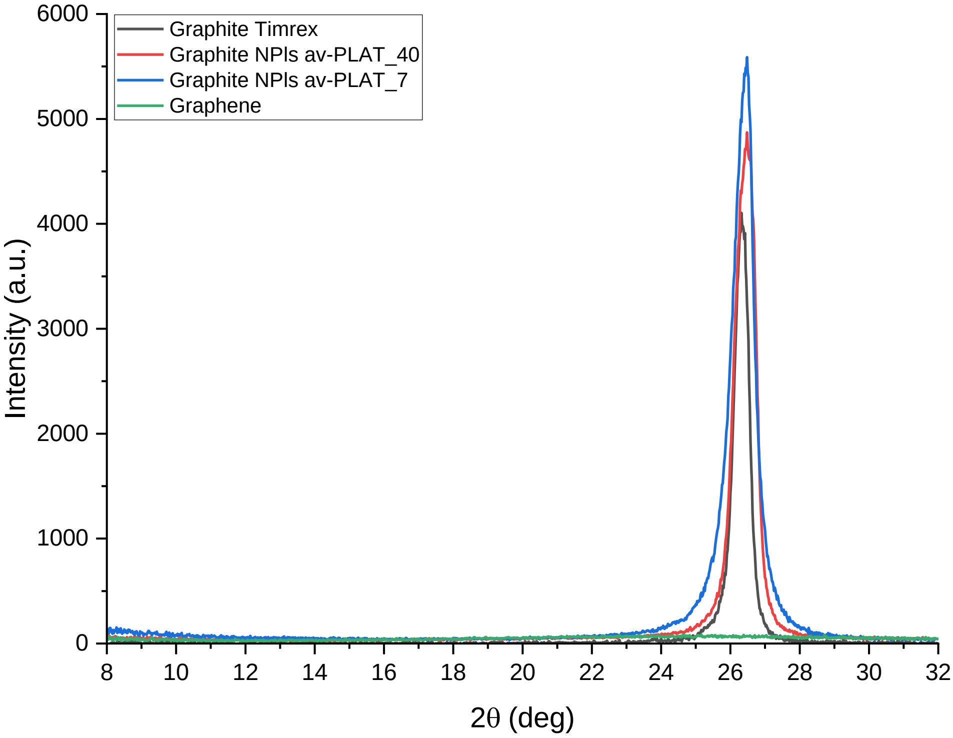

Figure 5.3 – XRD diffraction patterns of the different commercial graphitic and graphene materials

Table 5.3 – Summary of the XRD structural parameters of graphitic materials. [17]

Sample	**2θ** (deg)	**Interplanar spacing** (d, Å)	**FWHM** (deg)	**Thickness** (L_c, Å)	**Thickness** (nm)	**Layer Packing Density** (g cm^{-3})	n_{layer}
Timrex®	26.34	3.38	0.48	169	**17**	2.25	**39**
av-PLAT-7	26.37	3.38	0.84	97	**10**	2.26	**22**
av-PLAT-40	26.49	3.36	0.83	98	**10**	2.27	**23**

5.4 - Composites preparation and functional characterization

Materials: Sprintan SLR 4630 (Styrene Butadiene Rubber, SBR) supplyed from Synthos Group, while Europrene Neocis BR60 (Butadiene Rubber, BR) from Versalis; Silica Zeosil 1165MP from Solvay, bis(3-triethoxysilylpropyl)tetrasulphide (TESPT) from Aldrich; antioxidant N-(1,3-dimethylbutyl)-N-phenyl-p-phenylenediamine (6PPD) from Flexsys; stearic acid (Stearina TP8) from Undesa; N-cyclohexyl-2-benzothiazole sulfenamide (CBS) from Lanxess; sulphur from Redball Superfine; ZnO from Zincol Ossidi.

In a Brabender Plasti-Corder internal mixer SBR and BR was masticated at 130 °C for 1 min followed by inclusion of the silica, TESPT and the graphitic material and allowed to mix for 4 min. Subsequently, the antioxidant 6PPD, the curing activator ZnO and stearic acid as co-activator was added and mixed for 2 min. The compound was allowed to rest for 24 h and a second mixing was performed. The compound was successively masticated at 80°C for 1 min and then mixed with sulphur and CBS for 2 min. Compounds formulations are reported in Table 4. The composites were vulcanized in a hot press at 170°C for 10 minutes and dynamical and statical mechanical proprieties and λ was measured. A compound containing only 60 phr of silica was used as reference. In these first experiments, Timrex® graphite was not utilized.

Table 5.4 – formulations of graphitic material containing composites

Component	PHR		
BR	30	30	30
SBR	70	70	70
SiO_2	60	60	60
TESPT	4.8	4.8	4.8
Av-PLAT_7	**2**		
Av-PLAT_40		**2**	
Graphene			**2**
6PPD	2.5	2.5	2.5
ZnO	2	2	2
Stearic acid	1	1	1
CBS	3	3	3
Sulfur	1	1	1

DMA analysis was performed in compression, at three different temperatures (0, 23 and 70°C) utilizing a frequency of 10 Hz. The results (Fig. 5.4a) show that the E' values of the composites with Av-PLAT_7 and Av-PLAT_40 display values very similar or slightly lower than that of reference compound enclosing exclusively silica NPs, suggesting that no additional reinforcement can be obtained introducing these graphitic materials in SBR-BR rubber. Also, tan δ values are in line with that of the reference formulation (Fig. 5.4b). Remarkably higher E' and tan δ are obtained when graphene is used as filler (Fig. 5.4), suggesting, besides an improvement of the mechanical strength, an increase of energy dissipation for this compound.

Thermal conductivity of the composites was measured with the MTPS method. Results are summarized in Figure 5.5. Notwithstanding the very low filler loading, significant enhancement of the λ value can be observed upon introduction of carbon-based filler in the SBR-BR matrix. In particular, concerning the graphitic materials, the composite enclosing Av-PLAT_40 display the best performance, with an upgrade of the thermal conductivity of +65% if compared to reference compound. This can be probably connected to the presence of large sheets in Av-PLAT_40 which can more easily provide continuous thermal conductive pathways in the rubber matrix. As expected, the composite with graphene sheets, despite their lateral dimensions close to those of Av-

PLAT_40, shows the highest λ value, most likely due to the higher intrinsic λ of graphene (3080–5150, in plane [19]) compared to that of graphite (500-1000 [20]).

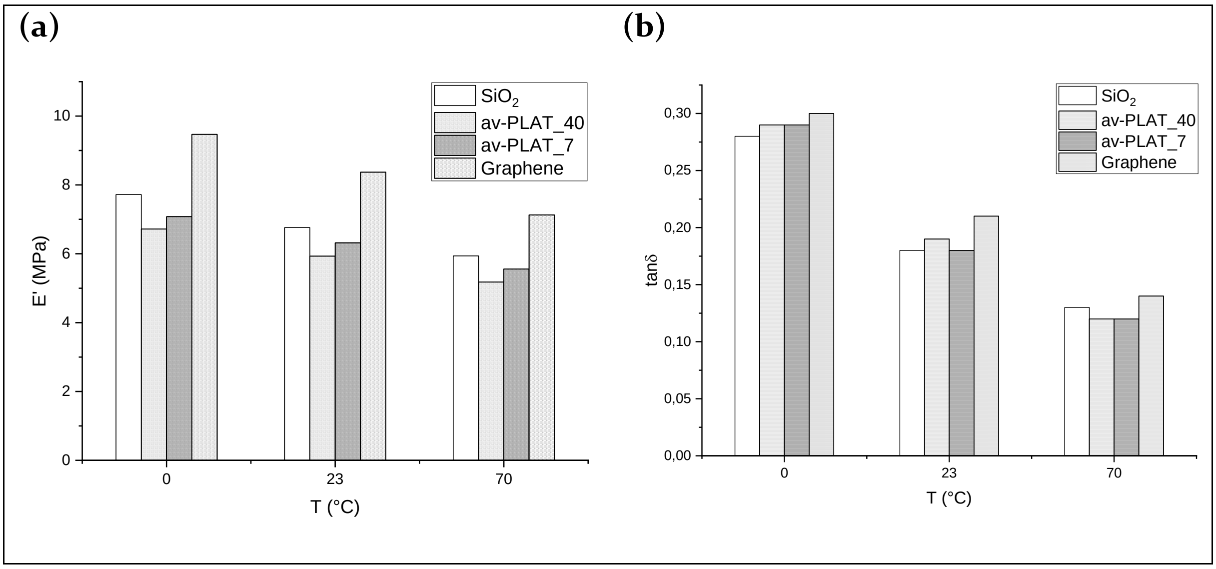

Figure 5.4 – DMA analysis at different temperature of reference SBR-BR compound containing exclusively 60 phr of commercial silica NPs and of SBR-BR composites including also 2 phr of different graphitic and graphene materials.

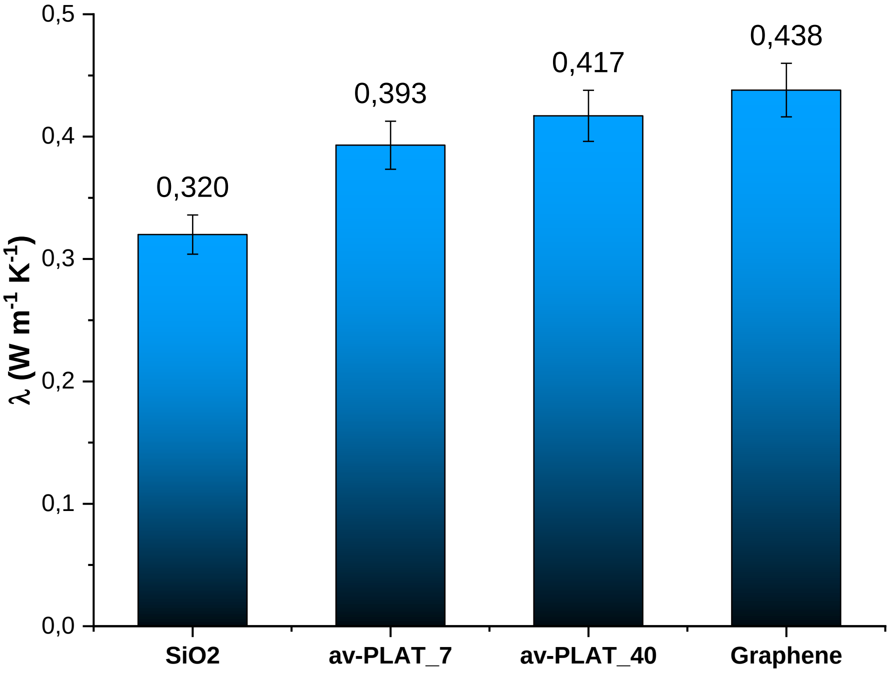

Figure 5.5 – Thermal conductivity of compounds SBR-BR compound containing exclusively 60 phr of commercial silica NPs and of SBR-BR composites including also 2 phr of different graphitic and graphene materials.

5.5 - EG@SiO_2 hybrid filler synthesis and characterization

Materials: Timrex® graphite (EG) was purchased from Imerys, Ethanol, Tetraethylortosilicate (TEOS) and ammonia solution 25% was purchased from Sigma Aldritch and cetyltrimethylammonium bromide (CTAB) from Alfa Aesar.

Introduction of graphite in polymer is generally associated with delamination and peeling of the composites. To enhance the interaction between graphite and rubber and the dispersion, EG was covered with silica modifying an easy synthetic procedure already present in literature [21]. Typically, in a round bottom flask, 0.575 g of expanded graphite was suspended by sonication in a solution of 2 mL of distilled water and 48 mL of EtOH. 0.0109 g of CTAB was then added and the flask heated at 65°C by oil bath for 15 minutes with magnetic stirring. Then 10.6 mL of TEOS was added followed by 2.4 mL of NH_4OH 25% solution after 5 minutes. The flask was kept for 2 hours at 65°C and after natural cooling the suspension was centrifuged, washed with EtOH and dried at 70°C for 12 hours. A scale up of this method was also conducted, the suspension in this case was vacuum filtered instead of been centrifuged.

The quantitative amount of SiO_2 grafted on the surface was evaluated by TGA and the morphology of the material by SEM and TEM. TGA analysis of the graphite and the hybrid filler material have been performed, measuring the weight loss from 30 to 1000°C in air (50 mL min^{-1}). As shown in Figure 6, graphite degradation starts to at 600°C and at about 900°C is completed and graphite results fully converted into CO_2 without any residue. When silica is deposited on the surface of the graphite (i.r. EG@SiO_2 sample), a better thermal stability is observed, and at 1000°C a residual mass (~18.5 wt. %), which is attributable to the grafted SiO_2 NPs.

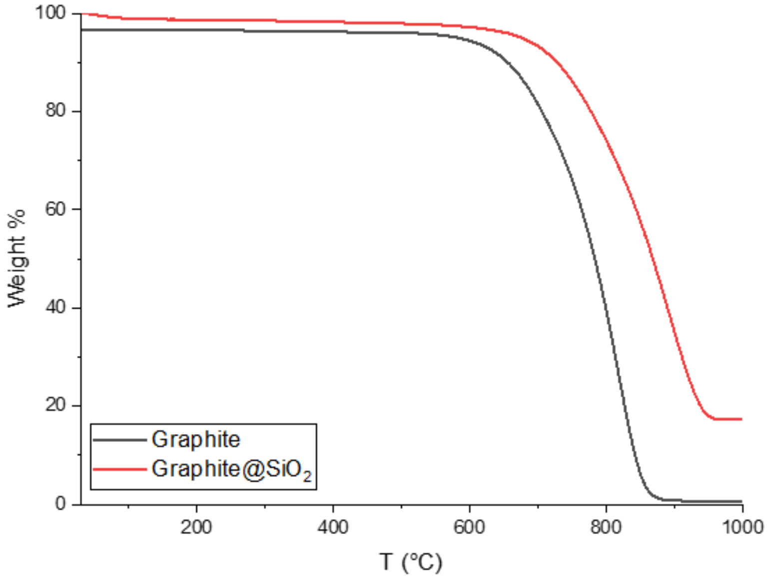

Figure 5.6 – TGA curves of Timrex® graphite (black line) and of EG@SiO_2 hybrid filler (red-line).

Morphological analysis was carried out by SEM and TEM (Fig. 5.7). In particular, SEM images shows silica grafting does not improve the disaggregation of graphite sheets (Fig. 5.7a). Interestingly, sub-micrometric aggregates composed of almost spherical SiO_2 NPs are clearly visible at the surface of graphite layers (Fig. 5.7b). TEM images of a single graphite layer are reported in Figure 5.7c, d. The occurrence of nanometric particles and aggregates is observable (Fig. 5.7c) and, at a higher resolution (Fig. 5.7d) SiO_2 NPs appear partially "socketed" in the graphite sheet. These results confirm the successful modification of the graphite surfaces with silica.

5.6 - Preparation and functional characterization of SBR-BR composites enclosing EG@SiO$_2$ filler

Following the procedure previously described, different compounds have been produced utilizing 60 phr of commercial SiO$_2$ NPs and different concentrations of EG@SiO$_2$ hybrid filler. For comparison compounds with 60 phr of silica and loadings of EG corresponding to the quantities of graphite present in EG@SiO$_2$ filler were also prepared (i.e. EG+SiO$_2$ composites). Details on the formulations are reported in Table 5.5.

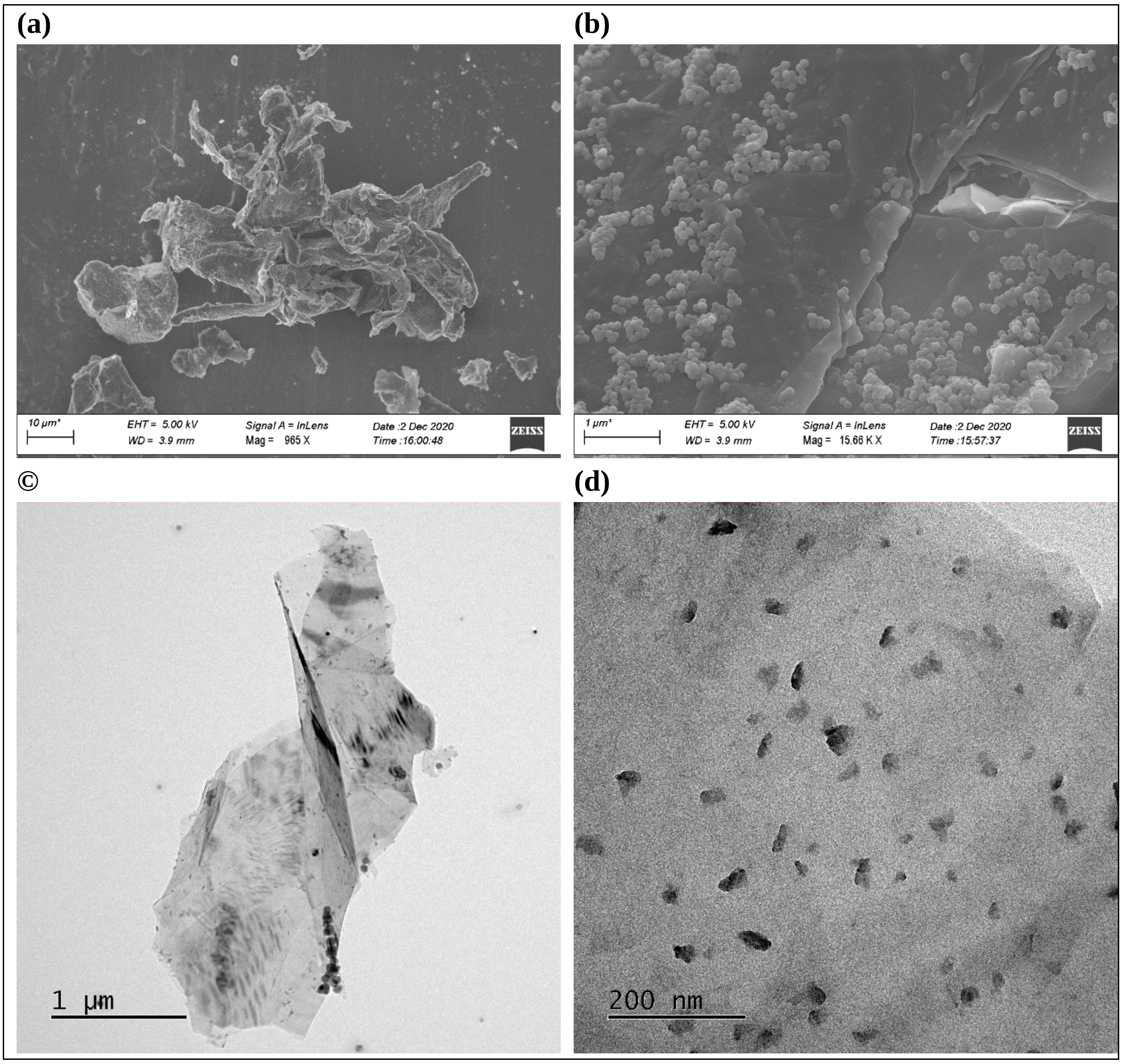

Figure 5.7 – (a, b) SEM and (c, d) TEM images of EG@SiO$_2$ hybrid filler

Table 5.5 – rubber formulation of composites containing graphite and silica/graphite fillers

Compound	PHR					
BR60	30	30	30	30	30	30
SBR60 4630	70	70	70	70	70	70
Graphite (EG)	4	6	8			
EG@SiO$_2$				4.9	7.3	9.8
SiO$_2$	60	60	60	59.1	58.7	58.2
TESPT	4.8	4.8	4.8	4.8	4.8	4.8
6PPD	2.5	2.5	2.5	2.5	2.5	2.5
ZnO	2	2	2	2	2	2
Stearic acid	1	1	1	1	1	1
CBS	3	3	3	3	3	3
Sulfur	1	1	1	1	1	1

Compression DMA tests of the vulcanized samples were performed. An example of results obtained at 23°C and utilizing a stress frequency of 10 Hz are reported in Figure 5.8. The modulus E’ of the composites increases as a function of the filler loading (Fig.5. 8a). Noticeably, a slightly higher reinforcement effect is observed when EG@SiO$_2$ hybrid filler is utilized. The tan δ values are instead very similar to that of the reference compound (Fig. 5.8b). These results, besides indicating that the introduction of graphite-based filler in SBR-BR affords satisfactory mechanical properties, suggest that the surface decoration of EG with SiO$_2$ NPs in the hybrid filler makes a step forward, improving the compatibilization with the rubber matrix and partly enhancing the E’ and dissipation behaviour of the composite.

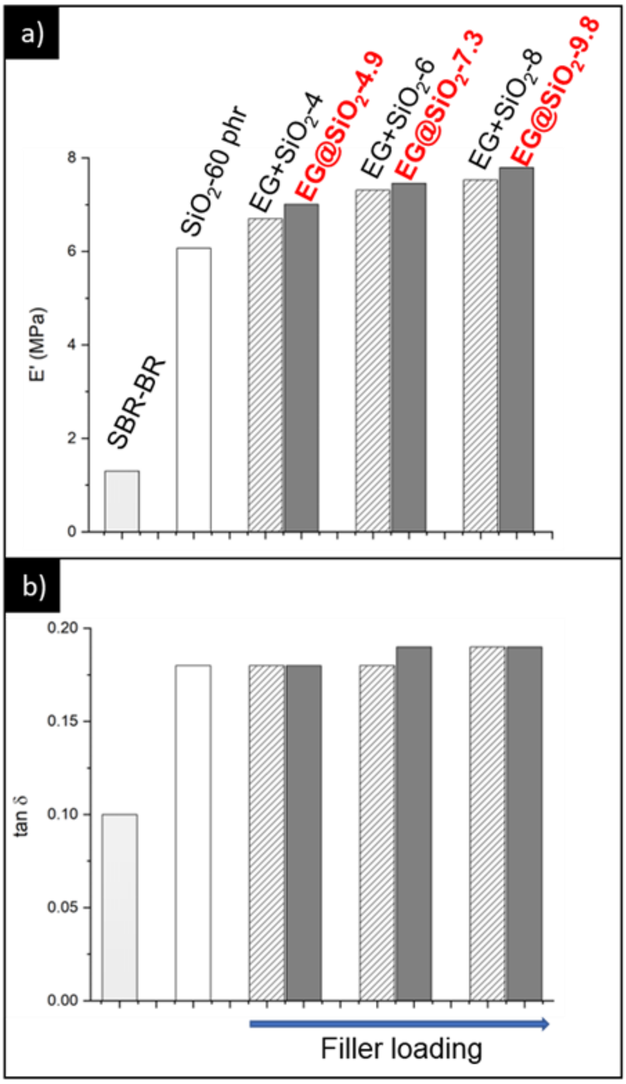

Figure 5.8 – E' and tan δ of the SBR-BR composites enclosing graphite-based filler at 23°C and stress frequency of 10Hz.

Thermal conductivity properties of the composites were evaluated by the MTPS method. The obtained λ values are reported in Figure 5.9. It can be clearly observed that the introduction of EG and EG@SiO_2 effectively raise the heat transfer in the composites. More interestingly, the presence of a layer of non-conductive silica NPs at the graphite surface in the hybrid filler does not hinder the thermal transport in the rubber matrix.

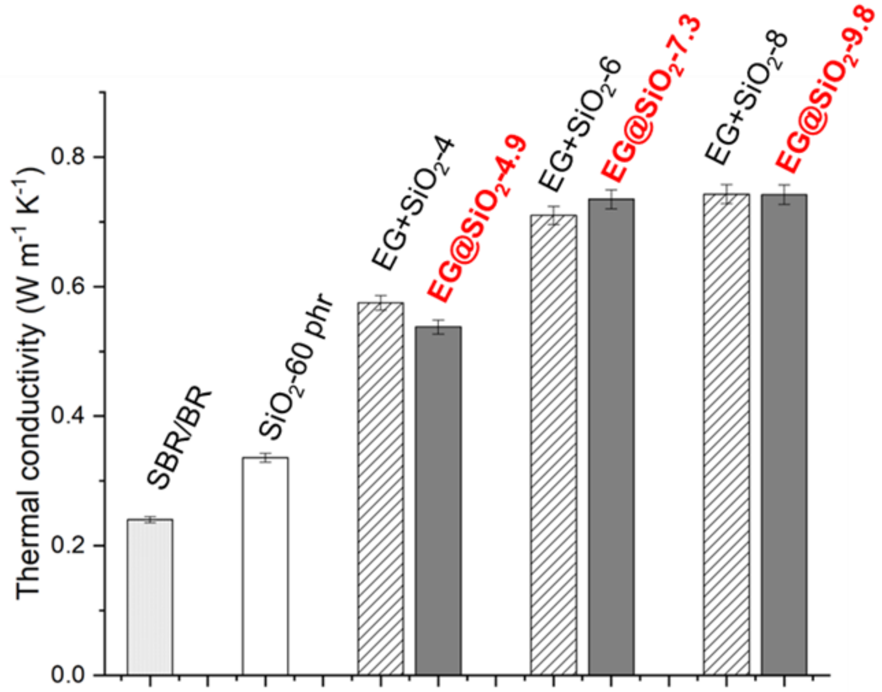

Figure 5.9 – Thermal conductivity of SBR-BR composites enclosing graphite-based fillers

Although very preliminary, these results prefigure a potential application for graphite-based filler and, particularly, for the EG@SiO$_2$ hybrid filler. Better structural and morphological characterizations of both filler and composites are needed, as well as the choice of graphite materials easier to exfoliate, in order to enable a more effective compatibilization with the rubber matrix, avoid peeling phenomena and make these materials readily applicable in large scale formulations for tires.

5.7 - Bibliography

[1] J. Nanda *et al.*, “Thermal Conductivity of Single-Wall Carbon Nanotube Dispersions: Role of Interfacial Effects,” *J. Phys. Chem. C*, vol. 112, no. 3, pp. 654–658, Jan. 2008.

[2] R. A. Hauser, J. A. King, R. M. Pagel, and J. M. Keith, “Effects of carbon fillers on the thermal conductivity of highly filled liquid-crystal polymer based resins,” *J. Appl. Polym. Sci.*, vol. 109, no. 4, pp. 2145–2155, Aug. 2008.

[3] I. M. Afanasov, D. V. Savchenko, S. G. Ionov, D. A. Rusakov, A. N. Seleznev, and V. V. Avdeev, “Thermal conductivity and mechanical properties of expanded graphite,” *Inorg. Mater.*, vol. 45, no. 5, pp. 486–490, May 2009.

[4] J. Gu, X. Yang, Z. Lv, N. Li, C. Liang, and Q. Zhang, “Functionalized graphite nanoplatelets/epoxy resin nanocomposites with high thermal conductivity,” *Int. J. Heat Mass Transf.*, vol. 92, pp. 15–22, Jan. 2016.

[5] A. A. Balandin *et al.*, “Superior Thermal Conductivity of Single-Layer Graphene,” *Nano Lett.*, vol. 8, no. 3, pp. 902–907, Mar. 2008.

[6] S. H. Song *et al.*, “Enhanced Thermal Conductivity of Epoxy-Graphene Composites by Using Non-Oxidized Graphene Flakes with Non-Covalent Functionalization,” *Adv. Mater.*, vol. 25, no. 5, pp. 732–737, Feb. 2013.

[7] L.-H. Liu and M. Yan, “Functionalization of pristine graphene with perfluorophenyl azides,” *J. Mater. Chem.*, vol. 21, no. 10, p. 3273, 2011.

[8] T. Ji *et al.*, “Thermal conductive and flexible silastic composite based on a hierarchical framework of aligned carbon fibers-carbon nanotubes,” *Carbon N. Y.*, vol. 131, pp. 149–159, May 2018.

[9] H. Chen *et al.*, “Thermal conductivity of polymer-based composites: Fundamentals and applications,” *Prog. Polym. Sci.*, vol. 59, pp. 41–85, Aug. 2016.

[10] Q. Mu and S. Feng, “Thermal conductivity of graphite/silicone rubber prepared by solution intercalation,” *Thermochim. Acta*, vol. 462, no. 1–2, pp. 70–75, Oct. 2007.

[11] M. J. Mochane, T. E. Motaung, and S. V. Motloung, “Morphology, flammability, and properties of graphite reinforced polymer composites. Systematic review,” *Polym. Compos.*, vol. 39, no. S3, pp. E1487–E1499, Jun. 2018.

[12] J. Song, L. Ma, Y. He, H. Yan, Z. Wu, and W. Li, “Modified graphite filled natural rubber composites with good thermal conductivity,” *Chinese J. Chem. Eng.*, vol. 23, no. 5, pp. 853–859, May 2015.

[13] S. Das, S. Halder, B. Paul, N. I. Khan, and M. S. Goyat, “Impact of silanized milled graphite nanoparticles on thermo-mechanical properties of epoxy nanocomposite,” *Mater. Chem. Phys.*, vol. 278, p. 125601, Feb. 2022.

[14] N. I. Khan, S. Halder, N. Talukdar, S. Das, and M. S. Goyat, “Surface oxidized/silanized graphite nanoplatelets for reinforcing an epoxy matrix,” *Mater. Chem. Phys.*, vol. 258, p. 123851, Jan. 2021.

[15] L. Cao, T. K. Sinha, L. Tao, H. Li, C. Zong, and J. K. Kim, “Synergistic reinforcement of silanized silica-graphene oxide hybrid in natural rubber for tire-tread fabrication: A latex based facile approach,” *Compos. Part B Eng.*, vol. 161, pp. 667–676, Mar. 2019.

[16] S. H. Song, “Graphene-Silica Hybrids Fillers for Multifunctional Solution Styrene Butadiene Rubber,” *J. Polym. Res.*, vol. 27, no. 6, p. 155, Jun. 2020.

[17] A. N. Popova, “Crystallographic analysis of graphite by X-Ray diffraction,” *Coke Chem.*, vol. 60, no. 9, pp. 361–365, 2017.

[18] A. S. Fialkov, “Carbon-graphite materials,” 1979.

[19] S. Ghosh *et al.*, “Extremely high thermal conductivity of graphene: Prospects for thermal management applications in nanoelectronic circuits,” *Appl. Phys. Lett.*, vol. 92, no. 15, p. 151911, Apr. 2008.

[20] J.-B. Donnet, *Carbon black: science and technology*. CRC Press, 1993.

[21] Y. Noma, Y. Saga, and N. Une, “Amorphous silica-coated graphite particles for thermally conductive and electrically insulating resins,” *Carbon N. Y.*, vol. 78, pp. 204–211, Nov. 2014.

CONCLUSION

The PhD research activity, in collaboration with Pirelli Tires, was focused on the **modification of commercially available materials and on the design of novel fillers able to impart, upon introduction in rubber matrix, improved thermal conductivity and satisfactory mechanical performances, trying also to reduce the filler loading**.

Al_2O_3 was selected as an appealing choice, due to its low cost, the stable chemical performance and the negligible toxicity, which compensate the not very high intrinsic thermal conductivity.

In particular by a proper tuning of crystal phase, morphology and surface properties of commercial and synthesized alumina particles, two **different filler systems have been developed by simple and easy to scale-up methods**:

i. Alumina nanosheets supported on silica: **SiO_2@Al_2O_3 binary filler** (see Chapter 2)

ii. Alumina decorated at the surface with polysilsesquioxanes units: **Al_2O_3@POSS hybrid filler** (see Chapter 3)

The structural, morphological and surface features of these materials have been comprehensively investigated and the novel fillers have been utilized for the production of butadiene rubber (BR)-styrene butadiene rubber (SBR) composites, which were then characterized in terms of mechanical and thermal conductive properties.

In particular, **SiO_2@Al_2O_3**, an innovative filler where silica NPs and alumina nanosheets belong to the same functional structure, has been proved to supply to SBR-BR matrix **satisfactory dynamic-mechanical properties and a considerable decrease of the hysteresis**, foreshadowing a **potential application in tire tread formulation**.

Furthermore, a **moderate but significant increase of the thermal conductivity** (+30% in comparison to reference compound enclosing only silica NPs) **has been detected in the presence of this filler**, envisaging the ambitious chance also **to tailor the thermal transport properties of tires**.

Al_2O_3@POSS hybrid filler where **alumina particles and POSS units belong to the same functional structure**, has been synthesized by grafting different loadings of OctaMethacrylPOSS onto silanized commercial alumina and alumina nanorods. **Upon incorporation**, by *solvent casting*, **in PB matrix**, **a remarkable increase of both thermal conductivity** (+ 60-70 % with respect to PB/Al_2O_3 and + 90 % compared to homopolymerized PB) **and elastic modulus has been observed**, even at relatively **low loadings of thermal conductive filler (15-10 v/v %)**, if compared with the literature studies. This has been associated to the peculiar hybrid structure of the hybrid filler, where the shell of POSS nanounits, **besides assuring the compatibility between filler and polymer host, allows a homogeneous distribution and a continuous networking** of the alumina NPs. This positively influences heat transport, **providing thermal conductive pathways** and **leading to the raise of the thermal diffusivity** even at low filler loadings, with a **potential reduction of filler utilization in rubber composite formulations**.

Since the mitigation overheating effects in tires, involves the issue of a permanent damage of the rubber composites, **a part of the research activity was dedicated** also **to the development of filler systems able not only to improve the thermal conductivity but also to enable self-healing effects,** in order to extend the service-life, the sustainability and the safety of the composites.

In collaboration with CSIC Madrid, the following actions have been pursued (see Chapter 4):

i. Exploitation of **Al_2O_3@POSS** (with methacryl terminations) in XNBR employed in automotive to verify their **potential self-healing ability**

ii. Development of an innovative filler composed by **alumina nanorods surface decorated with ZnO NPs (Al_2O_3@ZnO) able to ensure,** upon incorporation in XNBR, **both enhanced thermal conductivity and self-repairing properties**

The structural, morphological and surface features of Al_2O_3@ZnO have been investigated in depth as well as the ability of both the filler systems in imparting self-healing.

As concerns on **Al_2O_3@POSS hybrid filler**, the high number of carbonylic groups belonging to the methacrylic terminations of POSS units **has been exploited to provide H-bond interactions with the carboxylic groups of the XNBR rubber**. The results, besides supporting a **certain degree of self-repairing capability and the increase of λ** imparted by Al_2O_3@POSS to the rubber matrix, indicated that **an increased filler concentration is necessary to achieve a more satisfactory self-healing behavior**.

Al_2O_3@ZnO filler was developed in order to impart both remarkable λ and self-healing capability to XNBR, simultaneously. The idea was connected to the **chance of generating ionic dynamic interactions between the carboxylic groups of the XNBR matrix and the Zn^{2+} centers of ZnO clusters** grafted at the alumina surfaces. The results supported this possibility, indicating that **a careful modification of the ZnO NPs amount at the alumina surface activates selective healing mechanisms** and **provides enhanced thermal conductivity** to the composites.

Finally, though very preliminary, **the data obtained for the EG@SiO_2 hybrid filler**, **prefigure a potential application for graphite-based materials in rubber composites for tires**, since satisfactory mechanical properties and high λ values can be attained. However, further characterizations are necessary to investigate the potential occurrence of peeling phenomena, and, in this respect, the possibility of identifying a better strategy of exfoliation/compatibilization with the rubber matrix is essential.

In summary, the results of the PhD activities disclose the potentialities of alumina materials in upgrading the thermal conductivity of rubber composites for tires. In particular, the **most promising strategies appear those which enable targeted surface functionalization and aspect ratio tailoring**, simultaneously, assuring remarkable compatibilization with the rubber matrix and the generation of thermally conductive networks. In this frame and specifically for tires, **binary filler systems and hybrid fillers, like SiO_2@Al_2O_3, Al_2O_3@ZnO, Al_2O_3@POSS and EG@SiO_2, seem very promising candidates** since **they can combine high intrinsic thermal conductivity and the possibility of morphology, packing density and reinforcing ability tailoring**, thus significantly upgrading the advantages gained by using a single filler.

Appendix

Characterization Methods

The aim of this Appendix is to explain the analytical techniques employed for the chemical, structural and functional characterization of the fillers and their relative composites.

A1 - Attenuated Total Reflectance Fourier Transform Infrared Spectroscopy (ATR-FTIR)

Vibrational spectroscopy permits to qualitatively identify the functional groups of the materials. The different vibrational modes of bonds are associated to absorption of infrared radiation at different energy and thus at different wavelengths. When the angle of incidence at the interface between a crystal and a material is greater than the critical angle a total internal reflection arises and evanescent waves results (Fig. A.1).

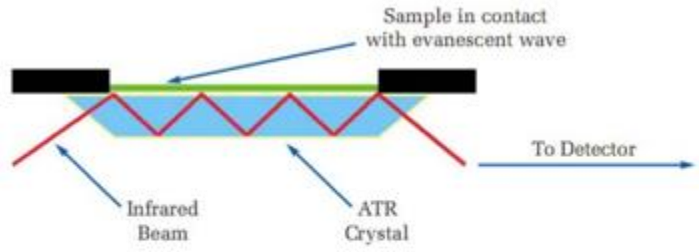

Figure A.1 - ATR-FTIR

ATR spectroscopy exploits this phenomenon to measure the IR absorbance of materials. When the material is in close contact with the reflecting surface, the evanescent wave penetrates the material and loses energy at the wavelength where the material absorbs. The radiation resultant is measured (absorption energy) and plotted as a function of the wavelength. In this thesis the measurements were performed utilizing a Nicolet™ iS20 FTIR Spectrometer instrument. (1 cm^{-1} resolution spectra, 650-4000 cm^{-1} region, 32 scan). This instrument was utilised to qualitatively characterize the filler before and after functionalization and the PB composites.

A2 – X-ray powder diffraction (PXRD)

XRD is an analytical technique that gives information about crystal structure of materials, that analyses the diffraction of X-ray at different θ angles that interact with an ordered structure. In the classical technique single crystal, material with perfect crystal lattice, are analysed in order to get information about the distances between atoms in the lattice utilising Bragg laws. [1] This technique is not suitable for common routine characterization. PXRD permits to have information of crystal structure directly on powder assuming that the sample is randomly oriented. Thus, a statistically significant number of each plane of the crystal structure will be in the proper orientation to diffract the X-rays and the resulting diffraction signal will be a distinctive diffraction pattern that contain the information about each plane present in the powder. Analysis were conducted on a Rigaki - Miniflex 600 diffractometer, that operates with a Bragg-Brentano geometry equipped with Cu X-Ray source (Kα radiation λ_1 = 1.5406 Å, λ_2 = 1.54443 Å). PXRD was utilized to study the structure of the aluminas and the graphitic materials.

A3 - Thermal analysis (TGA)

Thermo-gravimetric analysis (TGA) permits to study the changes of weight of a material as a function of the temperature in a controlled atmosphere. Lost in weight can be correlated to the degradation of organic molecules, solvent or humidity physically adsorbed on the surface or in the pores. Moreover, information about thermal stability of a sample can be obtained.

A typical TGA instrument consists of a precision balance and a furnace with a programmable control temperature. Temperature is fixed to a determined value or increased with a fixed rate to produce a thermal reaction.

The TGA analysis of this thesis were carried out on a Mettler Toledo TGA/DSC1 Star System. The sample were heated in air from 30 to 1000°C, following the thermal profile: 30 - 150°C at 5°C min^{-1}; dwell at 150°C for 10 min; 150 - 1000°C at 10°C min^{-1}.

A4 - Inductively Couple Plasma Optical Emission Spectroscopy (ICP-OES)

ICP-OES is a spectroscopic technique that permits to have quantitative information about elements present in a sample. This technique exploits the use of a plasma to atomize and ionize the sample. Moreover, due to the high energy of the plasma the atoms will be in and excited state. The transition to fundamental state will be associated to release of atomic characteristic photons that will be analysed by a spectrometer. In this thesis the amount of ZnO and Al_2O_3 was determined on ICP-AES Optima 7000 DV Perkin Elmer instrument. Solid samples have been analysed and thus a mineralization process was necessary. This step was conducted on a microwave mineralizer utilizing a mixture of strong acid (HNO_3, HF and HCl). For the determination of alumina deposited on the commercial silica, due to the strong resistance of alumina to acids, the analysis was conducted on the precursor and hot 2M NaOH solution was used to dissolve the material.

A5 - Solid State NMR

Solid-state NMR (ss-NMR) spectroscopy is an experimental technique that permits to analyse solid sample by nuclear magnetic resonance (NMR) spectroscopy. Unlike in conventional solution-state NMR where rapid motion averages out many of the spin interactions, in ss-NMR anisotropic part of many spin interactions are present. As results, solid-state NMR spectra are characterised by larger linewidths and thus low resolution. To reduce the anisotropic contribution, the sample can be spinned at a constant frequency (depending on the analysed nuclei) oriented at magic angle respect to the magnetic field. This technique is named as magic-angle spinning-NMR (MAS-NMR) and permits to produce better resolution NMR spectra. MAS-NMR spectra have been exploited for confirm functionalization of the alumina and to characterize some PB composites. The experiments have been performed at University of Trento in collaboration with Dr. E. Callone and Prof. S. Dirè (Klaus Laboratory).

A6 - Scanning Electron Microscope (SEM)

Scanning electron microscope (SEM) is an electron microscope that produces images scanning in a raster pattern a focused beam on a sample. When electrons interacts with the atoms of the sample, various signals are produced as visible in figure A.2 that give information about surface topography and composition of the sample. SEM utilizes secondary electrons and backscattered electron to produces images of the surface of the sample. Some microscopes can be equipped with X-ray detector that analyse the characteristic x-ray emission of atoms excited by the primary electron beam (SEM-EDX techniques).

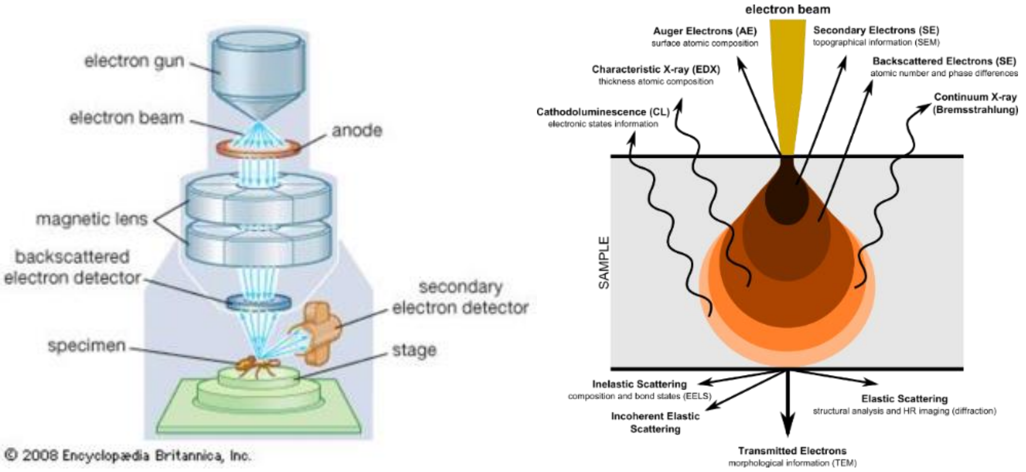

Figure A.2 - Scheme of SEM apparatus and typical “pear” form of the signal produced by interaction between electron and matter

For the morphological characterization of powder and the study of dispersion of filler in composites a Zeiss FEG Gemini 500 equipped with secondary electron and backscattered detector both out- and in-lens was used. Moreover, a Bruker QUANTAX detector was present for the EDX analysis. Metallization of the sample was conducted on Edwards S150B or Quorum Q150T ES instrument.

A7 - High-Resolution Transmission Electron Microscopy (HR-TEM)

TEM is an electron microscopy in which electrons beam pass through a thin layer of sample and it is attenuated depending on the interaction between the beam and the matter. The transmitted electrons are directed to a fluorescent screen or a detector that forms the image of the sample. Due to the lower wavelength associated to electron respect to photon, much higher resolutions are achieved. HR-TEM is a particular TEM technique that allows to obtain direct imaging of the atomic structure of samples.

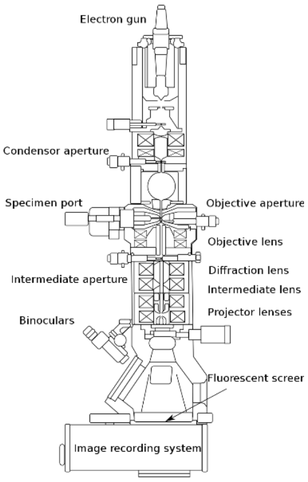

Figure A.3 - Scheme of TEM apparatus

TEM images were acquired on JEOL JEM 2100 Plus depositing a suspension of about 500 ppm of sample on a copper grid with carbon film. This technique was employed for the morphological characterization of nanometric materials.

A8 - Swelling experiments

Swelling experiments was conducted to calculate the crosslink density (ν) of the vulcanized rubber exploiting the Flory–Rehner equation (1). [2]

$$\nu = \frac{[\ln(1-V_r) + V_r + \chi V_r^{2}]}{-2\cdot\rho_p\cdot V_s\cdot(V_r)^{1/3}} \quad (1)$$

Where V_r is the volumetric fraction of the swelled rubber, χ is the Flory solvent-polymer interaction term, ρ_p the density of the polymer and V_s is the molar volume of the swelling solvent. In order to calculate the V_r parameter, squared sample of about 300-400 mg was weighted (m_1) and soaked in toluene for 72 hours. The mass of the sample after this process was measured (m_2) placing the sample in a closed vessel. The samples were then dried and weighted again (m_3).

V_r was determined according to (2):

$$V_r = \frac{(m_d - f m_0)\cdot\rho_p^{-1}}{(m_d - f m_0)\cdot\rho_p^{-1} + m_{so}\cdot\rho_s^{-1}} \quad (2)$$

where: m_1 and m_3 are the mass of the composite specimen before and after swelling/extraction experiments, respectively; $m_{so} = (m_2 - m_1)$ is the weight of the solvent in the swollen mass; ρ_s is the solvent density and f is the fraction of the filler in the composite. At least 4 sample for compound have been examined and the average ν and relative error reported. Crosslink density of XNBR compounds have been measured with this method.

A9 - Rheometer

In the rubber industry is important to know the behaviour of crosslinking of rubber, with temperature and time, in order to define its processability, curing time and final characteristics. In our works an oscillating disk rheometer was utilized. The instrument consists of a cone-shaped disk which is embedded in the rubber specimen and oscillated through a small angle while the specimen is heated under pressure (Fig. A.4).

The curing curves are obtained by the instrument measuring the rotational modulus of force (torque) necessary to move the disk as function of time at constant temperature. As the curing proceeds with time the torque rises due to the hardening of the material. Different characteristic parameter can be obtained from this analysis, in this thesis only t_{90} has been utilized. The t_{90} is the moment in which 90% cross-linking has been reached.

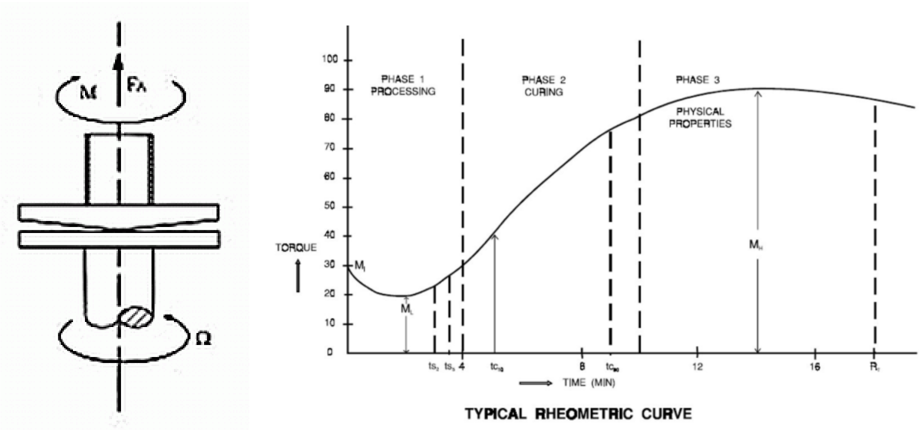

Figure A.4 – scheme of an oscillating disk and a typical curing curve with its characteristic parameter

A10 - Compression Dynamo Mechanical Analysis (DMA)

Elastomers that are subjected to a mechanical stimulus show viscoelastic response. This response will be the combination of the an elastic solids and a Newtonian fluids that are generally modelled as mechanically combinations of springs and dashpots. [3] Following this model two mechanical modulus arise. The first one is connected to the spring and so to the elastic part of the rubber that store energy (E') while the second one is related with the dashpot and so on the viscous part that is correlate with the dissipation of the energy (E"). DMA permits to mechanically characterize elastomeric material measuring these two moduli. Typically, rubber specimen is subjected to periodic sinusoidal shear strain γ ($\gamma t = \gamma + \sin(\omega t)$, *at defined frequency* ω *and temperature* T), the material response is a sinusoidal stress σ, offset by a certain phase angle (δ) respect to the shear strain applied, and expressed as:

$$\sigma t = \sigma + \sin(\omega t) + \delta = \sigma [\sin(\omega t)\cos\delta + \cos(\omega t)\sin\delta] \ (1)$$

σt can be split into two contributions, respectively in phase and out of phase with the strain, defined as follows:

(2) $$\sigma_0 \sin(\omega t)\cos(\delta)$$

(3) $$\sigma_0 \cos(\omega t)\mathrm{sen}(\delta)$$

Indicating $\sigma_0 \cos(\delta) = \sigma_0'$ and $\sigma_0 \sin(\delta) = \sigma_0''$, E' and E" can be rewritten as follows:

(4) $$E' = \sigma_0'/\gamma_0$$

(5) $$E'' = \sigma_0''/\gamma_0$$

Where E' and E" are the real and imaginary part of a complex modulus G*, representing respectively the elastic and the viscous behaviour of the material, written as:

(6) $$E^* (\gamma) = E'(\gamma) + i \cdot E''(\gamma)$$

δ, the phase angle between stress and strain, is given by equation (7):

(7) $$\tan[\delta(\gamma)] = E''(\gamma) / E'(\gamma)$$

DMA can be also conducted along a wide temperature range, obtaining information about glass transition and other chains relaxations if present. In this thesis two instruments were utilized. SBR/BR compounds was testes in the Instron Universal Testing Systems equipped with compression DMA set. Measures was done at three temperature 0, 23 and 70°C and for each temperature three frequency was used, 1, 10 and 100 Hz. PB/alumina composites were instead analysed on a DMA Q800 apparatus from TA Instruments (New Castle, DE, USA) in tensile mode, at 1 Hz frequency and performing a temperature sweep from -120°C to 100°C (3°C/min).

<u>AII - Tensile Tests</u>

Tensile testing is a simple test in which a sample is subjected to a controlled tension until failure. It permits to directly measured the ultimate tensile strength, maximum elongation and the reduction in area of the sample. From these measurements the following other properties can also be calculated: Young's modulus, Poisson's ratio, yield strength, and strain-hardening characteristics. Beside its simplicity, the information this test provide are commonly used for quality control, in the selection of specifical application material and to predict how a material will react under other types of forces. The common testing machine has two crossheads; one is fixed the other can be moved to adjust to the length of the sample and apply tension to the test specimen by a motor. Dogbone shape specimens are generally used which essentially are sample with a narrow middle and wide ends. This shape permits to concentrate the stress in the middle which is also the testing area. Tensile tests were conducted on an Instron 5800 apparatus at 25 °C and a speed of 50 mm min^{-1}.

Bibliography

[1] "The reflection of X-rays by crystals," *Proc. R. Soc. London. Ser. A, Contain. Pap. a Math. Phys. Character*, vol. 88, no. 605, pp. 428–438, Jul. 1913.

[2] P. J. Flory and J. Rehner, "Statistical mechanics of crosslinked polymers. Rubber like elasticity," *J. Chem. Phys*, vol. 11, p. 521, 1943.

[3] J. D. Ferry, "Some reflections on the early development of polymer dynamics: viscoelasticity, dielectric dispersion, and self-diffusion," *Macromolecules*, vol. 24, no. 19, pp. 5237–5245, Sep. 1991.